UNIVERSITY OF OKLAHOMA

GRADUATE COLLEGE

DEPOSITIONAL HISTORY AND RESERVOIR CHARACTERISTICS OF STRUCTURALLY CONFINED FOREDEEP TURBIDITES, NORTHERN CHICONTEPEC BASIN, MEXICO.

A DISSERTATION

SUBMITTED TO THE GRADUATE FACULTY

in partial fulfillment of the requirements for the

Degree of

DOCTOR OF PHILOSOPHY

By

SUPRATIK SARKAR
Norman, Oklahoma
2011

DEPOSITIONAL HISTORY AND RESERVOIR CHARACTERISTICS OF STRUCTURALLY CONFINED FOREDEEP TURBIDITES, NORTHERN CHICONTEPEC BASIN, MEXICO.

A DISSERTATION APPROVED FOR THE
CONOCOPHILLIPS SCHOOL OF GEOLOGY AND GEOPHYSICS

BY

_____
Dr. Roger M. Slatt, Co-Chair

_____
Dr. Kurt J. Marfurt, Co-Chair

_____
Dr. Richard D. Elmore

_____
Dr. Deepak Devegowda

_____
Dr. Sergio Chavez-Perez

Dedicated to my wife Nabanita and my parents

Acknowledgements

The journey towards the PhD degree, one of the most coveted goals in my life, has been an eventful and enriching experience through these four years at the University of Oklahoma. I could have never achieved this goal without the help, support, guidance and effort of a lot of people. I am indebted to all of them.

This dissertation would not have been complete without the guidance, support and constant encouragements of my advisor and mentor Dr. Kurt Marfurt, the 'king of seismic attributes'. I am deeply indebted to him for giving me the opportunity to work with him and his confidence on me for whatever I wanted to do. He made me to stretch my little geophysical ability to such an extent that I never imagined being able to do. He was always there for me for both the academic and non academic issues and helped me immensely to navigate through some rough periods in life. I feel extremely fortunate today that I got an opportunity to work with Dr. Marfurt, one of the most wonderful persons I have ever met in my life.

I want to express my gratitude to Dr. Roger Slatt, one of my principle advisors, who was the main reason for me to come to the University of Oklahoma. He has always been a great inspiration for me for his love towards work and for his students. I am grateful to him for his guidance and support through all these years.

I want to convey my sincere thanks to Dr. Sergio Chávez-Pérez, one of the principle support system behind our 'Chicontepec' project and one of my eminent committee members. Despite my poor long distance communication skills, he showed a great patience and kept faith in me. His suggestions through this project and his help

during the Pemex visit in Poza Rica (2010) have provided means to significantly improve this dissertation. I will always remember his presence and encouragement during our Chicontepec field trip despite of his busy schedule.

I thank Dr. Deepak Devegowda for his comments and critical suggestions which played a great role to improve this dissertation. He always cheerfully accepted me whenever I needed to discuss any problem. I want to thank Dr. Richard D. Elmore for being in my committee and supporting me through my years at the University of Oklahoma both as a committee member and department chair.

I wholeheartedly thank the AASPI consortium and its sponsors for the financial support of my research. Special thanks to Dr. J. Timothy Kwiatkowski for his help with the Chicontepec prestack seismic along with numerous helps with AASPI software and computer hardware. Without that help, I could not have progressed this far in the project.

I want to express my gratitude to Dr. Stephen P. Cossey who conducted the Chicontepec field trip voluntarily for the OU students. This field trip and several discussions with him played a big role to construct the background of the dissertation.

I thank Pemex Exploración y Producción for permission to use subsurface information for my work and publish the research. I am greatly thankful to Dr. Juan M. Berlanga and his colleagues Elba Alderete-Lozada, Javier Méndez de León, and many others who allowed us to work in Pemex's core facility at Poza Rica, Veracruz, Mexico, and provided me several important datasets that enabled me to address several puzzles of the Chicontepec project. I am also indebted to Marco Vázquez-García, Pemex Geophysics Manager in Villahermosa, for technical support and access to seismic data.

I would like to thank Donna S. Mullins, Nancy Leonard, Adrianne Fox, Teresa Hackney, Nicky Chapin and Robin Van Dyke; the great team at the ConocoPhillips School of Geology and Geophysics office. Thank you so much for all your love and support during these four years.

I want to thank all the student members at the AASPI consortium and also my fellow graduate students at the ConocoPhillips School of Geology and Geophysics. I thank Brad Wallet, who was a partner in the Chicontepec project and was a pioneer to start the project. We had a good time together during the Chicontepec field trip. Special thanks to Sunday Amoyodo for his companionship along with several academic and non academic discussions. I also want to thank my dear friends at CPSGG during these years: Atish, Alejandro, Kui, Bunmi, Debapriya, Roderick, Alfredo. I am grateful for their help

I will not be able to express in a few words about how deeply I am indebted to my parents and how much I love them. Living several thousand miles away- they worry about me all the time. My father has been a great support system to everything whatever I have achieved today. My mother always preferred to be in the background and provided silent support and encouragements. Thank you *Baba* and *Ma* for your endless support, love and constant encouragements in every step of my life. I am thankful to my little brother, Pinku, with whom I spent several great moments of life. I also want to thank my father-in-law and mother-in-law for their love and encouragement.

A special thanks to my friend and elder brother Sanjay da. Despite of living far away from me, he was always ready with any kind of help and suggestions for me. Thanks a lot Sanjay da.

I deeply thank my wife Nabanita, who has been by my side as best friend, since we started studying geology together thirteen years ago. Being in the same subject, she has always been the best critic of my research. She helped me with her expertise in several subjects to enrich my dissertation. We had several ups and downs during the years here at Norman, Oklahoma that we endured together and hopefully we will be able to persevere in the coming months. Her love and support through all the situations enabled me to finish my research and progress towards the goal to get a PhD.

Table of Contents

List of Tables

List of Figures

Abstract

Turbidite deposits within structurally confined and tectonically active basins often exhibit complex sediment distribution patterns and facies relationships. In this dissertation, I concentrate on unraveling the deepwater depositional history of the Chicontepec foreland basin followed by characterizing the turbidite reservoirs resulting from the complex depositional process and later affected by extensive diagenesis and volcanic emplacement. I augment this study with a seismic geomorphologic analysis of turbidites of a tectonically dynamic salt minibasin in the Gulf of Mexico and establish its relationship with sequence stratigraphy and sea level changes.

One of the key contributions of this dissertation is the reconstruction of the geologic history of the complex north Chicontepec basin turbidites, which represent one of the most important hydrocarbon plays in Mexico. I integrated seismic geomorphology, outcrop information, well log and core interpretation and tied with geologic time and tectonic history to unravel the progressive changes in depositional patterns and facies associations. The Chicontepec reservoir interval is subdivided into stratigraphic units equivalent to global 3rd order sequences. Based on those subdivisions, I propose a new depositional history model for the northern Chicontepec basin which is comprised of two major flow components from different directions and their variable interactions through geologic time with changes in basin floor geometry. The changes in depositional pattern are broadly correlated with the changes in reservoir quality.

Chicontepec turbidites are characterized by unique rock types containing abundant carbonate rock fragments with quartz, feldspar and clay. Chicontepec deposition was followed by complex diagenetic processes inducing extensive

cementation resulting in the low porosity, low permeability Chicontepec Sandstone. A key aspect of this dissertation is to illustrate a simple and effective methodology to characterize the complex Chicontepec reservoir interval and outline prospective areas for further hydrocarbon exploration. Correlating the stratigraphic units to producing and non-producing intervals provided the link between rock properties and different Chicontepec reservoir zones. These links provide the means to map the potential reservoir zones from prestack inversion-driven rock property volumes.

I also evaluate the potential effect of volcanic bodies on the adjacent Chicontepec reservoir intervals. Volcanic bodies are an integral part of Chicontepec petroleum system. I study their interactions with the Chicontepec sediments from the outcrop and well log patterns in a seismic geomorphologic framework. I propose a dual porosity model and map the potential zones within the Chicontepec Formation with predicted enhanced permeability by the influence of shallow volcanic bodies.

Chapter 1

Introduction

DISSERTATION STRUCTURE

This dissertation consists of six chapters, including an introduction and a conclusion. The chapters are in the form of scientific papers and have been presented at international conferences.

Chapter 2 presents an integrated methodology to reconstruct the depositional history of the Chicontepec turbidites in the northern part of the basin. This chapter forms the primary focus of my thesis. I also discuss the potential of extending the depositional concept in other parts of the basin and analyze the change in reservoir quality with change in depositional pattern. This chapter was presented in the AAPG Annual Convention and Exhibition in Houston (2011) and will be submitted to 'AAPG Bulletin' in August, 2011.

Chapter 3 introduces a simple and effective methodology to characterize the Chicontepec reservoirs in the northern part of the basin. Similar methodology can be used in other tight and complex reservoirs. I use the link established between the rock properties and known reservoir units to predict prospective areas with the aid of pre stack inversion driven maps. This chapter will be submitted to Geophysics in August, 2011.

Chapter 4 provides an overview of the effect of volcanic bodies on the adjacent hydrocarbon reservoirs in the north-eastern part of the Chicontepec foredeep. I provide a

practical recipe to understand the effect of volcanic bodies and use the concepts to predict the affected zone from seismic geomorphologic interpretation. These zones have good potential of enhanced permeability. This chapter was presented in the AAPG Annual Convention and Exhibition in New Orleans (2010) and was awarded the 2nd best student paper in the Convention.

Chapter 5 establishes strong connection between sequential seismic geomorphologic study with the aid of several seismic attributes and successful prediction of sea level change history. This study was carried out within a tectonically dynamic salt minibasin illustrating the turbidite facies association within such structurally confined area with the aid of comprehensive seismic geomorphology analysis. This chapter has been published in The Leading Edge (Sarkar et al., 2010) and its different sections were presented in the 78th Annual International SEG Meeting at Las Vegas (2008) and AAPG Annual Convention and Exhibition in Denver (2009).

OBJECTIVES

The principle objective of this dissertation is to delineate the spatial and temporal pattern of the deepwater sedimentary processes and facies assemblages followed by reconstructing the depositional history in the northern part of the structurally confined Chicontepec foreland basin. A second objective is to systematically characterize the depositionally complex and compositionally immature tight Chicontepec reservoirs to define and predict prospective reservoir zones and develop a methodology for similar complex and tight reservoirs in other areas. A final objective is to characterize the impact of the shallow volcanic bodies on the turbidite reservoirs. Establishing close link between

modern seismic attribute based seismic geomorphology and sequence stratigraphy had been a broad objective of this research.

BACKGROUND AND MOTIVATIONS

Deepwater sedimentation patterns in structurally-confined basins including foreland basins and salt minibasins are significantly different than the passive margin deepwater settings owing to the dominant tectonic influence on sedimentation. There has been increased attention and several publications in the recent years on salt minibasins primarily due to the exploration targets in Gulf of Mexico. On the other hand, there has been considerably less recent work on the structurally complex foredeep basins in front of the fold and thrust belts. Using the Chicontepec foredeep as an example, one of the principle motivations of this study is to investigate the spatial and temporal patterns of deepwater sedimentation and intrinsic complexity of facies association within such tectonically active areas and to calibrate it within a sequence stratigraphic framework. Although the Chicontepec basin has been studied for more than one hundred years, none of the existing depositional models explain the changes in facies distribution, the progressive changes in facies assemblage with geologic time, and reservoir performance (Perez, 1967; Busch and Govela, 1978; Carrillo, 1980; Cuevas, 1980; Bitter, 1983; Cantú Chapa, 1985; Bitter, 1993; Cossey, 2006; Cossey, 2008; Diaz, 2008; Cossey and Nieuwenhuise, 2011).

In addition to the depositional complexity, the Chicontepec turbidite reservoirs are tight and need hydraulic fracturing for hydrocarbon production. Pattern drilling is common practice in the unconventional Chicontepec play. There is a need for a

methodology to characterize the reservoirs and to delineate potential prospect areas based on the stratigraphic subdivisions in order to improve Chicontepec exploration and production. This methodology should be applicable to other tight sand reservoirs, which are common worldwide in this age of unconventional reservoirs.

In general, volcanics may harm the reservoir and are avoided by drillers. However shallow volcanic bodies form an integral part of the Chicontepec petroleum system specifically in the northern part of the foredeep. In many of the instances, they are emplaced close to the Chicontepec reservoir interval.

One of my principle activities in the industry supported "Attribute Assisted Seismic Processing and Interpretation" (AASPI) consortium at the University of Oklahoma, is to calibrate the attribute expression of depositional processes in a seismic geomorphology context. Different seismic attributes enhance different structural and stratigraphic aspects. Is it possible to use seismic geomorphology within a structurally confined basin with a reasonably good seismic data to predict sea level changes over the depositional period?

INTRODUCTION TO THE FORELAND BASIN SYSTEM

DeCelles and Giles, (1996) define a foreland basin as an elongate depression of potential sediment accommodation zone that forms on continental crust between a contractional orogenic belt and the adjacent craton, mainly in response to geodynamic processes related to subduction and the resulting peripheral or retroarc fold–thrust belt. A foreland basin system consists of four discrete depozones, referred to as the wedge–top, foredeep, forebulge and back–bulge depozones. The foredeep depozone is the thickest

sedimentary zone and thickens toward the orogen (Figure 1). DeCelles and Giles (1996) state that Aubouin's (1965) term 'foredeep' is commonly used interchangeably with foreland basin. Basinal turbidite systems form in deeper water elongate highly subsiding troughs (foredeeps) that developed in front of advancing thrust system (Mutti et al.,2003).

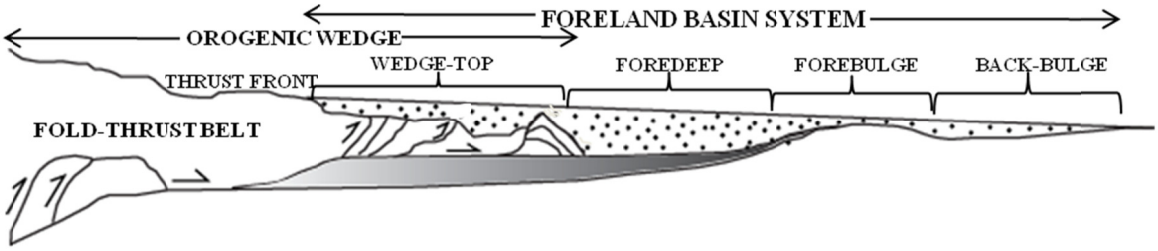

Figure 1: Schematic cross section of a foreland basin system indicating different zones. (Modified from DeCelles and Giles, 1996).

INTRODUCTION TO THE CHICONTEPEC BASIN

The Sierra Madre Oriental (SMO) is one of the major fold thrust belts created due to the Late Cretaceous–Early Tertiary Laramide Orogeny in Mexico. The Chicontepec foredeep was formed as a retroarc foreland basin developed parallel to the mountain belt (Morán –Zenteno, 1994), forming an elongated trough (Figures 1 and 2) in front of the SMO that developed as a subbasin of the Tampico Misantla Basin located in East Central Mexico. The Cretaceous Tuxpan Platform is situated on the eastern side of the Chicontepec foredeep (Figure 2).

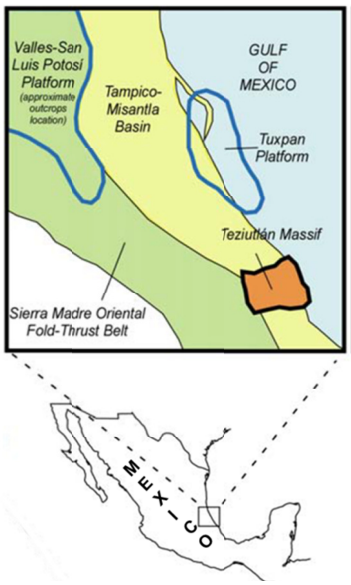

Figure 2: Location of the Tampico Misantla basin showing structural elements around the basin (modified from Bermudez et al., 2006).

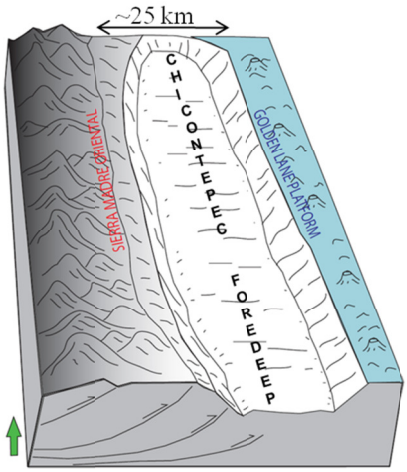

Figure 3: Schematic diagram showing the Chicontepec foredeep forming an elongated trough-like accommodation zone in between the Sierra Madre Oriental and the Golden Lane (Tuxpan) platform.

Deepwater turbidite systems that occur in foredeep setting are usually very complex due to variations in the basin formation history, basin morphology, seafloor topography, sediment provenance and later tectonic pulses. Pickering and Corregidor (2005) report that mass transport complexes dominate many such deepwater systems.

Tectonic pulses and related structural activities may deform previously deposited sediments, change the accommodation space by basin subsidence and modify the sedimentation rate by increasing sediment erosion. Volcanic intrusions and extrusions are common in foreland basins as they are very close to the subduction zone.

The Chicontepec foredeep trends NW-SE and was filled up with both thin and thick bedded turbidites. My study takes advantage of a recently acquired 3D seismic survey in the northern part of Chicontepec foredeep. Several Chicontepec outcrops are exposed in the foothill regions of SMO (Figure 4), which were exhumed by the post depositional tectonic activities.

After the formation of Chicontepec foredeep during Late cretaceous- Early Paleocene; Lower Paleocene Velazco Formation deposited within the trough (Figure 5). Chicontepec strata started depositing from Upper Paleocene and continued till Lower Eocene (Figure 5). The Chicontepec Formation can be broadly subdivided into three parts; Lower, middle and Upper Chicontepec. The average thickness of Chicontepec Formation varies from 300-400 meters in the area of interest. Maximum thickness of Chicontepec strata has been reported to be up to 2000 meters (Bitter, 1993).

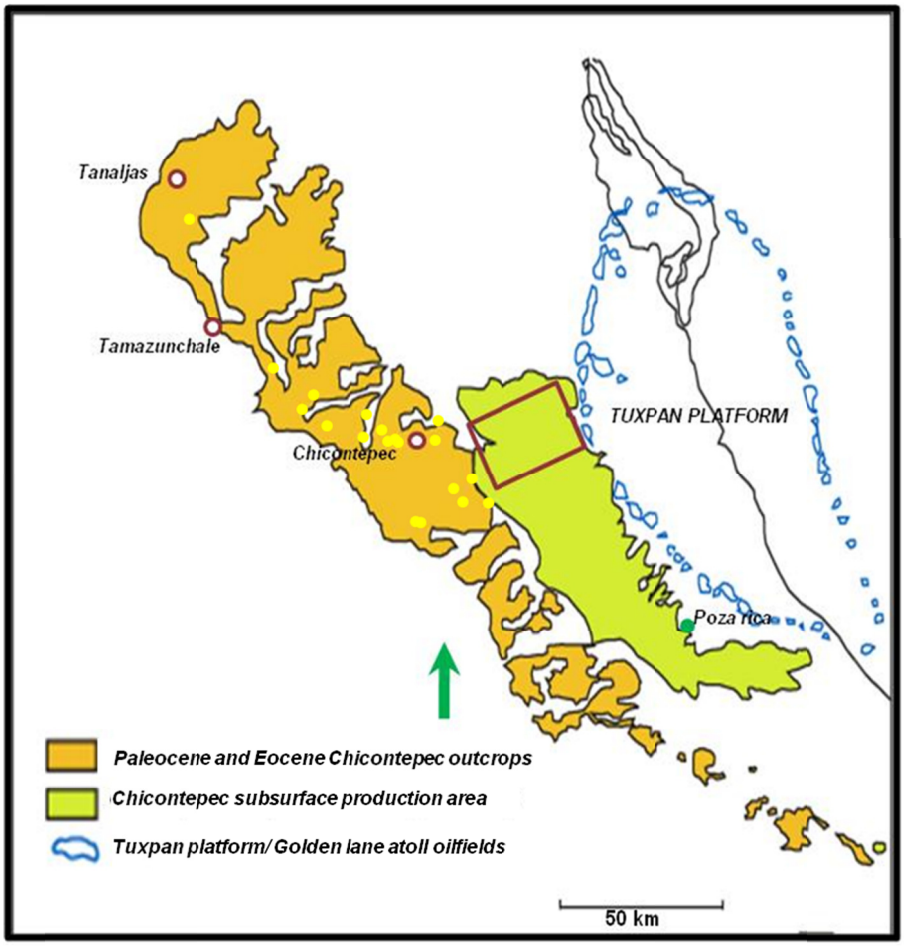

Figure 4: Location map of the Chicontepec foredeep in the East-Central Mexico (Modified after Bermudez et al., 2006). The orange area indicate the foothill region of Sierra Madre Oriental fold thrust belt along which several Chicontepec outcrops are exposed. The green area indicates the main Chicontepec subsurface production area. Cyan polygons indicate the Tuxpan Platform or Golden Lane atoll oilfields. Yellow dots indicate outcrops used in this study. The red rectangle is the outline of the 3D seismic coverage within the northern part of Chicontepec basin where this study is concentrated.

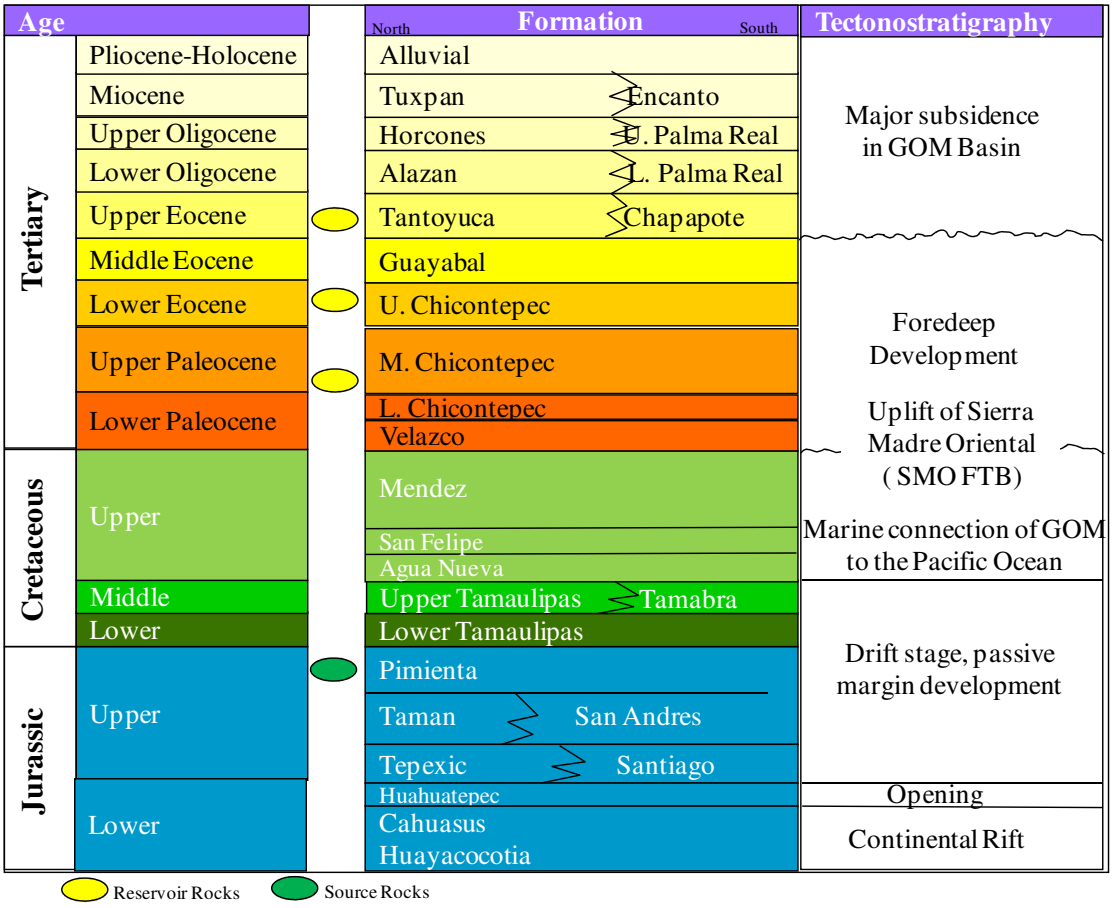

Figure 5: Generalized stratigraphic column of the study area (based on a stratigraphic column courtesy of Pemex).

EXISTING DEPOSITIONAL CONCEPTS OF THE CHICONTEPEC FORMATION

Turbidite deposition within the Chicontepec foredeep was first recognized primarily from well logs and a few 2D seismic lines in the late 1970s and early 1980s (Barker and Bargen, 1977; Busch and Govela, 1978; Carrillo, 1980; Cantú Chapa, 1985). These findings were followed by Chicontepec outcrop studies (Bitter, 1983; Bitter, 1993; Cossey, 2006; Cossey, 2008; etc.) and the Chicontepec reservoir characterization (Abbaszadah et al., 2003; Tyler et al., 2004; Bermudez et al., 2006; Takahashi et al.,

2006; etc.). While providing information about the depositional pattern and reservoir quality, there is no comprehensive study about the turbidite facies association throughout the foredeep basin.

Perez (1967) suggested the presence of a paleocanyon south of Poza Rica on noting the absence of Jurassic and Cretaceous strata (Figure 8). Studying the distribution of Chicontepec strata around Poza Rica, Busch and Govela (1978) also described a paleocanyon which deeply eroded the Cretaceous and Jurassic strata during Paleocene time which was subsequently filled with the Chicontepec formation (Figure 7 and 8). Carrillo (1980) and Cuevas (1980) extended the Chicontepec paleocanyon to the north, thereby proposing the presence of a paleocanyon throughout the Chicontepec foredeep (Figure 8). Given the absence of chronostratigraphic control and difficulty in correlating wells and seismic horizons, Cantú Chapa (1985) rejected these hypotheses and concluded that the presence of a paleocanyon can be interpreted only within a much smaller area in the south of Poza- Rica (Figure 8).

Recently Cossey and Nieuwenhuise (2011) have proposed a “fill and spill” concept of several subbasins separated by local highs or sills for the ultimate subsurface paleocanyon creation. He also connected the source of the paleocanyon to an entry point near the Tanlajas canyon in the far northern part of the basin. Cossey and Nieuwenhuise's (2011) studies are based on outcrops and paleocurrent measurements and the concepts cannot be fully verified from the subsurface seismic study done in the southern part of the basin by Diaz (2008).

The early Chicontepec paleocanyon concept has been superseded by a basin floor fan model. In this concept, a series of basin floor fans originating as eroded sediments

from uplifted Mesozoic units of the Sierra Madre Oriental fold thrust belt perpendicular to the foredeep axis and were deposited within the Chicontepec foredeep (Bitter, 1983, 1993; Cheatwood and Guzman, 2002; Cossey, 2006; Tyler et al., 2004) (Figure 9).

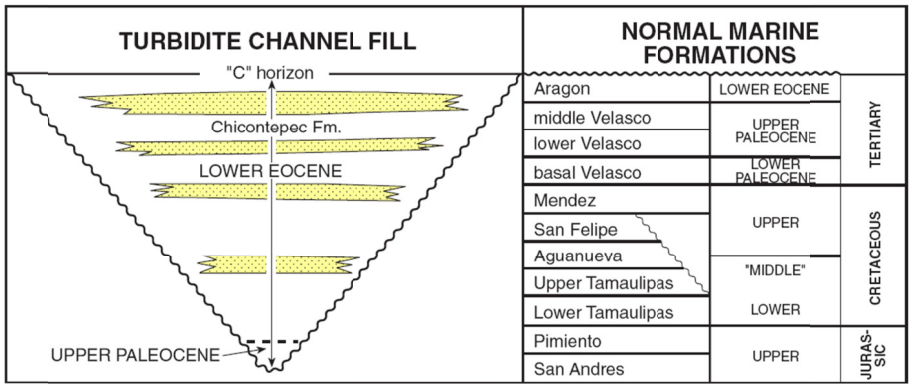

Figure 6: Stratigraphic subdivisions of Upper Jurassic, Cretaceous and lower Tertiary strata showing the relation of the unconformity at the base of the Chicontepec canyon and the nature of the canyon fill (Busch and Govela, 1978; Busch, 1992).

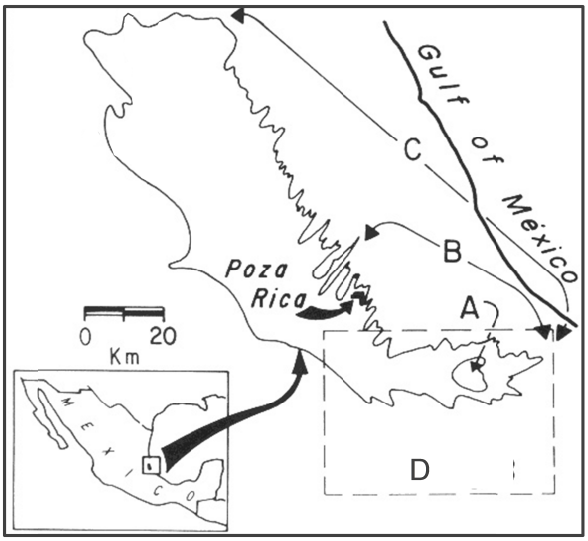

Figure 7: Evolution of the Chicontepec paleocanyon concept in East-Central Mexico as described by Cantu Chapa (1985). A is the first paleocanyon interpretation by Perez (1967); B is the extent of the 'Chicontepec Paleocanyon' by Busch and Govela. C is the extent of the paleocanyon proposed by Carrillo (1980) and Cuevas (1980) as they extend the paleocanyon throughout the whole production zone. D is the interpretation of Cantu Chapa (1985).

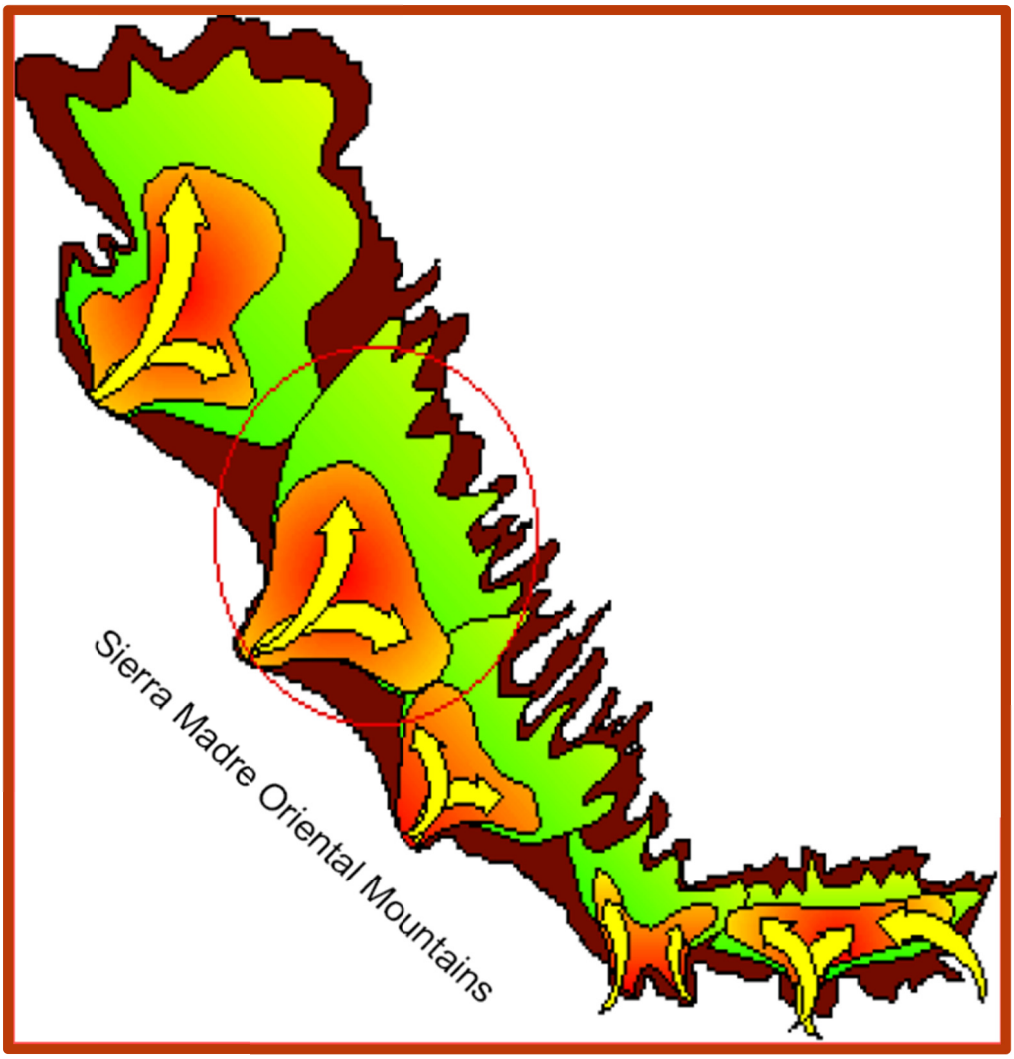

Figure 8: The most accepted concept for deposition of the Chicontepec Formation, where all the sediments within the basin are contributed by a series of basin floor fans originating from eroded sediments from the Sierra Madre Oriental fold thrust belt (after Cheatwood and Guzman, 2002).

REFERENCES

Abbaszadeh, M., T. Shimamoto, F. M. Sandria, D. H. Zamora Guerrero and F. Rodriguez de la Garza, 2003, Integrated Geostatistical Reservoir Characterization of Turbidite Sandstone Deposits in Chicontepec Basin, Gulf of Mexico: Proceedings of the Society of Petroleum Engineers Annual Technical Conference and Exhibition, October 5-8, Denver, Colorado, U.S.A., p. 1-15, SPE paper 84052.

Aubouin, J., 1965, Geosynclines: Elsevier, New York.

Bermúdez, J. C., J. Araujo–Mendieta, M. Cruz–Hernández, H. Salazar–Soto, S. Brizuela–Mundo, S. Ferral–Ortega, and O. Salas–Ramírez, 2006, Diagenetic history of the turbiditic litharenites of the Chicontepec Formation, northern Veracruz: Controls on the secondary porosity for hydrocarbon emplacement: Gulf Coast Association of Geological Societies Transactions, v. 56, p. 65–72.

Bitter, M.R., 1993, The sedimentation and provenance of Chicontepec sandstones with implications for uplift of the Sierra Madre Oriental and Teziutlán Massif, East-Central Mexico, Proceedings 13th Annual SEPM Gulf Coast Section Reservoir Conference, Houston, p. 155-172.

Bitter, M. R., 1983, Sedimentation and petrology of the Chicontepec Formation, Tampico-Misantla Basin, Eastern Mexico: M.Sc. thesis, University of Kansas, Lawrence, 117 p.

Busch, D.A., and S.A. Govela, 1978, Stratigraphy and structure of Chicontepec turbidites, southeastern Tampico–Misantla Basin: AAPG Bulletin, v. 62, no. 2, p. 235–246.

Cantu Chapa, A., 1985, Is there a Chicontepec paleocanyon in the Paleocene of eastern Mexico?: Journal of Petroleum Geology, v. 8, no. 4, p. 423–434.

Carrillo, B. J., 1980, Paleocanones Terciarios de la Planicie Costera del Golfo de Mexico: Bol. Asociation Mexicana de Geologos Petroleros Boletin, v 32(1), p. 1419-1447.

Cheatwood, C. J., and Guzmán, A. E., 2002. Comparison of reservoir properties and development history – Spraberry Trend Field, west Texas and Chicontepec Field, Mexico, Proceedings SPE International Petroleum Conference and Exhibition, Villahermosa, Mexico, 19p, SPE Paper 74407.

Cossey, S. P. J., 2008, Debrites in the Chicontepec Formation, Tetlahuatl, Mexico in Nilsen, T. H., Shew R. D., Steffens, G. S., and Studlick, J. R. J., eds., Atlas of Deep-Water Outcrops, AAPG Studies in Geology 56, p. 231-234.

Cossey, S. P. J., 2006, Slumps and debrites in Paleocene Chicontepec Formation, Mexico: Implications for subsurface identification: American Association of Petroleum Geologists, Abstracts with Program, Annual Convention, April 9-12, CD-ROM publication.

Cossey, S. P. J. and D. V. Nieuwenhuise, 2011, A New Depositional Model for the Chicontepec Basin, Onshore Eastern Mexico: American Association of Petroleum Geologists, Abstracts with Program, Annual Convention, April 10-13, CD-ROM publication.

Cuevas, S. F., 1980, Exploración petrolera en sedimentos terrígenos: 35.° Reunión a nivel de expertos de ARPEL, Nuevos Conceptos Geológicos en Exploración Petrolera, México, v. 1, 14 p.

DeCelles, P.G. and K.A. Giles, 1996, Foreland basin systems: Basin Research, 8, p. 105–123.

Diaz Cadenas, G. E., Sequence stratigraphy of Chicontepec play, Tampico–Misantla basin, Mexico: MS thesis at University of Oklahoma.

Morán-Zenteno, D., 1994, Geology of the Mexican Republic: AAPG Studies in Geology, no. 39, 160 p.

Mutti, E., R. Tinterri, G. Benevelli, D. di Biase, and G. Cavanna, 2003, Deltaic, mixed and turbidite sedimentation of ancient foreland basins: Marine and Petroleum Geology, v. 20, p. 733–755.

Perez, M. J. D., 1967, Estudio del Yacimiento San Andres. Inst. Mex. del Petróleo, Rama de Expl.

Pickering, K. T. and J Corrigidor, 2005, Mass–transport complexes (mtcs) and tectonic control on basin–floor submarine fans, Middle Eocene, South Spanish pyrenees: Journal of Sedimentary Research, v. 75, p 761–783.

Takahashi, S. , M. Abbaszadeh, K. Ohno and H.S. Soto, 2006, Integrated Reservoir Modeling for Evaluating Field Development Options in Agua Fria, Coapechaca and Tajin Fields of Chicontepec Basin: Pcoceedings of the First International Oil Conference and Exhibition in Mexico, 31 August-2 September 2006, Cancun, Mexico, p. 1-14, SPE paper 103974.

Tyler, N., R. Gachuz-Muro, J. Rivera, J. M. Rodríguez, S. Rivas-Gomez, R. Tyler, and V. Núñez-Vegas, 2004, Integrated characterization for low permeability, submarine fan reservoirs for waterflood implementation, Chicontepec Fan System, Mexico: Proceedings of the Society of Petroleum Engineers International Petroleum Conference in Mexico, November 8-9, Puebla, Puebla, Mexico, p. 1-12, SPE paper 92077.

Chapter 2

Delineating turbidite patterns and facies distribution within the Chicontepec Foredeep, Mexico

ABSTRACT

The turbidites in the Chicontepec formation were deposited in an elongated foreland basin between the active Sierra Madre Oriental (SMO) fold thrust belt and Tuxpan Platform during the Paleocene and Eocene. Even after extensive exploration for more than forty years, the deepwater depositional model of the Chicontepec Formation is poorly understood. I propose a model for progressive changes in deepwater patterns in the northern part of the Chicontepec foredeep which would facilitate an improved geologic understanding and to a superior perspective for the reservoir distribution patterns in this important hydrocarbon play.

Integration of 3D seismic data, well logs and core information with the Chicontepec outcrops adjacent to the 3D seismic area facilitates the complex spatial and temporal geologic patterns in the northern part of the Chicontepec foredeep. Outcropping Chicontepec strata at the foothills of the SMO expose the deepwater patterns of the Chicontepec Formation and provide important indication about paleoflow direction which progressively changed from predominantly NW-SE direction to SWW-NEE direction from Paleocene to Eocene period. Regionally correlated wells indicate the presence of six extended shale layers which divide the zone of my study into five

stratigraphic units, which can be calibrated to Haq et al.'s (1987) condensed sections of global 3rd order sequences. Detail facies distribution patterns delineated within those five stratigraphic units by integrating seismic geomorphology and core studies, indicate the presence of dominant axial channel system during the Late Paleocene Lower Chicontepec deposition. Depositional pattern progressively changed from the Upper part of the Late Paleocene with maximum sedimentation was sourced from the direction of SMO. The interaction of the two systems created mixed deposition in some areas. Reservoir quality within the stratigraphic units varies in accordance with the progressive changes in depositional pattern, where Eocene stratigraphic units show better reservoir quality than the Paleocene units.

INTRODUCTION

Existing depositional models of the Chicontepec Formation have not yet been successful in explaining the complexity of deepwater deposits and its relation to the reservoir quality and performance. My primary objective for this paper is to delineate the deepwater processes and facies distribution patterns, explain interrelationships among the deepwater architectural elements and their progressive changes through geologic time within the Chicontepec reservoir interval in the northern part of the Chicontepec foredeep. Identifying the change in depositional pattern in a chronostratigraphic framework would facilitate a depositional history model for the Chicontepec turbidites. I wish to correlate the change in reservoir properties to the change in depositional pattern in time and space.

Reservoir characteristics of Chicontepec Formation

This complex turbidite system is characterized by very low porosity (1% –10%) and permeability (.01– 5 mD) (Bermudez et al., 2006). Several factors contribute towards the low porosity and permeability of the reservoir, including poor grain sorting, composition of the framework grains and extensive diagenesis. Due to poor reservoir quality, only 0.1% of the original oil in place, equal to 140 million barrels of oil–equivalent, had been recovered till 2002 (Cheatwood and Guzman, 2002).

Background geology

The Sierra Madre Oriental (SMO) is one of the major fold thrust belts created due to the Late Cretaceous–Early Tertiary Laramide Orogeny in Mexico. The Chicontepec foredeep was formed as a retroarc foreland basin developed parallel to the mountain belt (Morán –Zenteno, 1994), forming an elongated trough (Figure 1b) in front of the SMO that developed as a subbasin of the Tampico Misantla Basin located in East Central Mexico. The Cretaceous Tuxpan Platform is situated on the eastern side of the Chicontepec foredeep (Figure 1).

The Chicontepec foredeep trends NW-SE and was filled with both thin and thick bedded turbidites. My study takes advantage of a recently acquired 3D seismic survey in the northern part of the Chicontepec foredeep. Several Chicontepec outcrops are exposed in the foothill regions of SMO (Figure 1), which were exhumed by the post depositional tectonic activities.

After the formation of the Chicontepec foredeep during Late cretaceous- Early Paleocene time the Lower Paleocene Velazco Formation deposited within the trough

(Figure 2). The Chicontepec strata started depositing from Upper Paleocene and continued until Lower Eocene (Figure 2). The Chicontepec Formation can be broadly subdivided into three parts: Lower, middle and Upper Chicontepec. The average thickness of the Chicontepec Formation varies from 300-400 meters in the area of interest. Maximum thickness of the Chicontepec strata has been reported to be up to 2000 meters (Bitter, 1993).

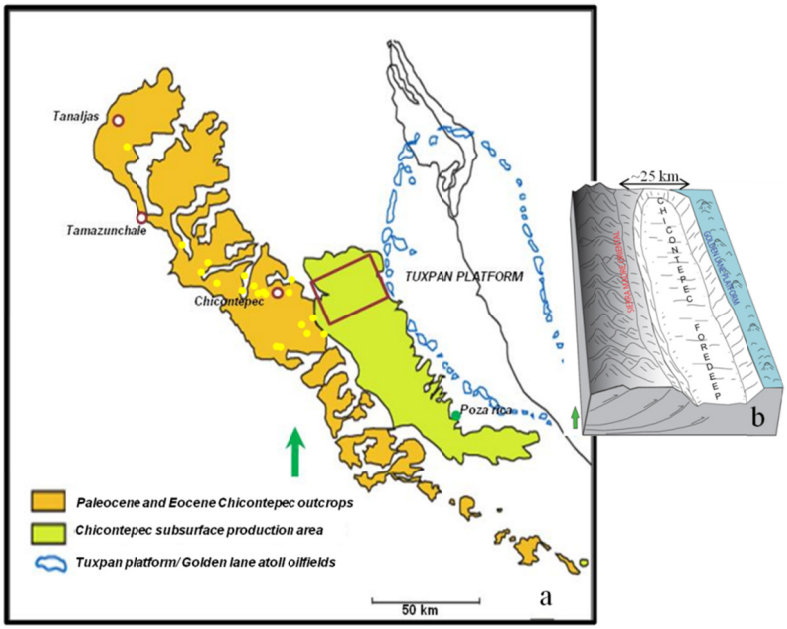

Figure 1: (a) Location map of the Chicontepec foredeep in East-Central Mexico (Modified after Bermudez et al., 2006). The orange area indicates the foothill region of the Sierra Madre Oriental fold thrust belt along which several Chicontepec outcrops are exposed. The green area indicates the main Chicontepec subsurface production area. Cyan polygons indicate the Tuxpan Platform or Golden Lane atoll oilfields. Yellow dots indicate outcrops used in this study. The red rectangle is the outline of the 3D seismic coverage within the northern part of the Chicontepec basin where this study is concentrated. (b) Schematic diagram showing the Chicontepec foredeep forming an elongated trough-like accommodation zone between the Sierra Madre Oriental and the Golden Lane (Tuxpan) platform.

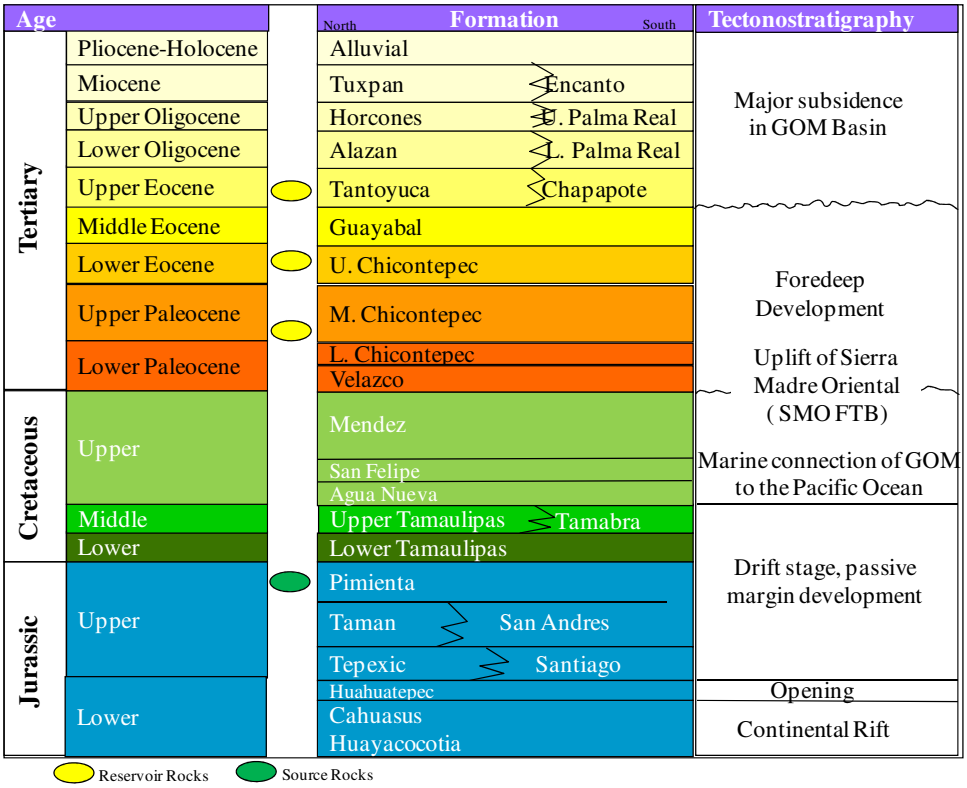

Figure 2: Generalized stratigraphic column of the study area (based on a stratigraphic column courtesy of Pemex).

Foreland basin turbidite depositional concepts

Significant foreland basin turbidite analysis has been based on outcrop studies done over the years (e.g., Ricci Lucchi, 1990; Thornburg et al., 1990; Sinclair, 1997; Plink-Bjorklund et al., 2001; Mutti et al., 2003; Pickering and Corregidor, 2005). Fewer foreland basin turbidite analyses have been described based on modern sea floor data (e.g., Prior et al., 1986; Romero Otero, 2009). De Ruig and Hubbard (2006), and Covault et al. (2009) have described the turbidite architecture and seismic geomorphology for the Tertiary Molasse foreland basin system in Austria on the basis of 3D seismic and well information. Although, these studies describe a variety of turbidite depositional patterns, all the patterns can be divided into two primary categories followed by a third category

representing a combination of the first two. The first pattern consists of one or more slope channels originating on or cutting through the fold thrust belt that fills the trough with channel-fan complexes flowing perpendicular to the foredeep axis (Figure 3a). The second pattern consists of an axial channel complex parallel to the foredeep axis, which provided the major mode of sediment transportation and accumulation (Figure 3b). These channels also form channel lobe complexes parallel to the basin axis and splays.

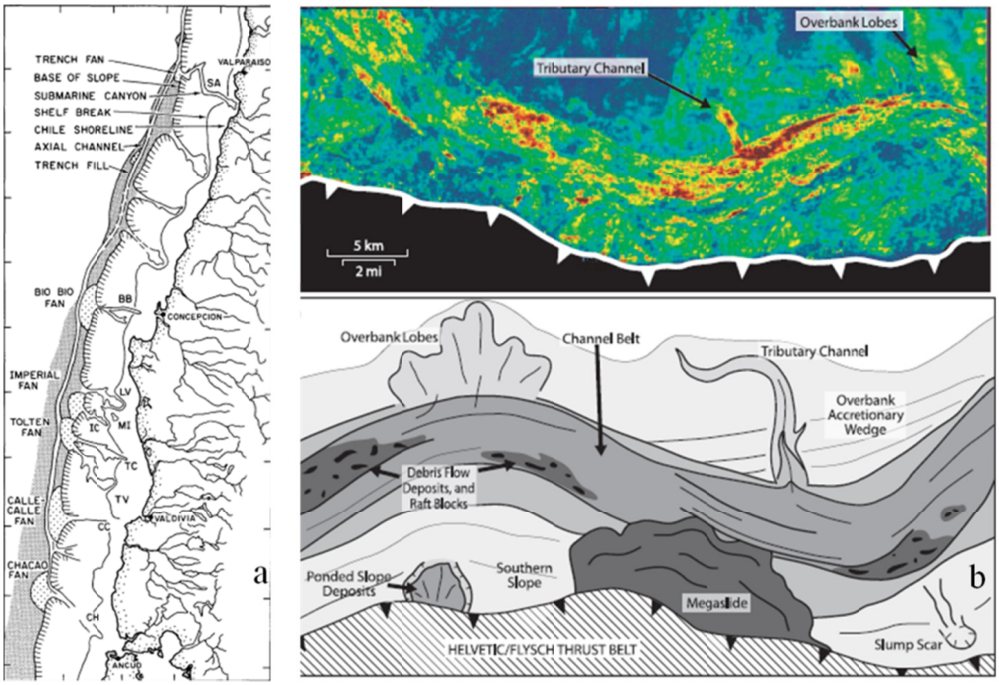

Figure 3: Example of two primary categories of depositional flow patterns within a foreland basin. (a) Series of channel fan complexes perpendicular to the foredeep axis (Thornburg et al., 1990). (b) Axial channel system flowing subparallel to the foredeep axis along with associated splay and tributaries (DeRuig and Hubbard, 2006).

In the Chicontepec Basin, the most well known depositional concept was the 'Chicontepec paleocanyon' concept (Perez, 1967; Busch and Govela, 1978; Carrillo, 1980; Cuevas, 1980; Cantú Chapa, 1985) which illustrates deposition of the Chicontepec turbidites within an erosional canyon. This paleocanyon concept has been superseded by

a basin floor model similar to the second pattern defined in this section and is mentioned in most of the recent papers on the Chicontepec Basin (Bitter, 1983, 1993; Cheatwood and Guzman, 2002; Cossey, 2006; Abaszadeh et al., 2003) (Figure 4).

Figure 4: The most accepted concept for deposition of the Chicontepec Formation, where all the sediments within the basin are contributed by a series of basin floor fans originating from eroded sediments from the Sierra Madre Oriental fold thrust belt (after Cheatwood and Guzman, 2002).

Depositional history model

When seismic geomorphologic patterns from seismic sequences are related to geologic time and the sedimentological details from core and log analysis, we start to explore the progressive changes in depositional systems and architecture over a geologic time period. Using information from an outcrop analogue can add an extra dimension to the identified depositional patterns. Thus, a good depositional history model within a reservoir zone helps to map lateral and vertical reservoir heterogeneities and identify the best prospects for potential drilling (e.g. Zeng et al., 2001; Singh et al., 2004; Calavan and Garfield, 2004; Sprague et al., 2005; Porter et al., 2006; De Ruig and Hubbard, 2006.).

DATA AVAILABILITY AND METHODOLOGY FOR THIS STUDY

Data availability

The primary area of this study is defined by a modern 700^2 km 3D prestack time migrated, Amatitlan 3D seismic survey in the northern part of the Chicontepec play (Figure 1a). This seismic survey provides a unique opportunity to examine the subsurface characters of the Chicontepec reservoirs and deepwater elements. Although the bandwidth is good, ranging 0-60 Hz (Figure 5), the 60 Hz component corresponds to a wavelength of ~70 m within the Chicontepec Formation whose velocities range between 2800 m/s to 5200 m/s on sonic logs. Individual reservoir components consist primarily of thin sands which range between 0.2-15 m thick as observed from core description and well logs. Comparing this range to the ¼ wavelength resolution at 60 Hz of 70 m, we note that all these thin sands fall below the limits of seismic resolution. Although, we cannot resolve such sands, we can still detect them (e.g., Widess, 1973; Kallweit and Wood, 1982) either through their geomorphological form, or through anomalous reflectivity validated by the generation of synthetic seismograms from sonic and density logs. Apart from complexity of foredeep deepwater deposits, population centers, terrain and swamps gave rise to areas of low fold of the seismic data (Figure 6). Data quality has been severely affected in places by the presence of several igneous sills and extrusives (Figures 6 and 7).

Well log information is available from around 300 wells from four major oil fields in the eastern part of the northern Chicontepec basin (Figure 8). I had access to conventional core sections from 10 of those wells. A biostratigraphic report is available

from the P1 well, which is situated in the middle of the survey (Figure 13). Several thin sections were made mainly from the outcrop locations and from conventional cores from two wells.

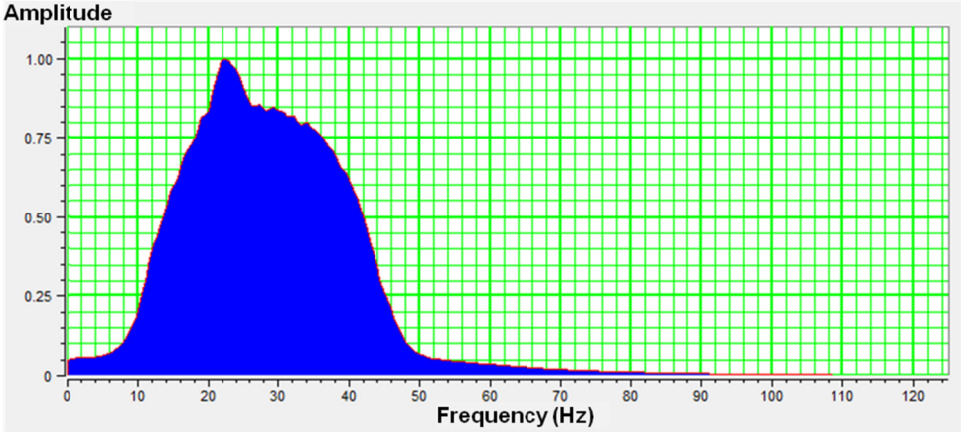

Figure 5: Seismic bandwidth (Hz) within the Chicontepec Formation.

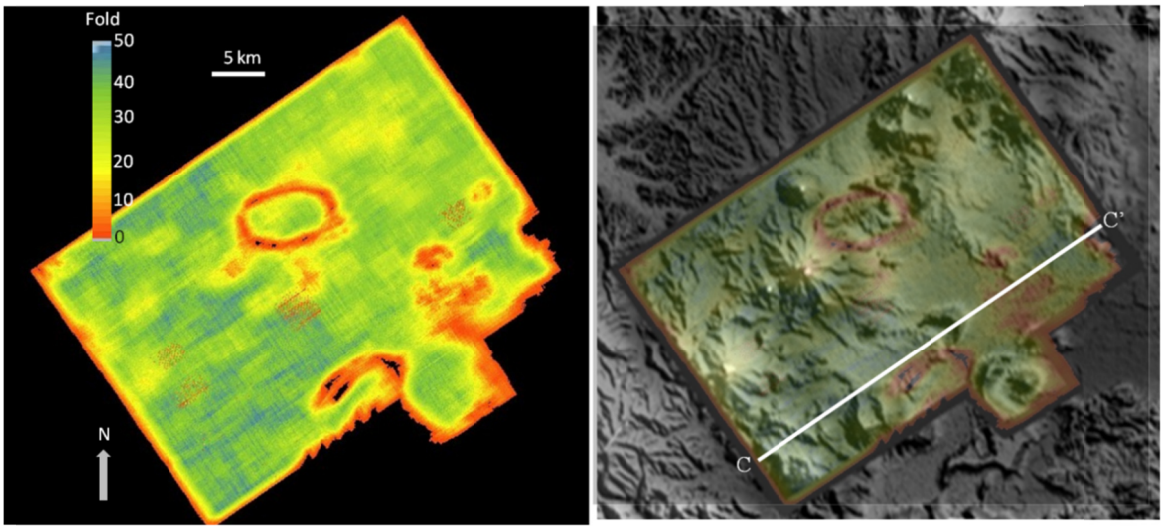

Figure 6: (a) Seismic fold map of Amatitlan seismic survey. (b) Digital elevation map blended with the seismic fold map. Several extrusive volcanic mounds can be observed throughout the survey area (modified from Pena et al., 2009).

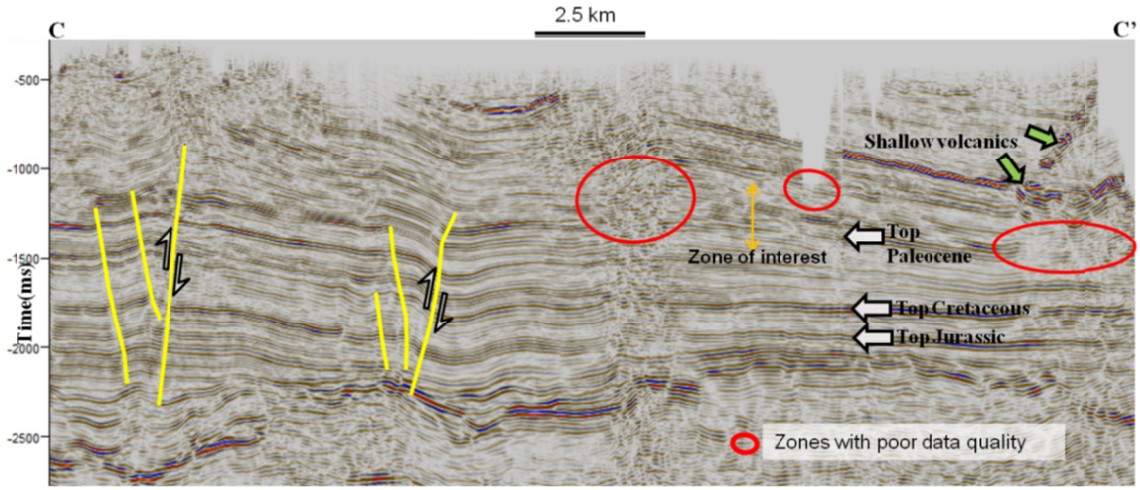

Figure 7: A representative vertical seismic section from the Amatitlan 3D seismic survey. Red ellipses indicate poor data quality within the zone of interest due to shallow volcanic bodies and low fold of acquired seismic data. Two major thrust faults are marked in yellow (along with their antithetic faults), which represent the extended part of SMO in the subsurface. These thrust faults can be referred to the thrust faults in the schematic diagram in Figure 1b.

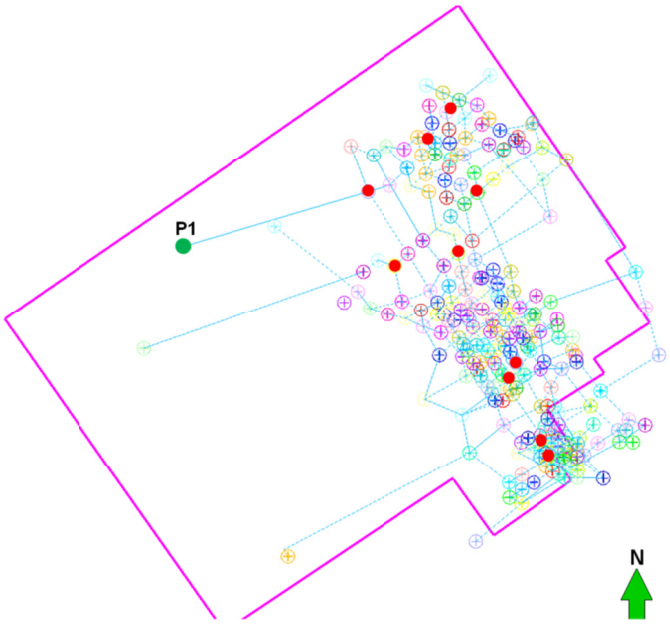

Figure 8: Location of the wells with well logs. Pink polygon demarcates the Amatitlan 3D seismic survey. Red circles indicate the wells where core interpretations were done. Green circle indicates the well with biostratigraphic information.

Methodology

I begin with an overview of the outcropping Chicontepec Formation in the foothills of Sierra Madre Oriental fold and thrust belt (SMO) and identify the probable depositional flow directions from the outcrop paleocurrent measurements. Next, I subdivide the Chicontepec turbidites into depositional facies from outcrop and core descriptions to provide constraints on architectural elements that fall below seismic resolution. Then, I perform regional stratigraphic correlation from well logs and correlate within the chronostratigraphic framework to calibrate the stratigraphic divisions with global sequences. These stratigraphic units are then transferred to the 3D seismic volume to delineate the facies distribution pattern with the help of seismic geomorphology and core description. Finally, I am able to build a depositional history model in the northern part of the Chicontepec basin as an outcome of this sequential analysis. I attempt to calibrate the change in rock composition from Paleocene to Eocene rocks with respect to the depositional history and estimate the possible continuation and changes in depositional patterns in other parts of the basin based on published literature. I will describe each of the components of the workflow shown in Figure 9.

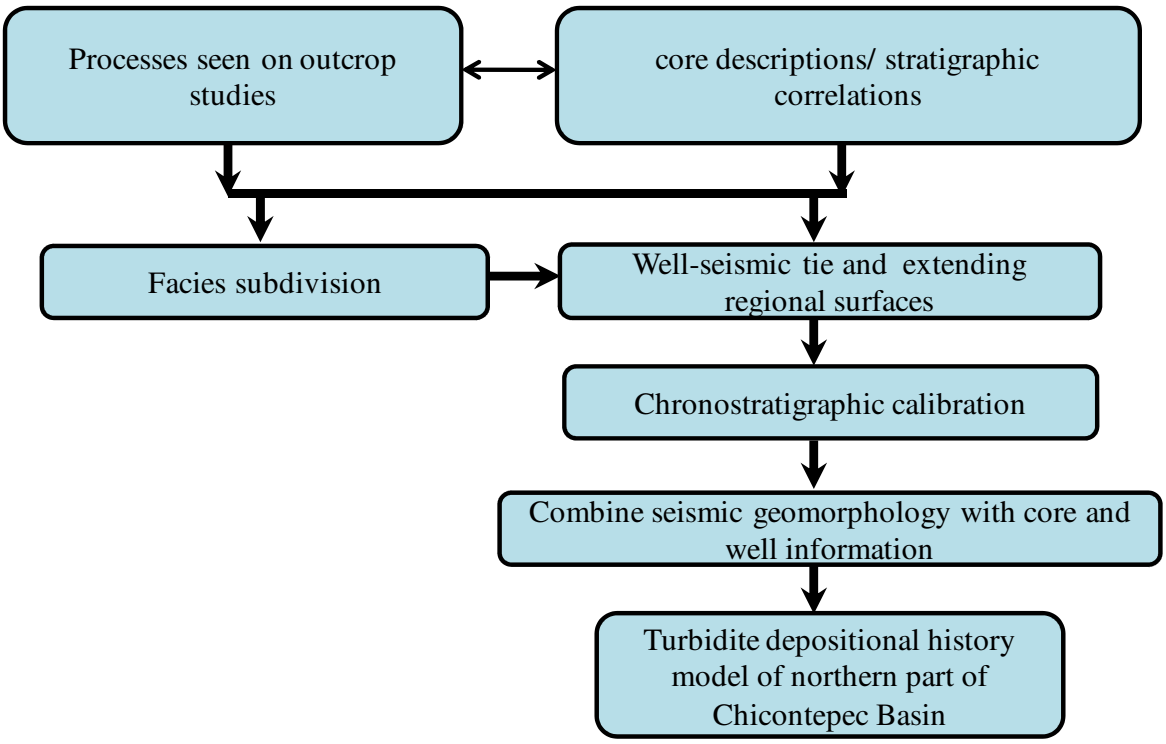

Figure 9: Workflow to delineate deepwater patterns and build a depositional history model for the northern part of the Chicontepec basin.

OUTCROP STUDY

Several Chicontepec outcrops are exposed in the foothill regions of SMO. I visited several of these outcrops situated to the west and northwest of the subsurface study area (spanning from 2.5 km to the west to 70 km to the northwest of the seismic coverage) (Figures 1, 10a and 12). These outcrop exposures provide a direct means of identifying depositional processes and establishing a statistical framework, if not an accurate estimate of relative facies distribution. The deepwater facies distribution and assemblages of the Paleocene and Eocene Chicontepec Formation form the Chicontepec reservoir units in the subsurface and thus allow us to study the Formation at different scales.

Deepwater architectural elements, including layered sheet, amalgamated sheet, channel-levee, channel/canyon fill, thin beds and mass transport complexes are readily visible in these outcrops (Figure 10b). The majority of the outcrops are of Paleocene age (Bitter, 1993), representing the Lower to Middle Chicontepec Formation. Accompanying Cossey in field work in 2010, we advanced from north to south in the outcrop belt and progressively encountered outcrops of younger age which might be a result of progressive advance of the deformation front from north to south (Diaz, 2008). An outcrop near Colatlan village extends from late Upper Paleocene to Early Eocene (biostratigraphic information from personal communication with Dr. Stephen P. Cossey, 2010) (Figure 11). The amount of deformation, presence of mass transport complexes and overall thickness of the Chicontepec Formation decreases significantly from the SMO fold thrust belt to the eastern part of the foredeep.

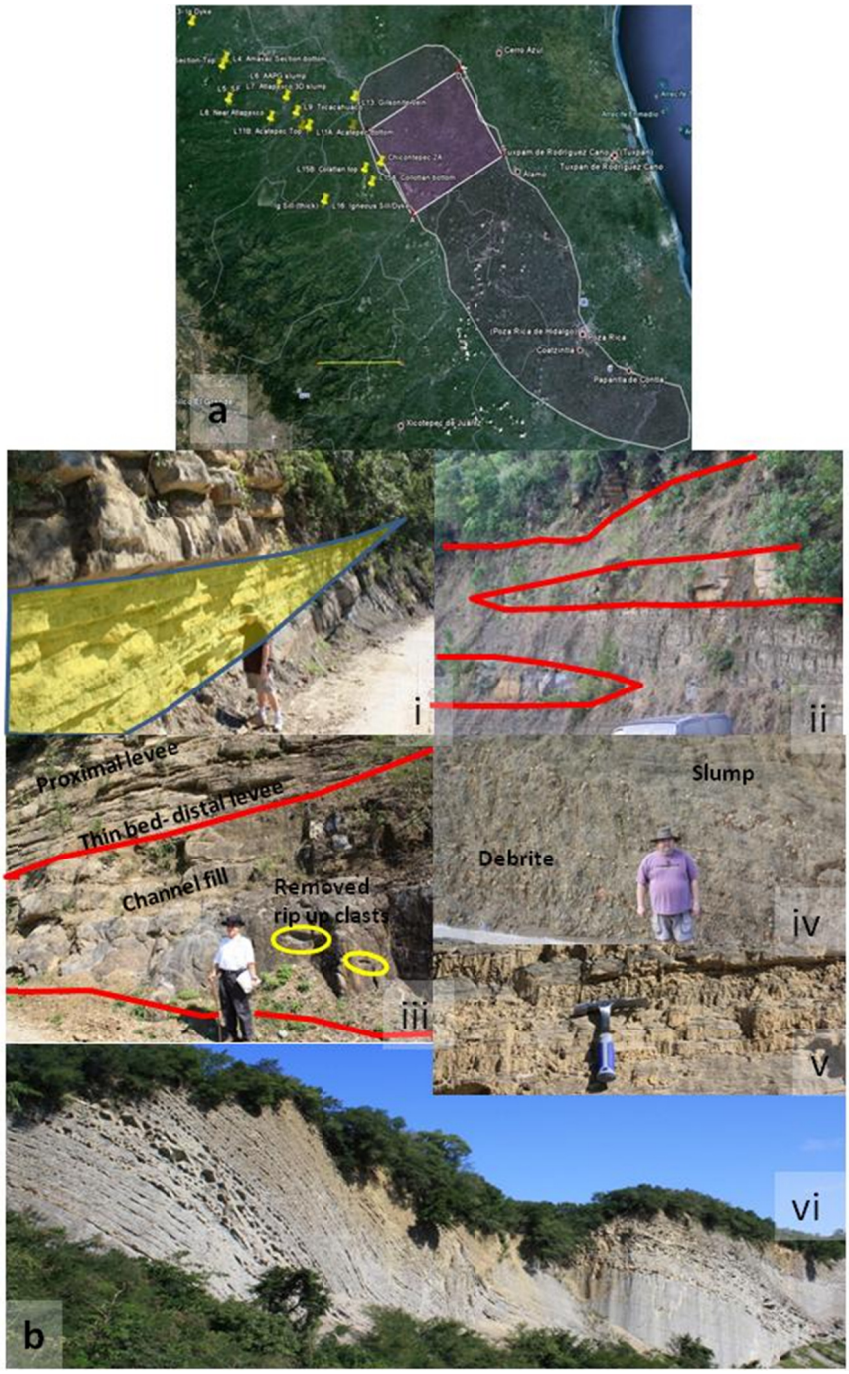

Figure 10: (a) Location of outcrop studies (yellow markers) with respect to the 3D seismic coverage and the Chicontepec production zones. (b) Deepwater architectural elements observed during outcrop studies: (i) Channel fill, (ii) splays, (iii) channel levee complex with plucked out remnants shale rip up clasts, (iv) MTC with slumps and debrites, (v) thin-bed levees and (vi) prograding basin floor fans including amalgamated and layered sheet sandstones.

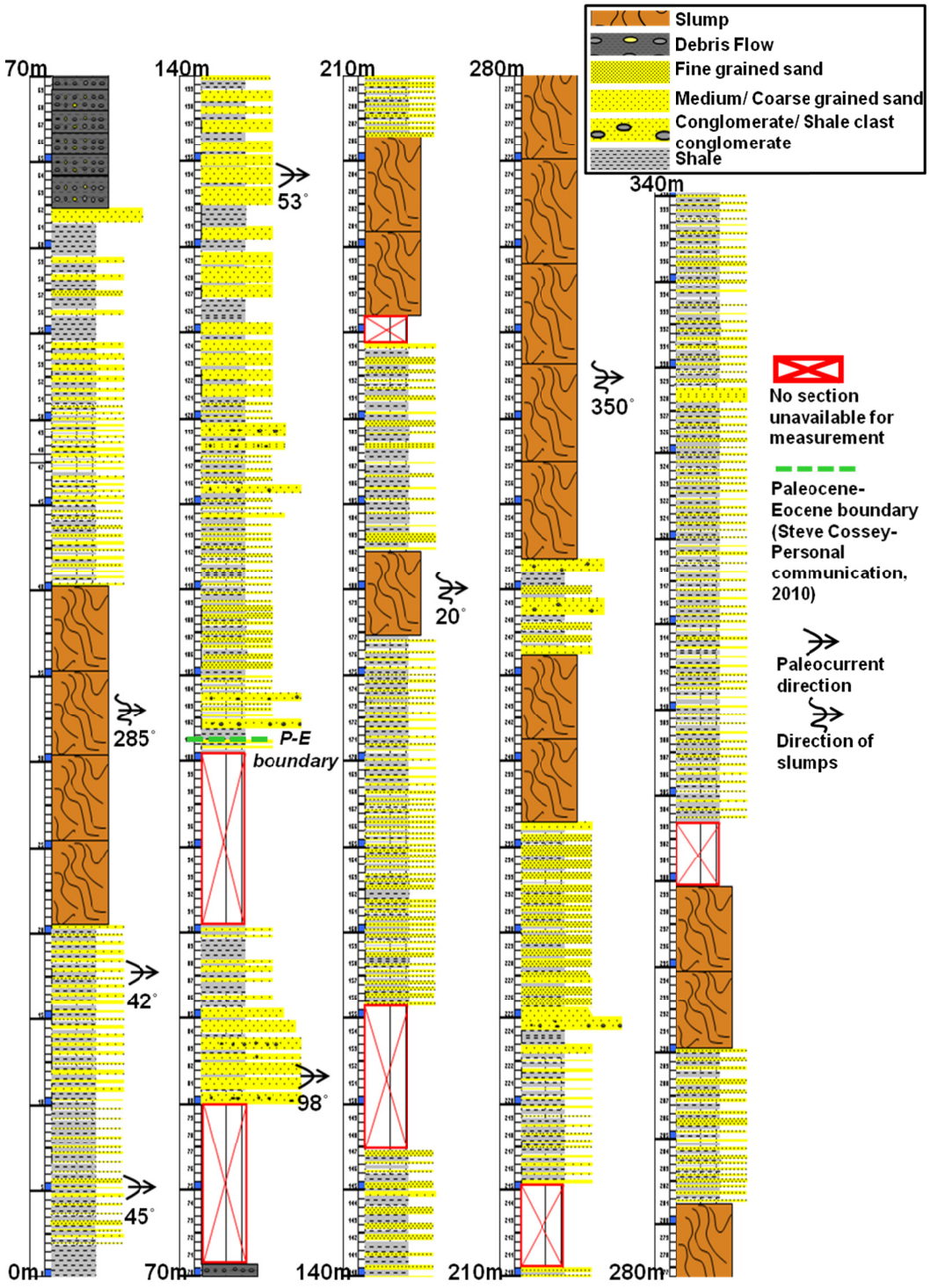

Figure 11: Stratigraphic description of a Chicontepec outcrop section near Colatlan, Mexico, representing sediments from late Upper Paleocene to Early Eocene (Biostratigraphy information: Steve Cossey-Personal communication, 2010).

Depositional flow direction

Unidirectional paleocurrent measurements from flutes and occasional cross bedding of the Chicontepec formation outcrops provide explicit constraints on the direction of deposition during the Paleocene and Eocene. Bitter (1983, 1993) published a large database of paleocurrent directions representative of the Chicontepec outcrops he studied (Figure 12). I augmented Bitter's database with paleocurrent measurements made on the additional outcrops shown in Figures 15a and 17. I also measured direction of slumps from the outcrops.

Paleocurrent measurements in the Paleocene outcrops show a predominant (77%) paleoflow direction from NW-SE (Figure 17b). Only 14% of the paleocurrent measurements were from SW-NE as predicted from Figure 8 and 9% of the paleocurrent data show a completely opposite trend (SE-NW). In contrast, slump directions in some of these outcrops are predominantly from SW-NE (Figure 17b). The major paleocurrent pattern is completely different in the late Upper Paleocene and Early Eocene Colatlan outcrop section (Figure 16) indicating a change in paleoflow direction (SW-NE) from the earlier Paleocene outcrops. This depositional flow pattern is perpendicular to the axis of the Chicontepec basin and SMO, consistent with Figure 8.

Paleocurrent directions provide statistical measures of the sediment dispersal direction and possible provenance during Chicontepec deposition. Since the strike of the Chicontepec basin is from NW-SE (average strike 145°- 325°), any sediment dispersal in the form of channel-fan complexes from SMO would follow a SW-NE direction (perpendicular to SMO), similar to the previous case studies from other foreland basins (e.g., Thornburg et al.,1990; De Ruig and Hubbard, 2006). The predominant paleocurrent

direction parallel to the basin axis (NW-SE) in the lower part of Upper Paleocene indicates a major axial flow and ancillary axial channel-fan complex in the Lower Chicontepec. From this outcrop pattern I can interpret that there was a dominant axial channel-fan complex during Lower Chicontepec. There are two possible provenances for this axial flow: (1) one or more large canyons entered from the northern extent of the basin as evident from Paleocurrent measurements (ESE paleocurrent direction near Tanlajas and Tancanhultz, from Bitter (1993) and also indicated by Cossey and Nieuwenhuise (2011)) (Figure 12); (2) multiple axis perpendicular flow from SMO merged and formed axis parallel channel-fan complexes. The paleocurrent directions towards the SW-NE possibly indicate reflected paleocurrent from preexisting paleo-highs. The W-E paleocurrent direction indicates some paleoflow originated from Golden Lane platform. The change in predominant paleoflow direction to SW-NE in Early Eocene (started below the Paleocene-Eocene boundary) indicate the major sediment dispersal from SMO in Mid- Upper Chicontepec deposition, which also resulted in much higher rate of sedimentation in Eocene (Diaz, 2008) as compared to Paleocene.

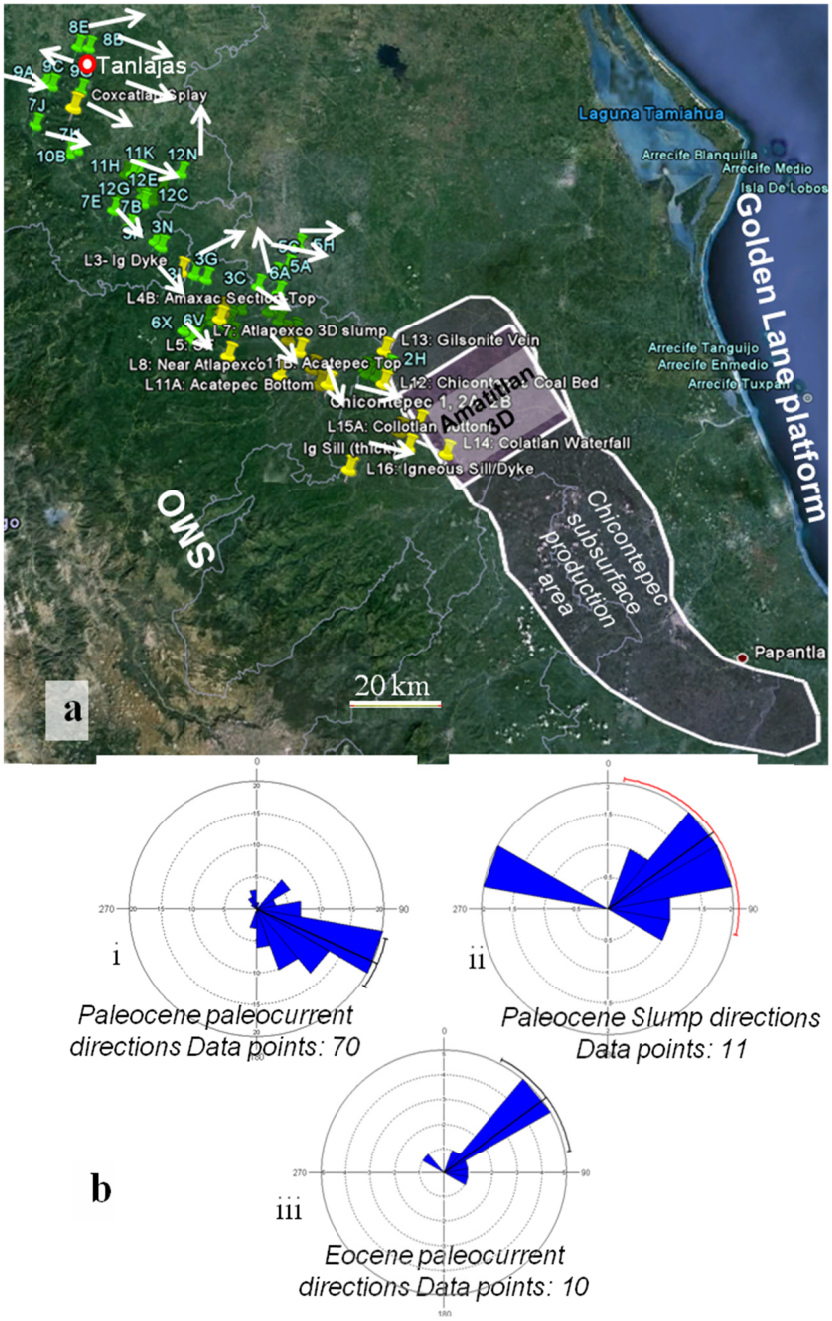

Figure 12: (a) Outcrop locations along the foothills of SMO, where we have information for paleocurrent and slump directions. Yellow points indicate the points of my field location and green points mark the locations obtained from Bitter (1983, 1993). White arrows indicate representative paleocurrent directions from Paleocene outcrops. (b) Rose diagrams representing (i) paleocurrent directions from Paleocene outcrops; (ii) slump directions from Paleocene outcrops and (iii) paleocurrent directions from Eocene outcrops.

Facies subdivisions

After outcrop analysis in the field, I described core sections available from 10 wells whose locations are shown in Figure 8, situated in the eastern part of the study area. Where possible, core sections were tied to the wireline logs to understand the regional changes in depositional pattern. I then identified a suite of lithofacies based on both outcrop and core descriptions. The Chicontepec Formation is subdivided into nine facies based on deepwater architectural elements (Weimer and Slatt, 2007) incorporating Bouma subdivisions: (1) conglomerates/pebbly mudstones, (2) amalgamated channel facies, (3) channel-levee facies, (4) amalgamated sheet facies, (5) layered sheet facies, (6) levee-overbank facies, (7) splay facies, (8) shale facies and (9) mass transport complexes (slumps and debrites). The facies characteristics are summarized in Table1.

STRATIGRAPHIC CORRELATIONS

Well logs were populated with corresponding lithologic descriptions in cored wells as well as in the nearby wells. Core-log depths were matched with the help of core gamma scans. Along with correlating local facies variations, I identified six regionally extensive shale layers within the Chicontepec reservoirs from stratigraphic correlations among 300 wells in the eastern part of the study area (Figure 13) denoted as shale1-shale6. In some of the wells, where the shale layers are absent possibly due to erosion, correlation was continued based on well log patterns. Since the shale layers could be correlated throughout the study area, these layers most likely represent marine flooding surfaces or condensed sections.

Table 1: Summary of different facies in the Chicontepec Formation.

Facies	Lithology	Bed Thickness	Facies Thickness	Bouma Subdivision	Bioturbation	Other Characteristics
Conglomerates/pebbly mudstones	Mud clast dominated. Conglomerates with muddy or sandy matrix; pebbly mudstone: mud supported.	0.4-4.0m.		T_a beds towards the top	Rare	Observed above erosional surface.
Amalgamated Channel facies	Fine to very coarse Sandstone often with shale clasts. Shale layers often seen between sand layers.	0.05-0.8m	0.5-3.8m	T_a, T_b and occasional T_c	Burrows are common.	Sharp/ erosional base. Bed thickness, facies thickness, the nature of amalgamation often changes laterally.
Channel-levee facies	Alternating sandstone and shale beds.	0.02-0.2m	0.6m – 5m	T_b, T_c most common; lesser presence T_a , T_d beds	Common horizontal and vertical burrows.	Common presence of carbonaceous layers, plant remains, ripple laminae.
Amalgamated sheet facies	Moderate- well sorted Fine-medium grained sandstone. Few coarse grained sandstone.	0.08-0.6m	1.5-10.0m	T_b most common. Occasional T_c	Common horizontal and vertical burrows.	Very high sand to shale ratio (4-8); indicates proximal basin floor environment.
Layered sheet facies	Fine-medium grained, moderate- to well-sorted sand and silt along with shale.	0.02-0.5m	1.5–20.0m	T_c is most common; T_b, T_d and T_e also present.	Abundant horizontal, vertical and inclined burrows.	Sand to shale ratio varies from 0.3 to 2.8, indicates mid-distal basin floor fan environments.
Levee-overbank facies	Thin bedded sand or silt.	0.01- 0.25 m	0.8 m-30 m	T_c,T_d, and T_e	Abundant horizontal, vertical and inclined burrows.	Sand to shale ratio (0.1-2.0) decreases from proximal to distal levee deposits.
Splay facies	Fine to coarse grained; moderately to well sorted single or a set of thick sandstone beds.	0.2– 1.6 m	0.7- 1.6 m	T_a,T_b, and T_c	Few burrows.	Individual splay beds pinch out laterally. High Sand to shale ratio (6-9).
Shale facies	Isolated shale bed/beds between other major facies.	0.02- 1.0 m	0.1m-2m	T_d,T_e	Abundant horizontal burrows.	Represent condensed sections and basin plain deposits.
Mass transport complexes	Debrites: Commonly shaly matrix; occasional sandy matrix. Slumps: Deformed form of other facies.		1->100m		Burrows common in debrites.	Disorganized and deformed non reservoir facies

Well tops were transferred to the seismic volume after performing well-seismic ties (Figures 14 and 15), which allowed me to extend the shale layers throughout the study area. Since the seismic data quality is poor in several areas, a combination of well picks and seismic horizons improved the accuracy of the correlations. These regionally extensive shale layers divide the Chicontepec reservoir zone into five stratigraphic units, denoted as unit A- unit E.

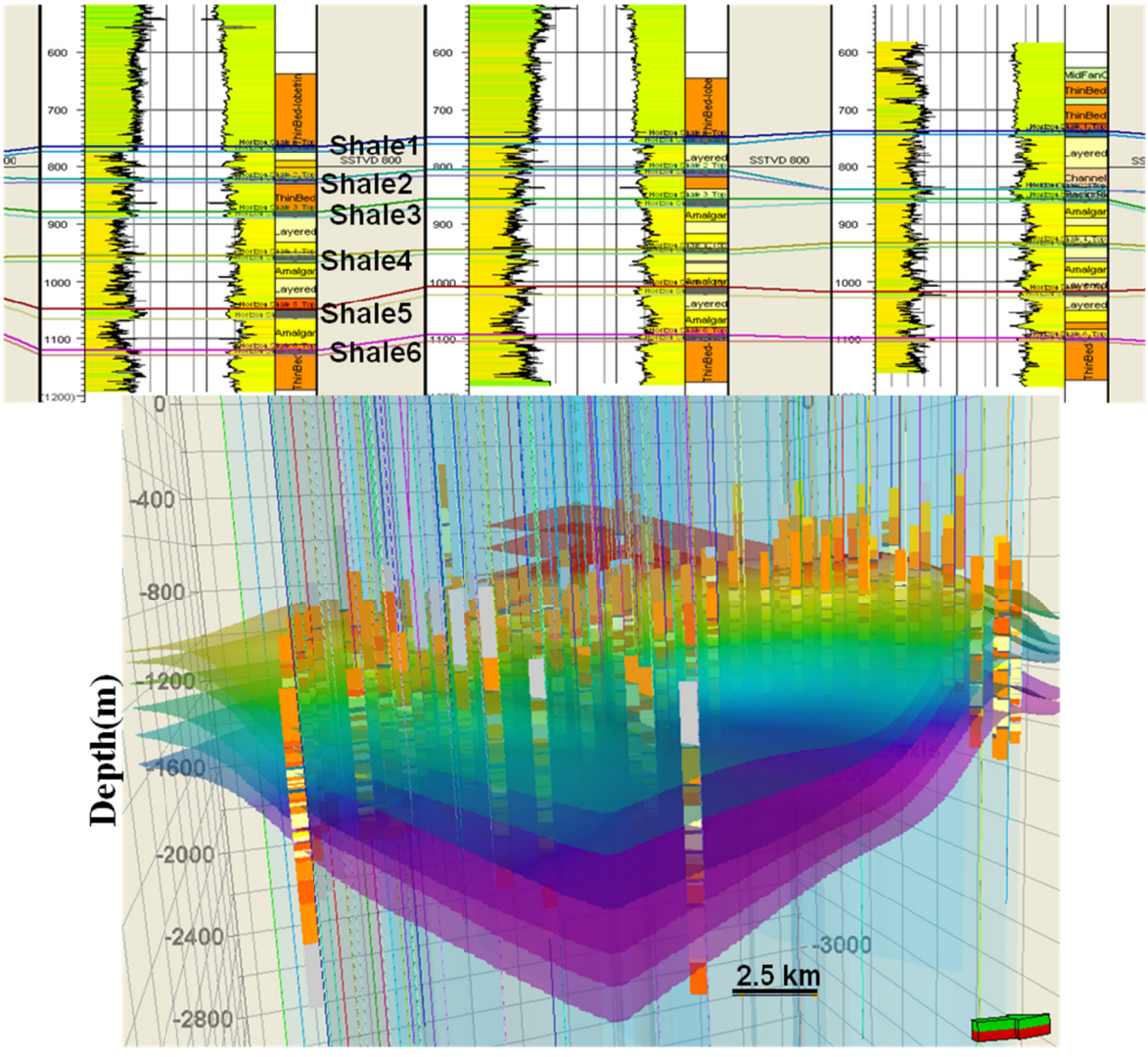

Figure 13: Six regionally extensive shale layers (condensed sections) correlated from well logs.

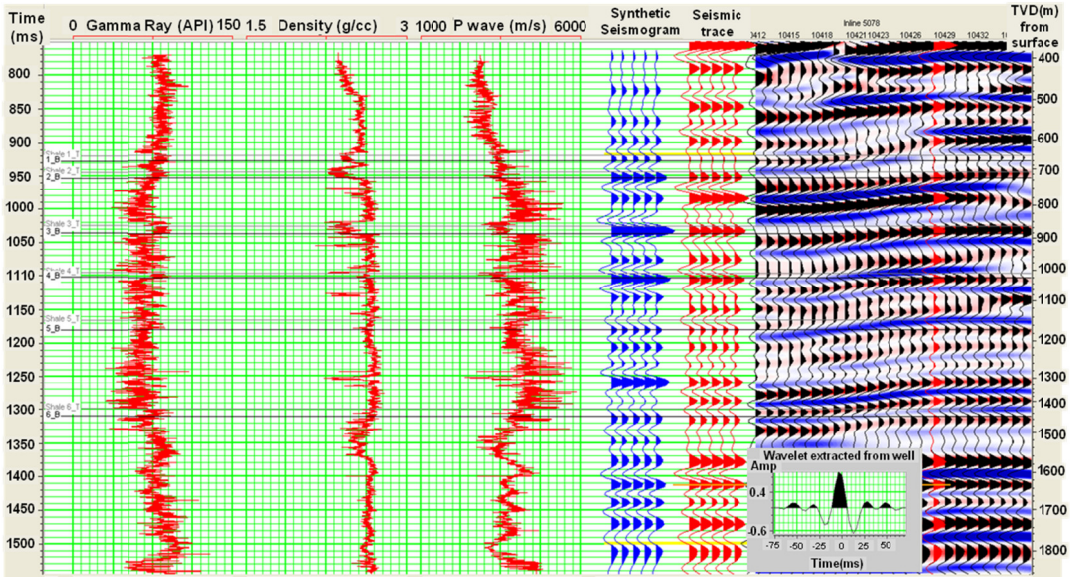

Figure 14: Well- seismic ties in the P1 well show a high correlation (R2=.851). The wavelet(inset) was extracted using the density and sonic logs for this well within the reservoir interval. 35 wells were tied to seismic having original sonic and density logs and unique extracted wavelet. The correlation coefficient for all the tied wells varies between 0.68 and 0.92.

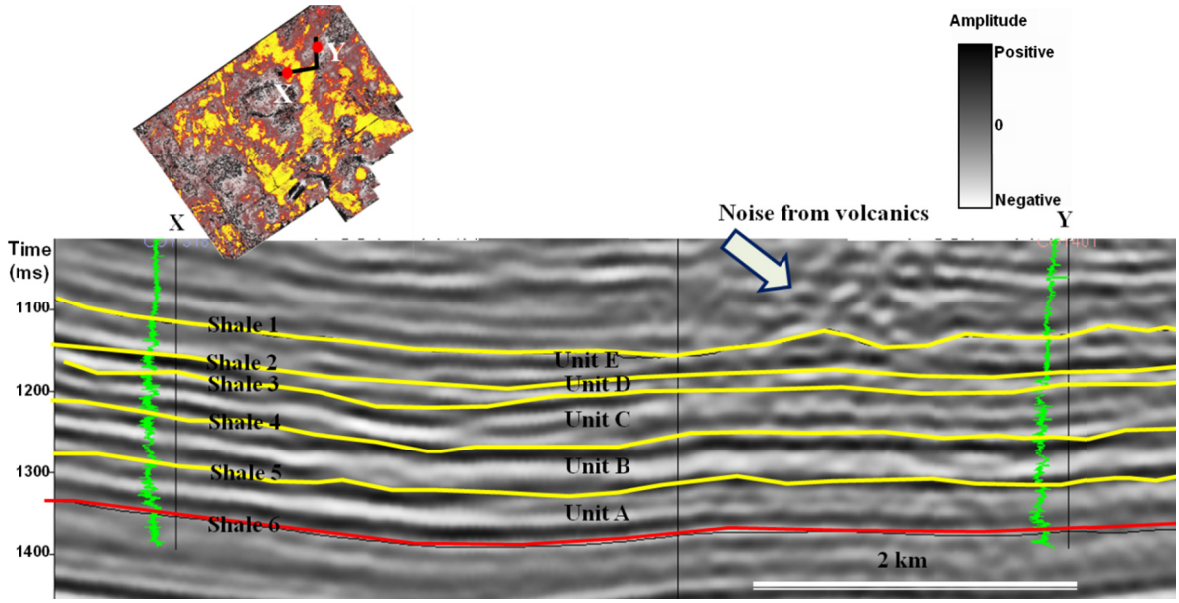

Figure 15: Combining stratigraphic correlations from well logs and seismic interpretation, the shale layers could be extended in the areas where no wells are present. This figure show gamma ray log from two tied wells.

CHRONOSTRATIGRAPHIC CALIBRATION

A biostratigraphic report was available from one well (P1) situated in the middle of the study area (Figure 8). Combining this biostratigraphic information with the detailed stratigraphic correlation facilitated the construction of a chronostratigraphic framework for the zone of study. The information from the biostratigraphic report was compared with the sea level changes and 3rd order cycles as described in Haq et al. (1987) and biostratigraphic chart of the Gulf basin from Paleo Data inc. (2011).

Figure 16 shows the well with biostratigraphic information and one of the stratigraphic correlation profiles. The biostratigraphic report indicates foraminiferal zones (P9, P5, and P4) as well as corresponding 3rd order cycles in Haq et al. (1987). According to the report, foraminiferal zone P12 changes to P9 and older at a depth of 440 m (290 m TVDSS (true vertical depth subsea)). This change is marked with the first appearance of planktonic foraminifera *Acarinina soldadoensis soldadoensis*. The biostratigraphic report indicates that the section starting from 440m (290 m TVDSS) may correspond to the 3rd order sequence boundary TA 3.1 (Early Eocene). Another three 3rd order sequence boundaries TA 2.2, TA 2.1, TA 1.2 corresponding to zones P5, P4 and P1d have been proposed at the depths of 1000m (850 m TVDSS), 1150m (1000m TVDSS) and 1820m (1670m TVDSS), respectively. The TA 2.2 sequence boundary at 1000m (850m TVDSS) is close to the Paleocene-Eocene boundary in the well. The Shale4 surface can be correlated with the Haq et al.'s (1987) condensed section corresponding to sequence TA 2.2. I can also correlate the shale5 surface with the corresponding condensed section of Haq et al.'s (1987) sequence boundary TA 2.1. Since these shale layers are regionally

extensive, these correlations provide a means to tie the zone of interest into a chronostratigraphic and sequence stratigraphic framework. Biostratigraphic studies do not provide any information about changes in sequence or zones within the thick interval between TA3.1 and TA 2.2 which corresponds to Early Eocene time. However, my correlation with the global sea level curve and 3rd order sequence chart by Haq et al. (1987) suggests that shale1; shale2 and shale3 can be correlated with condensed sections from the major 3rd order sequences TA2.9, TA2.6 and TA2.4 respectively (Figure 16). Shale6 might represent a condensed section corresponding to sequence TA 1.3. Calibrating my stratigraphic correlation with biostratigraphy as well as global sea level changes, I can correlate the stratigraphic units (unit A to unit E) between regionally extensive shale layers to the 3rd order sequences of Haq et al. (1987) (Figure 16). Such correlation indicates that Unit A represents the initiation of the Chicontepec turbidite deposition at the beginning of the Upper Paleocene and continues through the major part of Upper Paleocene. Unit B spans late Upper Paleocene to approximate Paleocene-Eocene boundary and primarily represents the Middle Chicontepec Formation. Unit C, D and E are part of the Upper Chicontepec (Early Eocene) Formation.

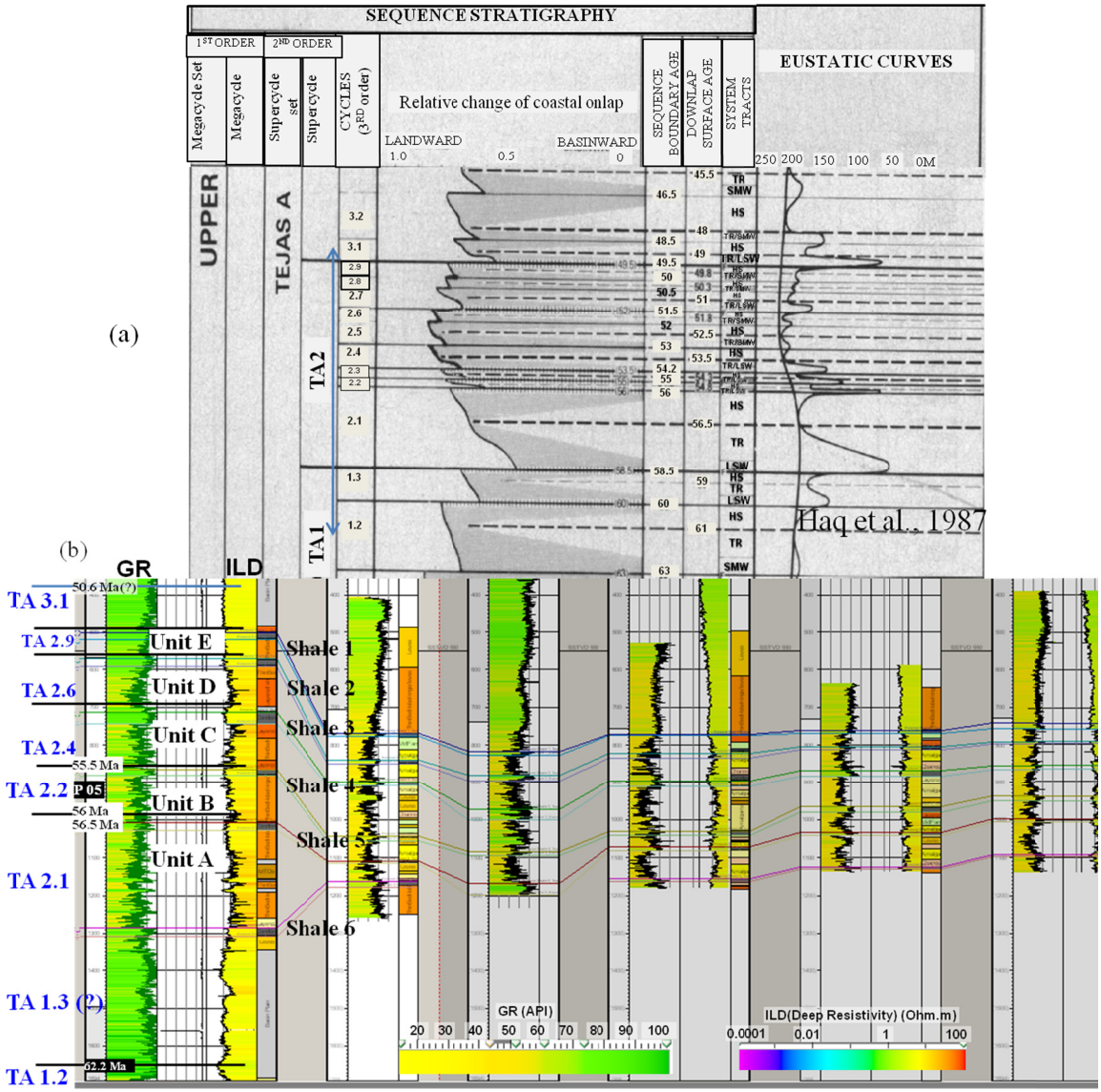

Figure 16: (a) Eustatic curves and global 3rd order sequences from Upper Paleocene- Early Eocene from Haq et al. (1987). (b) Six regionally extensive shale layers and possible condensed sections identified from stratigraphic correlation that divides the Chicontepec reservoir section in six stratigraphic units (unit A-E). Using biostratigraphic records, the stratigraphic units can be correlated with global sequences TA 2.1, TA 2.2, TA 2.4, TA 2.6 and TA 2.9.

DELINEATING DEEPWATER PATTERNS IN THE STRATIGRAPHIC UNITS

Seismic attributes

Seismic attributes are routinely used in the context of seismic geomorphology to map depositional components. Saller et al. (2004) used coherence and rms amplitude to map a deepwater turbidite system. Chopra and Marfurt (2008) found that curvature can map differential compaction within fluvial- deltaic systems. In this same survey (Amatitlan 3D), Mai et al. (2009) used coherence and curvature to map complicated deformation below the Paleocene-Eocene Chicontepec Formation. While Diaz (2008) successfully used coherence in the southern part of the Chicontepec basin to map MTCs and channels, coherence images from the northern Amatitlan survey are ambiguous at best to delineate the depositional features. I applied the coherence attribute to outline the most incoherent areas indicating poor seismic data quality zones. RMS amplitude often helps to delineate thin sands forming complementary images to coherence (e.g. Hadler-Jacobsen et al., 2010) especially when the sands are thin. I use a more robust measure of amplitude that measures the coherent component of the seismic energy within a 3 trace by 3 trace by 20 ms window. Spectral components provide additional delineation, particularly for thin beds (Zeng, 2011).

Such attributes are best interpreted along stratal slices within a seismic geomorphology context (Sarkar et al., 2010). I extend the core description and well log interpretation spatially, guided by the coherent energy attribute along stratal slices. As the

seismic is tied with geologic time, the progressive changes in depositional pattern along the stratal slices unravel the depositional history of the Chicontepec Formation.

Strata below unit A: The base of Unit A represents the base of the Chicontepec Formation. The strata underlying Unit A represents the Lower Paleocene Velazco Formation or equivalent unit. The coherent energy horizon slice 30ms below the base of unit A indicates widespread finer clastic deposition throughout the basin (Figure 17), which conforms to the shale lithology of the Velazco Formation.

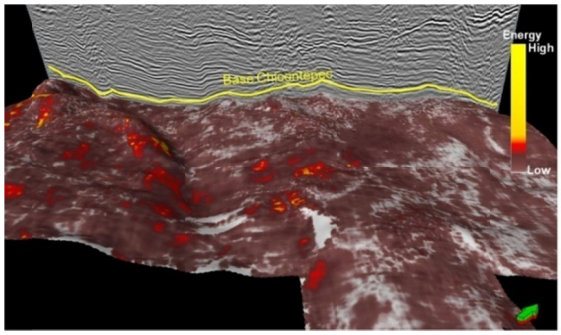

Figure 17: Phantom horizon slice 30 ms below the base of the Chicontepec interval shows a regionally monotonous low amplitude pattern indicating shale deposition. This unit is equivalent to the Lower Paleocene Velazco formation.

Unit A: Unit A represents the basal part of the Chicontepec Formation and it extends within a major part of Upper Paleocene; where shale6 probably represents the condensed section below sequence boundary TA 1.3 (~ 59 Ma; Haq et al., 1987). The most significant observation in unit A is the presence of high energy sediment conduits parallel to the axis of the foredeep in the form of channels or a canyon. In Figure 18, a horizon slice corendering coherent energy and incoherent values of coherent attribute 20 ms above the base of unit A (base of the Chicontepec) demonstrates the presence of two high energy possible major flow conduits trending from NW-SE direction along with other

smaller axial flow units. The zones of incoherent values of coherence attribute represent the poor seismic data areas. The two major flow conduits are interpreted as amalgamated channel complex and canyon fill respectively from vertical seismic section (Figure 19). To confirm the seismic geomorphologic interpretation I looked at the core data available from 3 wells for that particular zone (Figure 18, Table 2). The cored zone of well W1 (Figure 20), which is situated at the edge of one of the major flow conduits indicates alternating fine sand and shale beds comprised of Bouma T_b, T_c, T_d beds with abundant bioturbation. This pattern is reflected in the gamma ray log pattern as well (Figure 20a). These features indicate a proximal levee depositional environment with intermittent channel scours. Two other wells that have core at this zone are situated 2-2.5km away from the main flow zone (Figure 18). Core descriptions from both these wells show alternation of thin sand and clay beds (Bouma T_c, T_d) with abundant bioturbation. Thus, the core description indicates proximal to distal levee deposits. Figure 20 shows a change in well log pattern near the zone of interest moving away from the flow conduit. Gamma ray and resistivity log patterns at the study zone of well W11, can be interpreted as channel sands or part of an amalgamated channel complex. Well W12, situated at the edge of the flow conduit shows sand–shale alternations, indicating channel-levee deposits. In wells W13 and W14, the sediments become more shaly, indicating levee-overbank deposits. Several other well log correlation profiles were analyzed alongside other seismic attributes including spectral decomposition (Figure 21). Along with confirming the axial flow- amalgamated channel complex and channel conduits, some splays and fans were also interpreted. A few slope fans were identified originating from the SMO which are confined within a narrow region in front of the SMO (Figure 22).

Similar study was done along 5 other horizon and stratal slices within Unit A. Although, the predominant axial channel/canyon complex is present in all the slices, there are lateral facies changes and small variations in overall patterns. Unit A culminates with condensed section corresponding to TA 2.1 (Haq et al., 1987) (shale5). Combining these patterns, I illustrate the representative facies distribution model for Unit A (Figure 22). The axial flow pattern of Unit A as evolved from this study conforms to the basin axis-parallel paleocurrent directions from Paleocene outcrops (Figure 12).

Some preexisting paleo-highs and adjacent depressions partly governed the course of these flow conduits (Figure 23). These paleo-highs were generated as the effect of thin skin structures created by the Laramide Orogeny in Late Cretaceous to Paleocene time.

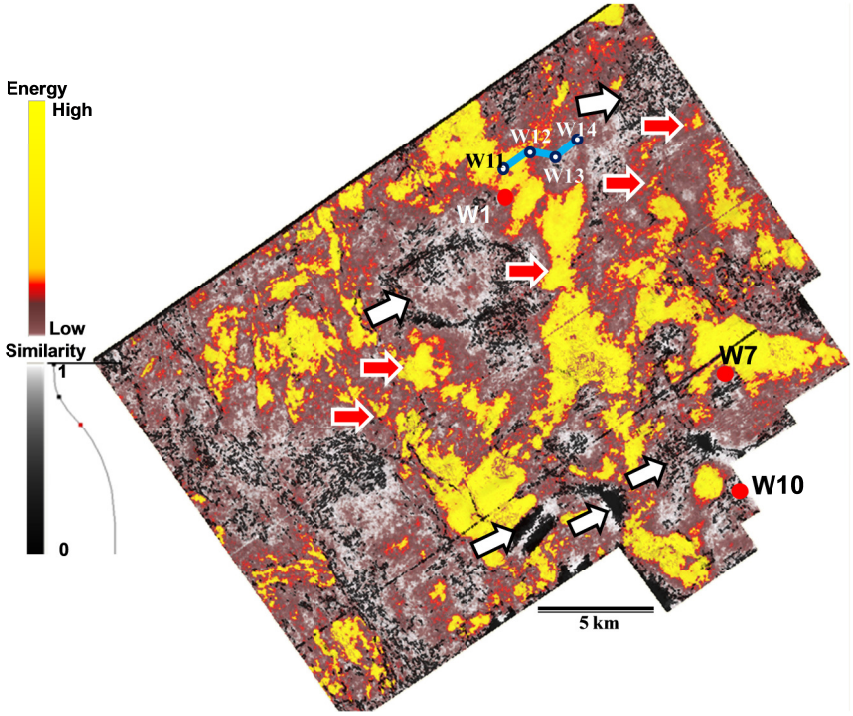

Figure 18: Phantom horizon slice through coherent energy attributes corendered with coherence, 20ms above the base of unit A (base of the Chicontepec). Zones of incoherent values of the coherence attribute primarily indicate poor seismic data areas shown by white arrows. Seismic geomorphologic pattern

indicates flows parallel to the basin axis as shown by red arrows. Red circles represent the well locations where core available for unit A (brief description in Table 2). Blue line represents the stratigraphic correlation profile shown in Figure 25.

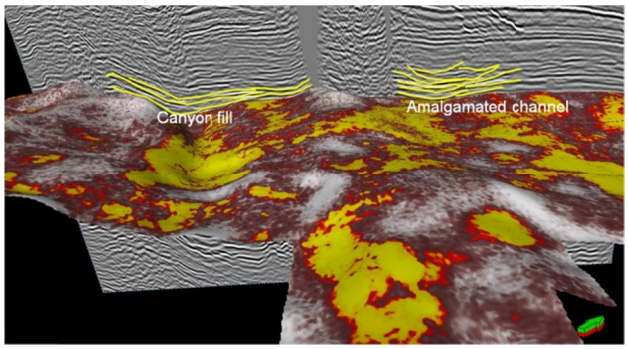

Figure 19: Vertical seismic section indicate the axial flow conduits as canyon fill and amalgamated channel complex.

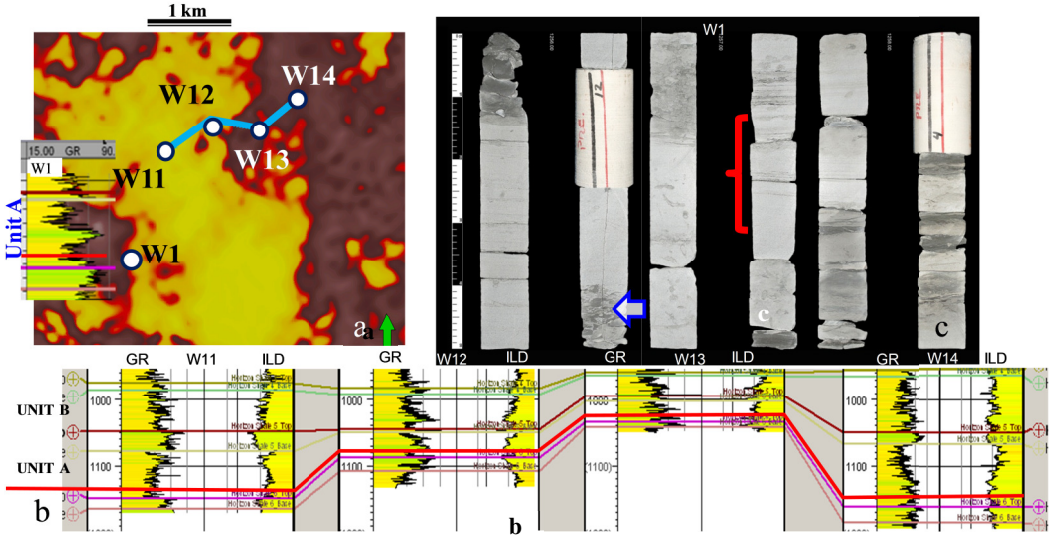

Figure 20: (a) Phantom horizon slice through coherent energy and gamma ray log pattern for well W1 within the stratigraphic unit A. (b) Stratigraphic correlation profile shows the changes in well log pattern as I move away from the main flow conduit or amalgamated channel complex. Red line indicates the relative location of the phantom horizon slice through coherent energy attribute. (C) Core section from well W1 near the zone corresponding to the horizon slice (indicated by a red double bracket). The core section represents a channel- levee depositional environment dominated by Bouma Tb, Tc and Td beds. A scour surface with shale rip up clast is also observed (indicated by a white arrow).

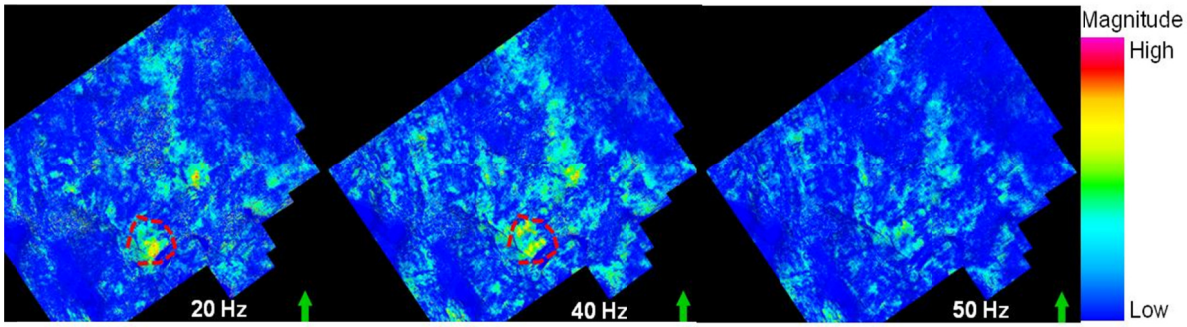

Figure 21: Spectral magnitude at 20 Hz, 40 Hz and 50 Hz emphasize different geomorphologic elements. A fan unit interpreted in red possibly occurs at the base of the SMO.

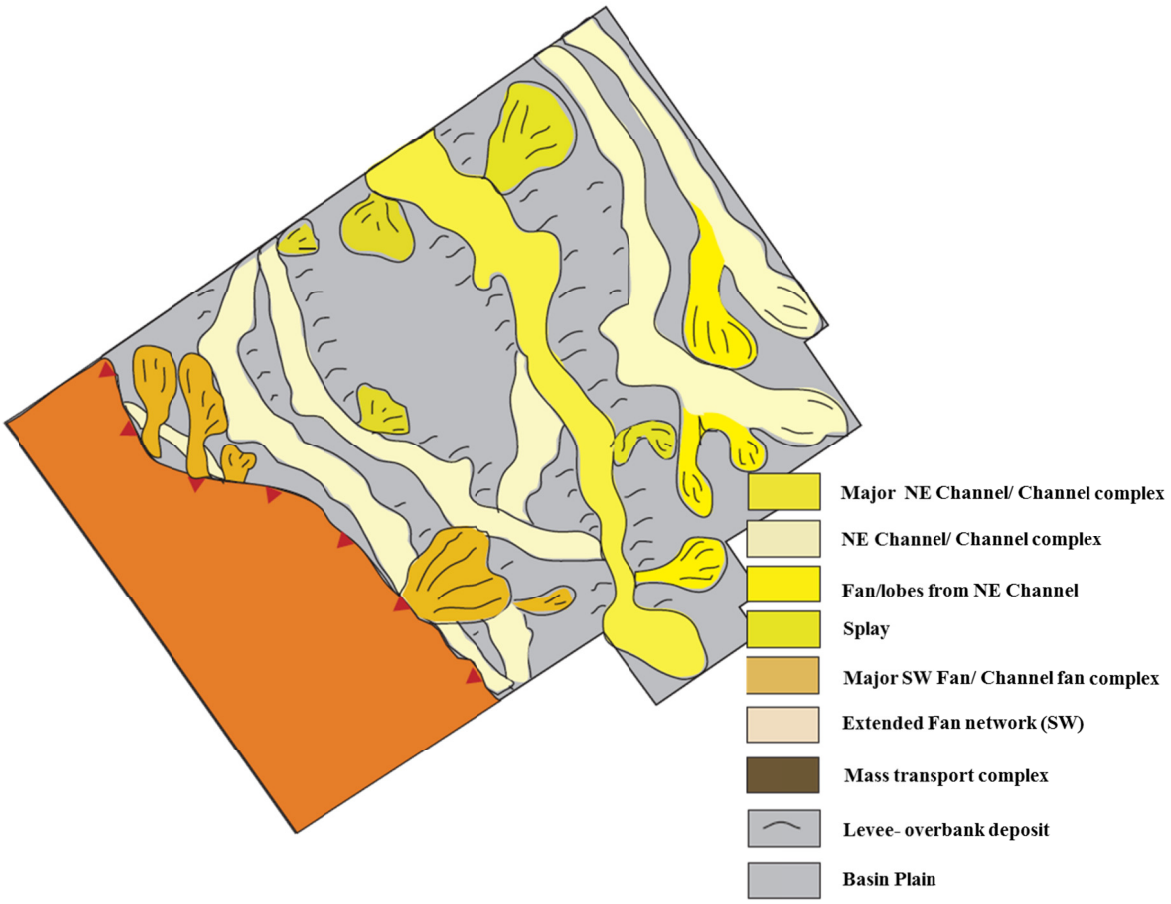

Figure 22: Deepwater facies distribution model for stratigraphic unit A.

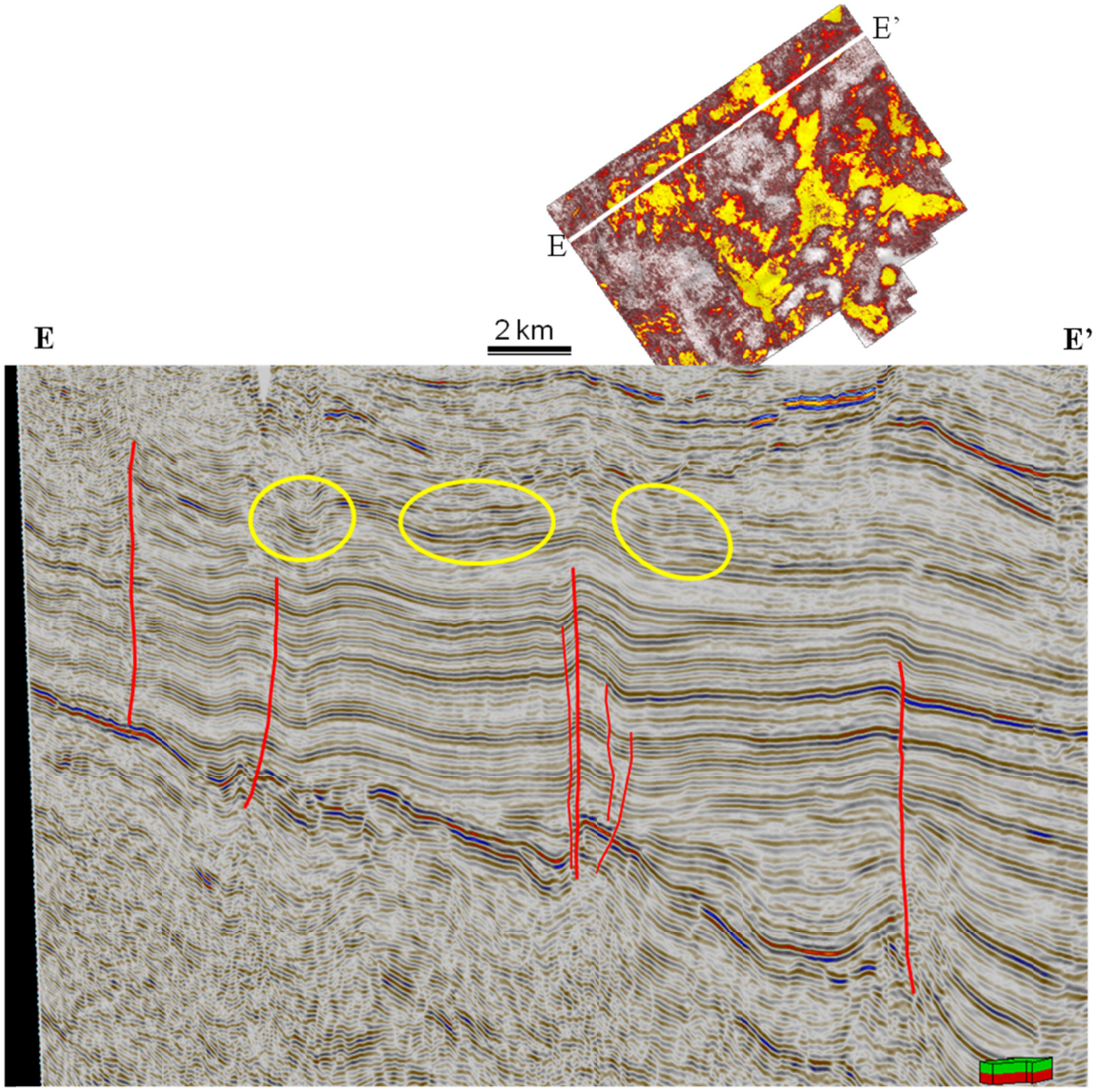

Figure 23: The course of the basin axis parallel flow conduits was partly affected by the presence of pre existing structures and their associated depressions as shown by the yellow ellipses.

	Unit A (Figure 18)	Unit B (Figure 24)	Unit C(Figure 26)	Unit D (Figure 28)	Unit E(Figure 30)
W1	*Proximal levee: Very fine sand and clay. Tb, Tc, Td with abundant bioturbation*	*Proximal to distal levee: Very fine sand and clay. Tc, Td, Te with abundant bioturbation*	*Channel-levee deposit.*		
W2		*Amalgamated sheet sand; Fine to very fine grained. Tb dominates with a few Tc and Td.*	*Layered sheet sand; fine-medium grained. Tb, Tc dominates.*		*Fine grained amalgamated sheet sand; Tb.*
W3		*Amalgamated sheet sand; Fine to medium grained. Tb dominates with a few Tc and Td.*	*Amalgamated and layered sheet sand; Fine grained. Tb, Tc, Td.*	*Medium grained Amalgamated sheet sand; Tb.*	*Medium grained amalgamated sheet sand;Tb.*
W4		*2 Ta beds with channel base conglomerate in alternation with fine to medium grained Tb beds (thin bedded amalgamated sheet) with bioturbation.*		*Distal levee or lobe fringe; Very fine grained sand and clay dominate. Tc with Tb and Td*	
W5		*Thin bedded layered sheet, Tc, Td with Tb. Bioturbated.*		*Thin bedded layered to amalgamated sheet; Tb, Tc.*	*Thin bedded layered sheet; very fine grained Tc, Td.*
W6			*Medium-Coarse grained amalgamated sheet. Three Ta beds within 20 meters.*	*Thin bedded Layered sheet sand (distal fan). Very fine grained Tc, Td.*	*Fine grained layered sheet; Tc with some Tb, Td.*
W7	*Tc, Td, Te. Mud dominated with some fine sand beds, highly bioturbated. Proximal- Distal levee overbank.*	*Amalgamated medium grained sand; Tb in alternation with debrite.*	*Amalgamated Channels. Many erosional surfaces topped by shale clast conglomerate (Ta). Alternation of channel sands and layered and amalgamated sheet sands (medium to coarse grained Tb).*	*Some Ta beds with scoured surface and shale clast conglomerate alternated with thick bed medium grained layered sheet (Tb, Tc). Extensive bioturbation.*	
W8		*Mud dominated Thin bedded Td; very fine grained.*	*Mud dominated Thin bedded Td; very fine grained.*	*Medium-Coarse grained amalgamated sheet sand*	
W9		*Muddy slump and debrite.*	*Fine-Medium grained Layered sheet sand.*	*Fine-Medium grained amalgamated and Layered sheet sand; Tb dominates.*	*Thin bedded silt and clay with a few fine sand streaks. Lobe fringe- basin plain deposits.*
W10	*Alternation of very fine sand and clay. Td, Tc dominated. Distal levee.*	*Muddy Debris Flow.*	*Fine-Medium grained Layered sheet sand.*	*Fine-Med grained amalgamated and layered sheet sand; Tb and Tc.*	

Table 2: Brief core descriptions corresponding to the representative horizon slices of the stratigraphic units shown in Figures 18,24,26,28 and 30.

Unit B: Unit B starts above shale5 (~56.4 Ma) and continues up to the condensed section represented by shale4. Shale4 can be correlated with the condensed section corresponding to sequence TA 2.2 of Haq et al. (1987). Thus, unit B is equivalent to sequence 2.2 and is comprised of sediments of the upper part of Late Paleocene, culminating near the Paleocene-Eocene boundary as seen from the chronostratigraphic calibration. Seismic geomorphologic analysis along horizon and stratal slices within unit B indicates a change in major flow and facies distribution patterns from unit A. Unlike the predominant basin axis-parallel sediment flows from NW-SE direction as observed in Unit A, sediment flows from SMO in SWW- NEE direction becomes major sediment source to the basin. The few flow conduits along with an amalgamated channel complex coming from NW-SE were minor contributor of sediments to the basin. To understand the geobodies seen from seismic attributes, I looked at the core sections available for this particular zone (Figure 24) and then at some stratigraphic correlation profiles in the eastern part of the study area. In Figure 24, I analyze a coherent energy stratal slice corendered with coherence attribute within unit B. Core descriptions available from 9 wells in this zone, are briefly described in Table 2. Two of the wells (W1 and W4) are close to the major flow conduit continuing from Unit A. Well W4 is situated within the channel complex according to seismic geomorphology and the corresponding core section indicates the presence of T_a beds with rip up clasts in alternation with medium grained Tb bioturbated beds. Well W1 is comprised of alternation of very fine sand and clay, dominated by bioturbated T_c, T_d, T_e beds. So I interpret the sediments in W1 to be a proximal to distal levee, whereas sediments in well W4 are part of a channel levee complex alternating intermittently with some layered sheet sediments. Other wells indicate amalgamated

sheet facies, (W2, W3), layered sheet facies (W5, W8), MTC (debrite in W9, W10) and alternation of debrite and amalgamated sheet facies. Stratigraphic correlations also indicate the presence of amalgamated, layered sheet, and channel-levee facies and largely calibrate with the seismic geomorphologic interpretation. Integrating all these studies, I illustrate the representative depositional and facies distribution pattern for unit B in Figure 25. The MTC-debris flow unit in Figure 25 is interpreted from core data.

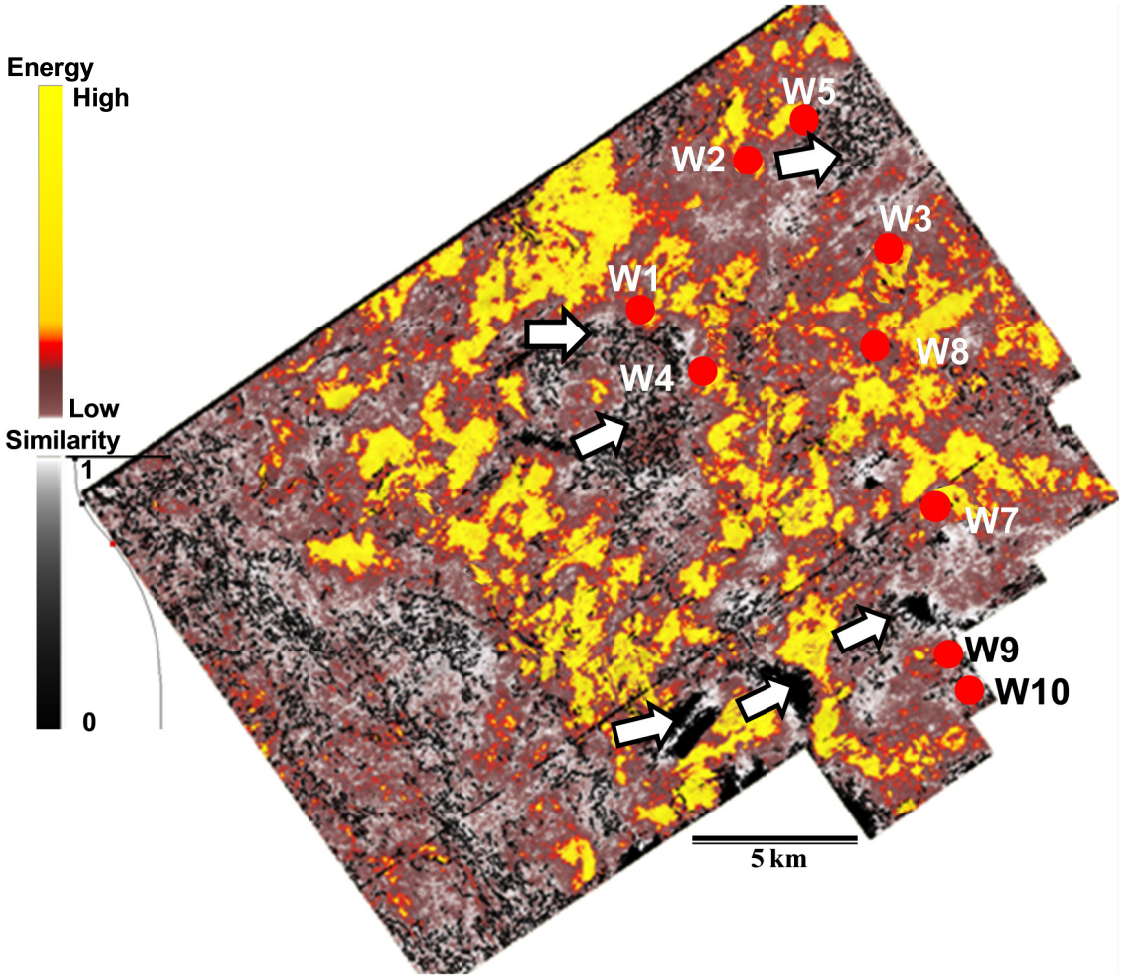

Figure 24: Coherent Energy stratal slice through stratigraphic unit B corendered with incoherent values of coherence attribute. Red circles represent the wells, where core descriptions used corresponding to this stratal slice (Table 2). White arrows indicate poor seismic data zones. Sediment dispersal pattern indicates presence of both basin axis- parallel and - perpendicular component for sediment deposition.

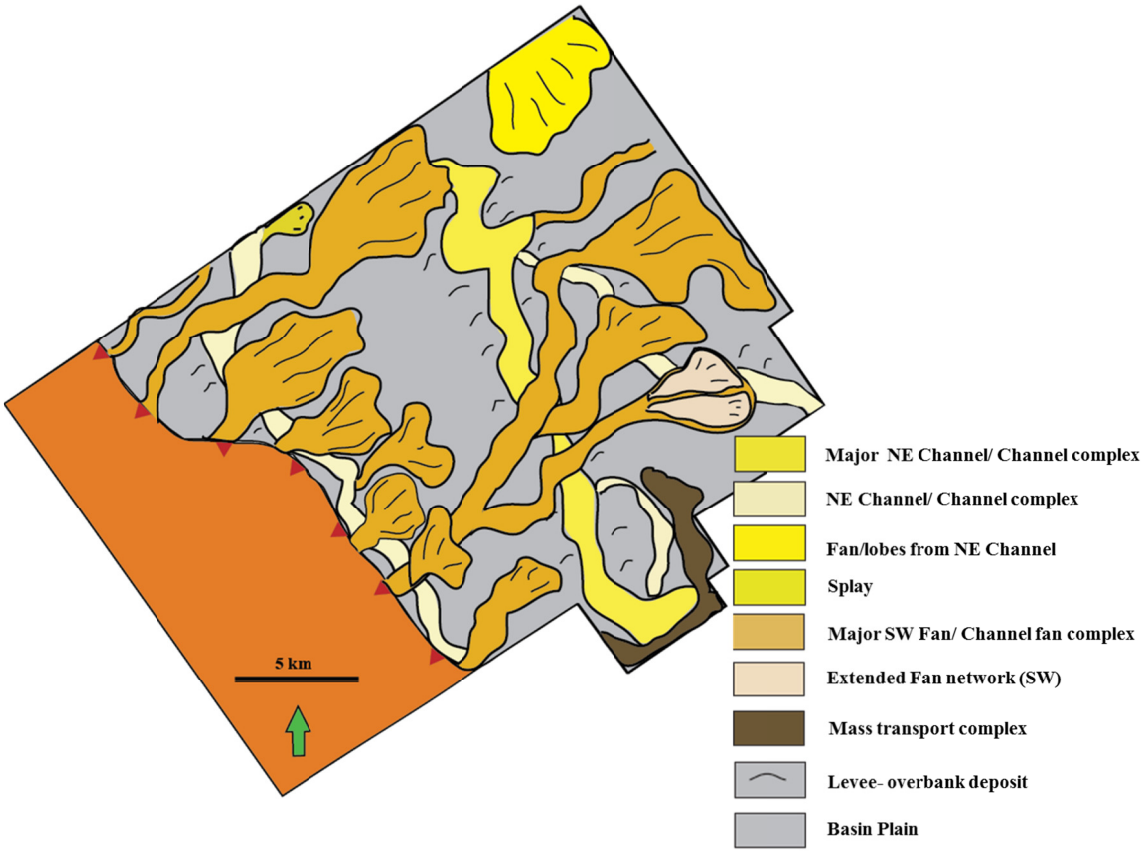

Figure 25: Type facies distribution for unit B based on Figure 24, core descriptions and stratigraphic correlations.

Unit C: Unit C is bounded by shale4 and shale3 which correlate with the TA 2.4 sequence of Haq et al, (1987). Unit C is comprised of sediments from the basal part of the Early Eocene. In Figure 26, I display a horizon slice 25 ms above shale4 top horizon where coherent energy is corendered with coherence attribute. Seismic geomorphological interpretation integrated with the core studies, indicates the presence of a mixed depositional system of basin axis-parallel and -perpendicular flows as in unit B, with basin axis perpendicular flows providing the majority of sediment fill within the basin. One of the core sections from well W7 is representative of sedimentation from this mixed system (Figure 26). In this section I observe multiple scoured surfaces topped by shale

clast conglomerate and massive/ plane laminated sands representing amalgamated channel facies (T_a, T_b) alternating with medium to fine grained, well sorted, amalgamated sandstone beds (T_b) representing amalgamated sheet facies. Figure 32 illustrate the depositional model and facies distribution pattern for Unit C. This Figure also reveals new courses of amalgamated channels in the south-eastern part of the study area.

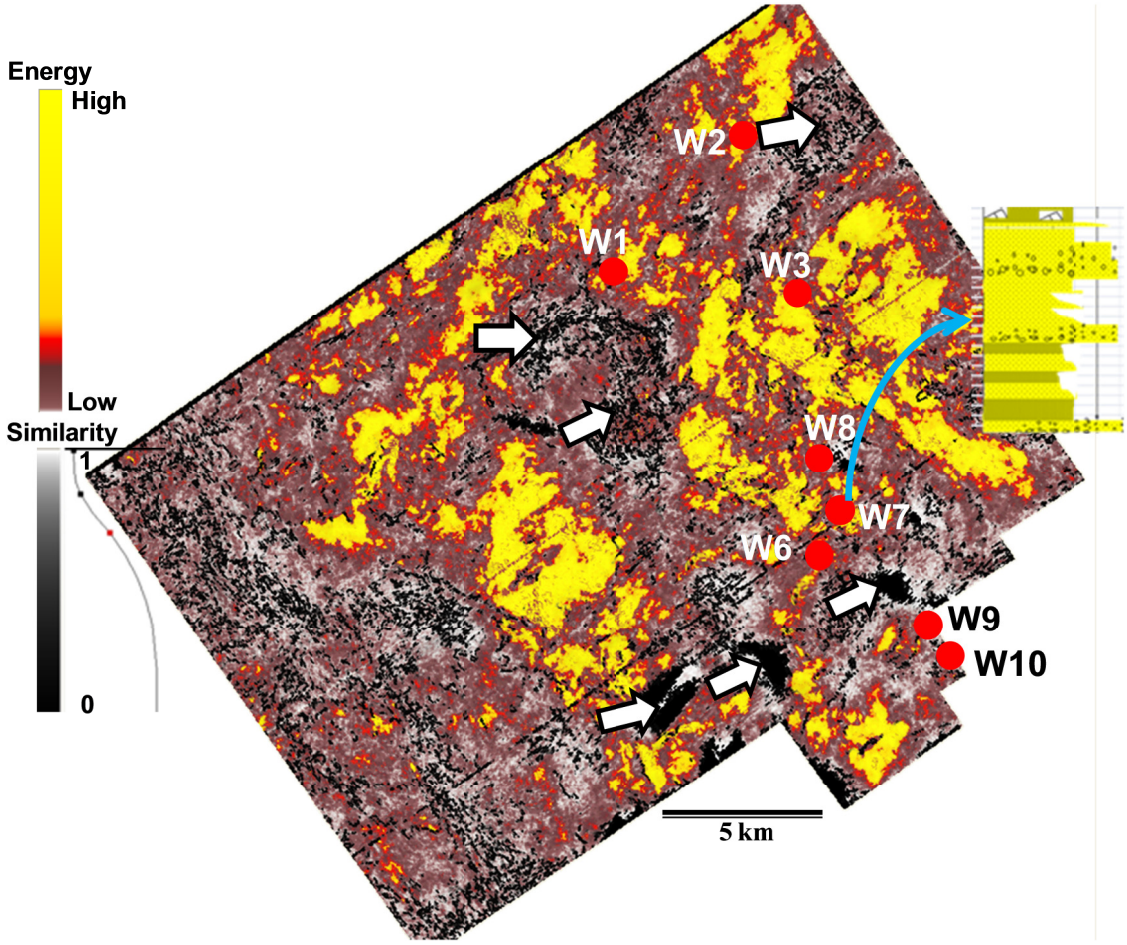

Figure 26: Coherent energy (corendered with coherence) horizon slice 25 ms above shale4 unit within unit C indicates mixed depositional pattern. Red circles indicate core data available corresponding to this stratal slice (brief description in Table 2). Core section from well W7 exhibits an example of alternating amalgamated channel and amalgamated sheet facies. White arrows indicate poor seismic data zones.

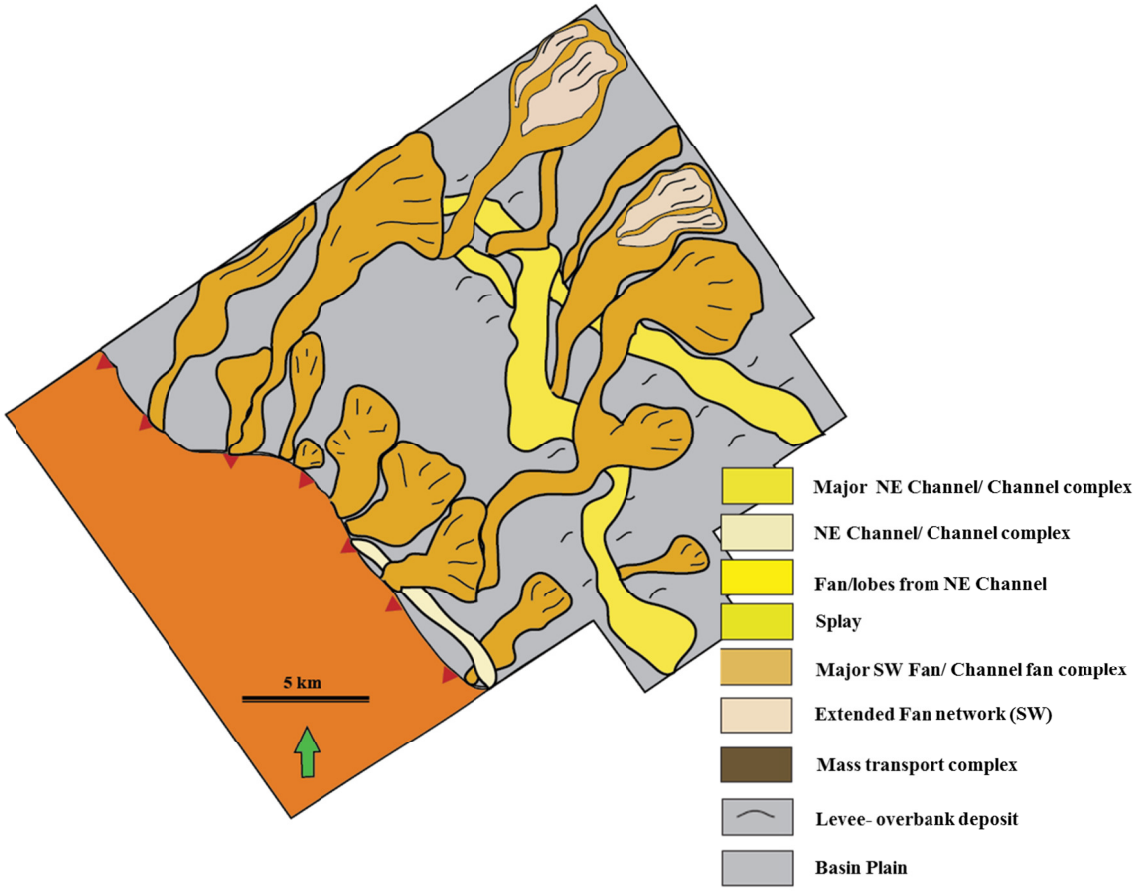

Figure 27: Type facies distribution of unit C.

Unit D and Unit E: Unit D and Unit E are two top stratigraphic units of the Chicontepec reservoir zone, which might be equivalent to TA 2.6 and TA 2.9 of the upper part of Early Eocene strata according to my calibration with and 3rd order sequences and sea level curve from Haq et al. (1987). Figure 28 and Figure 30 exhibit coherent energy stratal slices corendered with incoherent values of coherence attribute from unit D and unit E, respectively, and the core descriptions of the corresponding zones in the wells are enlisted in Table 2. Seismic geomorphologic study using coherent energy and other attributes combined with the core study reveals that a major amalgamated channel complex flowing parallel to the basin axis continues in these two stratigraphic units as

well, but becomes less prominent in unit E. Continuity of this amalgamated channel facies throughout my study zone is confirmed from the vertical seismic interpretation (Figure 19). Major sediment flow and channel- fan complexes approached from the direction of SMO (basin axis-perpendicular flow). My integrated interpretation has provided facies distribution maps as exhibited in Figure 29 and Figure 31, representing stratigraphic units D and E respectively. The overall sand to shale ratio decreases from unit D to unit E which might be correlated with the decreasing net to gross ratio in the corresponding reservoir units. These stratigraphic units equivalent to 3rd order sequences grade into a shaly sequence as evident from well logs (Figure 16) as well as seismic attributes; and it might possibly be a seal for the Chicontepec reservoirs. The stratigraphic unit above unit E is equivalent to sequence 3.1 of Haq et al. (1987).

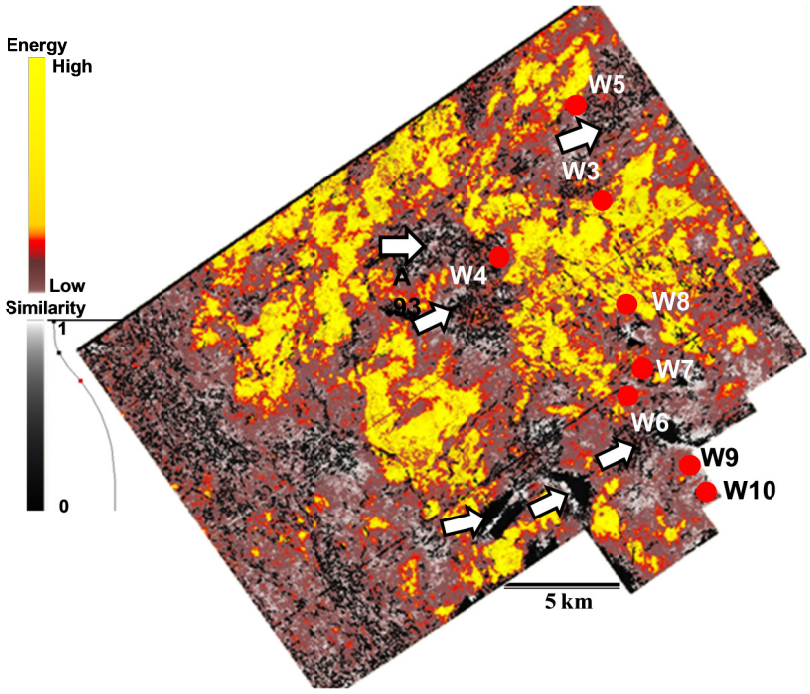

Figure 28: Coherent energy (corendered with coherence) stratal slice from unit D. Red circles indicate core data available corresponding to this stratal slice (brief description in Table 2). White arrows indicate poor seismic data zones.

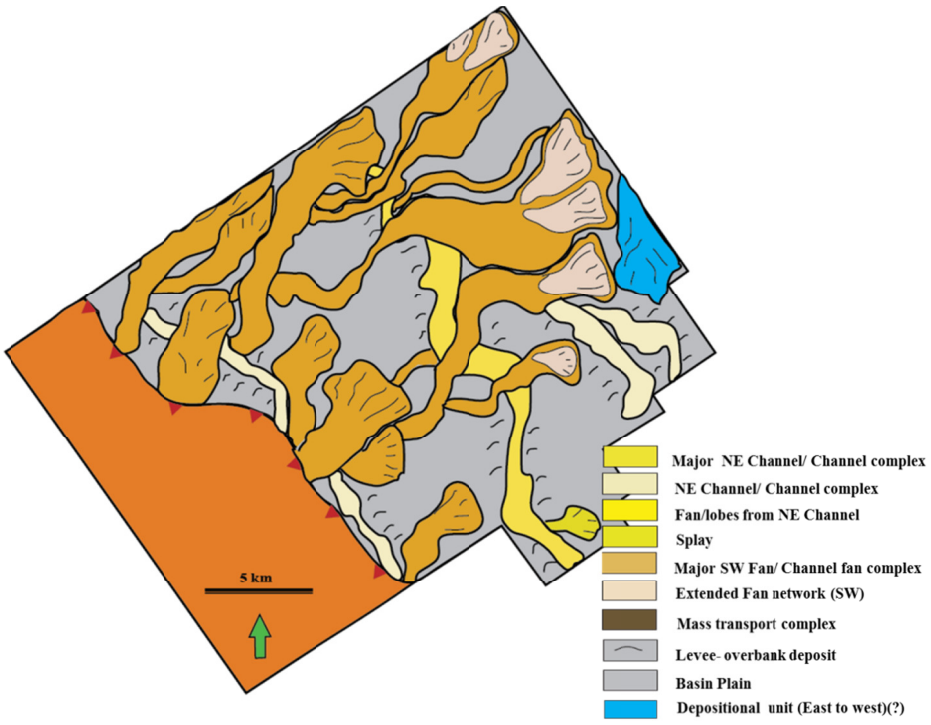

Figure 29: Type facies distribution for unit D.

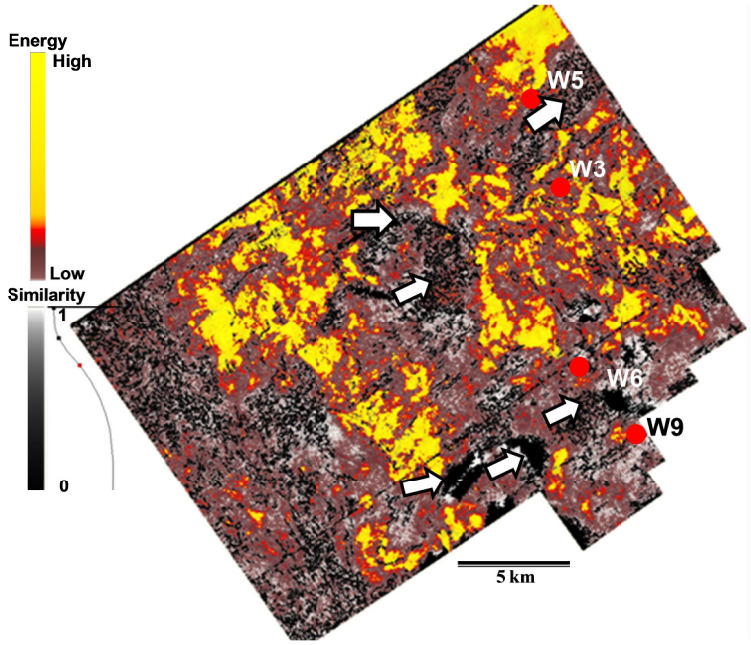

Figure 30: Stratal slice through unit E corendering coherent energy with coherence attribute. Red circles indicate well locations from which core description corresponding to this stratal slice is used. White arrows indicate poor seismic data zones.

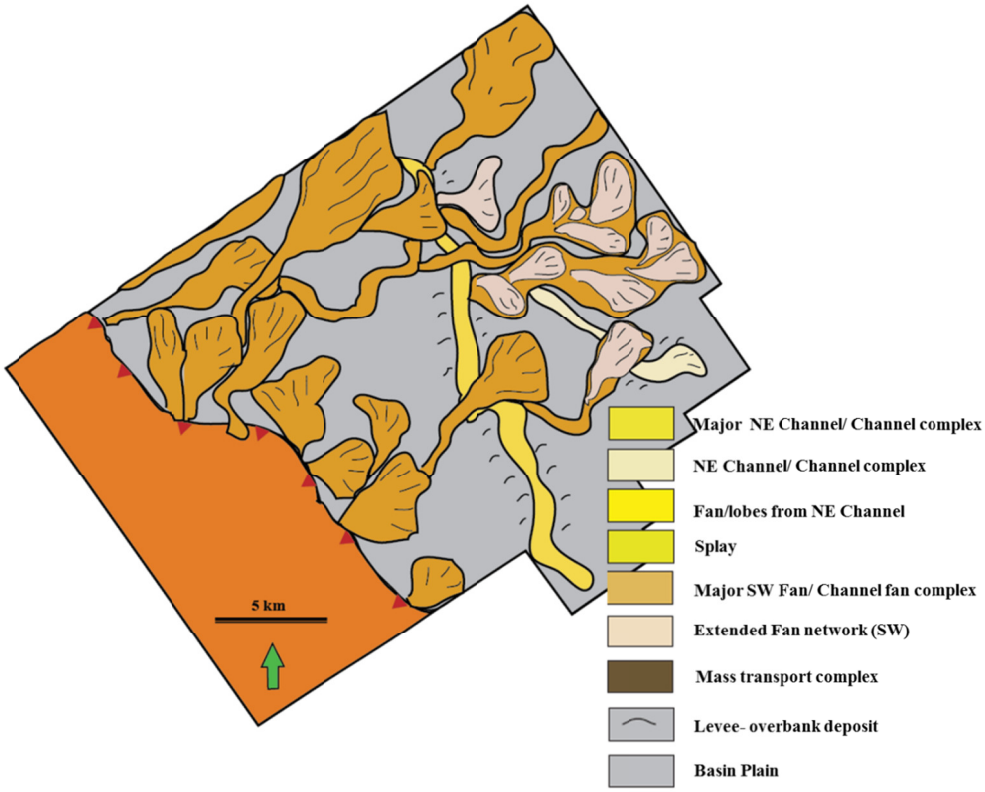

Figure 31: Type facies distribution of stratigraphic unit E.

Additional Information:

I interpreted cross bedding from one of the image logs analyzed from the study area (Figure 32) to obtain additional information about the paleoflow direction. This image log indicates flow from east to west, which is not one of the major flow directions interpreted. However during the outcrop studies there were a few measurements (Figure 12) showing SE-NW paleocurrent patterns. So, I can conclude from these observations that there were some rare but intermittent flows from the direction of Golden Lane platform, which contributed to the reservoir sediments.

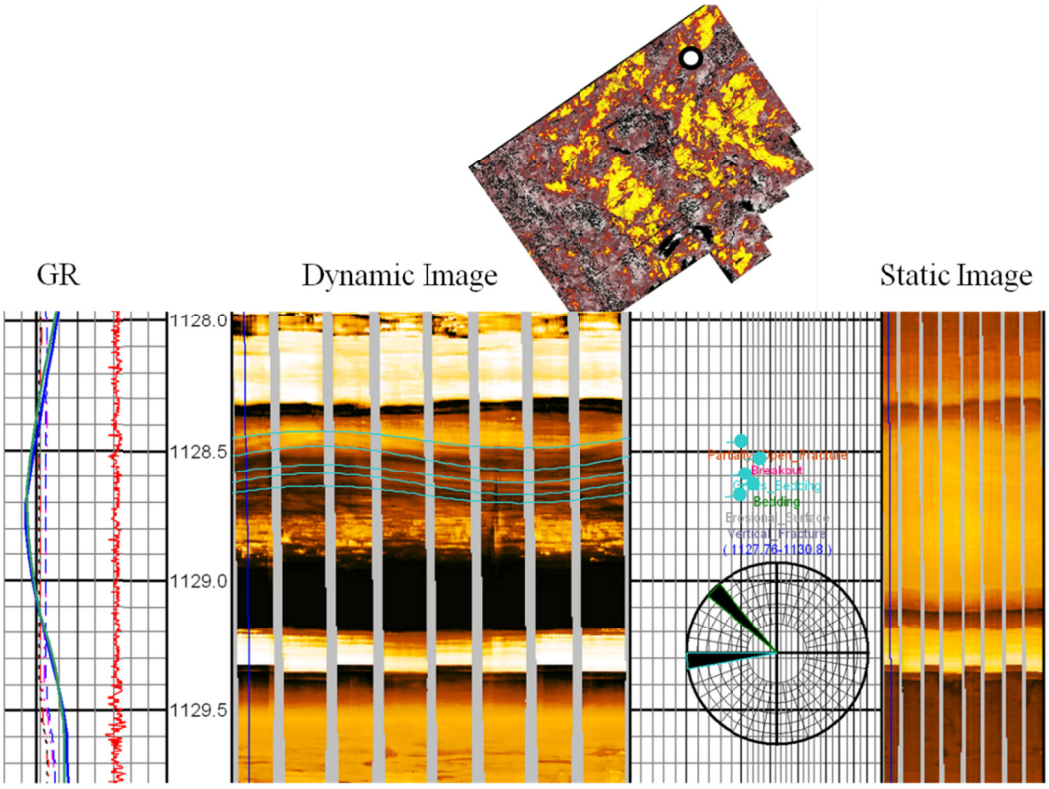

Figure 32: Cross bedding interpreted from image log indicate a flow coming from the direction of Golden Lane platform (E- W).

DEPOSITIONAL HISTORY MODEL

By systematically integrating information from outcrop, core, well log and seismic data, I propose a new deepwater depositional model for the northern part of the Chicontepec play.

The Chicontepec foredeep was developed in front of the Sierra Madre Oriental fold and thrust belt (SMO) during the Late Cretaceous- Early Paleocene Laramide Orogeny (Morán–Zenteno, 1994; Horbury et al., 2003). After this major tectonic activity, deepwater shales of the Lower Paleocene Velazco Formation were deposited within the foredeep (Figure 33). Rate of sediment deposition in the Chicontepec basin was low during this time (Horbury et al., 2003; Diaz, 2008) which conforms to the interpretation

that there were no major tectonic activities until the Late Upper Paleocene. Due to low sedimentation, steep foredeep margin slope existed through major part of the Paleocene period and that caused the majority of the sediments generated from the SMO to be confined within a narrow zone at the base of slope (Figure 22). During these early stages of the Upper Paleocene, some major and associated minor channel/canyon and amalgamated channel complexes were deposited in the foreland basin flowing parallel to its axis, from NW to SE direction. A major canyon outside the system or multiple flows generated from SMO, later converged to form this major axial flow. Paleocurrent measurement of Bitter (1983, 1993), indicate a possible onset or entry point of a major flow in the far north part of the basin near Tanlajas (Figure 12). Several major and minor flows, originating from this axial flow, along with associated splay and basin floor fans dominated deposition of the Lower Chicontepec and lower part of the Middle Chicontepec Formation (Figure 33). These sediments are equivalent to the global 3rd order Upper Paleocene sequence TA 2.1 defined by Haq et al. (1987). The flow path was governed in many cases by preexisting paleo-highs and adjacent depressions generated during the Laramide orogeny (Figure 23). Occasionally the axial flow was obstructed by these local highs and deflected to the opposite direction giving rise to alternating paleocurrent directions measured in Chicontepec outcrops. A few channels or MTCs originated from the Golden Lane platform and contributed in the Chicontepec Formation. The axis-parallel amalgamated channel complexes flowing through the narrow conduit at the base of the steep foredeep slope margin and the eroded sediments from the SMO gradually created a smooth gradient (like a shelf) between the foredeep margin and the middle part of the trough.

According to Horbury et al. (2003) and Diaz (2008), the sedimentation rate in the Eocene was much higher than in the Paleocene due to enhanced tectonic activity which according to the current interpretation began in the late Upper Paleocene time. During deposition of sediments equivalent to sequence TA 2.2 (Haq et al., 1987), basin axis-perpendicular flows coming from SMO and continued to the middle and eastern part of the basin were common. This sequence continues to the basal part of the Early Eocene. This flow pattern was confirmed from the paleocurrent measurements (45° N, 42° N) below the Paleocene- Eocene boundary in the Colatlan section outcrop (Figure 11). Eocene sediment studied from two of the outcrop locations also shows a majority of the paleocurrent measurements in a SW-NE direction. Axial flow pattern continued, giving rise to a mixed depositional system, although the rate of sedimentation in the axis perpendicular flows was higher. This mixed depositional pattern dominated by flows perpendicular to the basin axis continued through Early Eocene time with sedimentary sequences equivalent to TA 2.4, TA 2.6 (Figure 33). Enhanced tectonic activity also produced several MTCs and some large-scale MTCs continued into the eastern part of the basin. Some of the amalgamated channel systems and isolated channels/ canyons, and the system of axial flow continued through the entire interval of depositional system even though flow paths changed over time.

The sedimentation rate gradually decreased above these sequences with fewer channel-fan complexes and MTCs generated from SMO as the Laramide Orogeny reached culmination near the end of early Eocene ((Alzaga-Ruiz et al., 2008) . The axial flow system also weakened considerably towards the top of the reservoir zone. These patterns characterize the top sequence in the reservoir zone (equivalent to TA 2.9 of Haq

et al., 1987) (Figure 16) before it grades into a Early-Mid Eocene shaly sequence (equivalent to sequence TA 3.1 of Haq et al., 1987) .

In summary, I conclude that there were two distinct depositional patterns within the Chicontepec Formation. Most of the Paleocene deposition was controlled by basin axis-parallel amalgamated channel and channel fan systems although the overall sedimentation rate in the basinal part was low. This pattern began to change at the beginning of a late Upper Paleocene tectonic pulse; several basin axis- perpendicular flows from the direction of SMO deposited sediments in the foredeep giving rise to a mixed depositional system. Early Eocene sedimentation was a continuation of this pattern, even though in the lower part of Early Eocene, tectonic activity increased giving rise to higher sedimentation rate from the NW- SE direction.

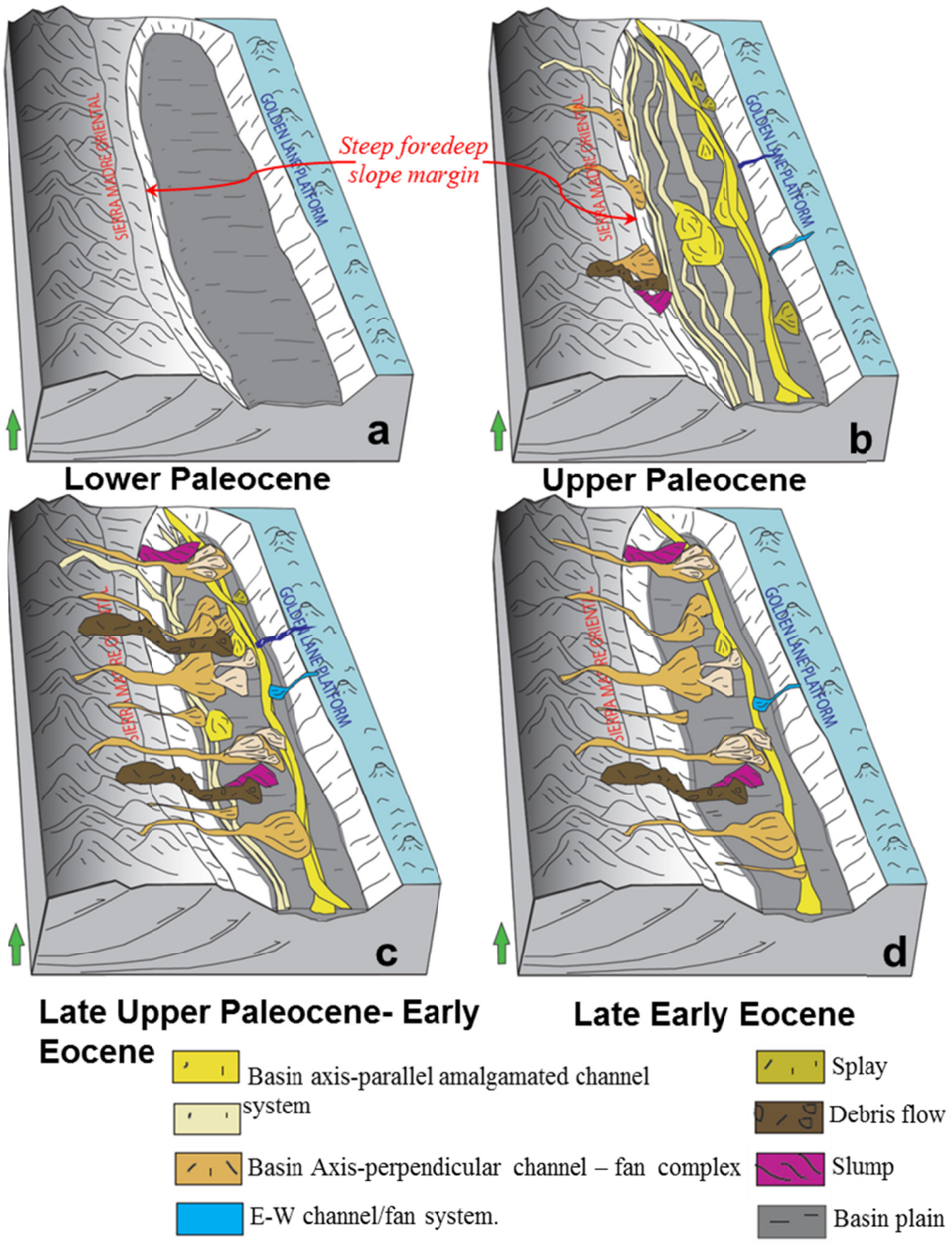

Figure 33: Summary of depositional history of the Paleocene-Eocene Chicontepec turbidites.

ROCK COMPOSITION

To link rock composition with the two different depositional systems, thin sections were prepared from Paleocene and Eocene outcrop samples as well as from core sections from a couple of wells (Figures 34 and 35). The rocks are broadly termed as *litharenite* according to the Folk's (1987) classification. Those can also be called as *calcilithite* as the carbonate rock fragments on average constitutes 85% of the rock fragments along with a few volcanic, sedimentary and metamorphic rock fragments. After point counting around 20 samples, I plotted them in two QFL (Quartz- Feldspar-Lithic fragments) ternary plots for outcrops and wells (Figure 34). The average composition of Paleocene outcrops is $Q_{22}F_7L_{71}$ and Eocene outcrops are $Q_{31}F_{10}L_{59}$. On the other hand, the average composition from stratigraphic unit A in wells is $Q_{24}F_8L_{68}$ and stratigraphic unit C, D, E is $Q_{39}F_{12}L_{49}$ (Figure 34). The cluster of points for the Paleocene and Eocene can be broadly differentiated from one another (Figure 34). Note the distinct decrease in the proportion of carbonate rock fragments and increase in the proportion of quartz.

The Chicontepec Sandstone is mineralogically immature, although the mineralogical maturity progressively increases from lower to upper Chicontepec stratigraphic units. Despite of difference in the sediment transport directions and facies associations, both the major flow patterns carried out sediments originating from erosion of same carbonate dominated Mesozoic formations resulting in abundance of carbonate rock fragments throughout the Chicontepec reservoir. The sediments deposited from the axis-parallel amalgamated channel systems is expected to be mineralogically and texturally immature, whereas the sediments deposited from the basin axis-perpendicular

channel-fan system would show comparatively higher maturity which would increase away from the provenance or SMO. Rock composition of the stratigraphic units confirms the interpretation.

Presence of higher carbonate fragments is directly proportional to the higher cementation within the rocks in Chicontepec formation primarily due to more available cementation source. Higher quartz and lower carbonate, makes a rock more brittle and increase the fracability, which is an important reservoir property for the Chicontepec reservoirs, where 99% of the wells are hydraulically fractured to produce oil. On the other hand overall grain size and angularity decreases and sorting marginally improves from Paleocene to Eocene sections. So, reservoir quality improves from Paleocene to Eocene sections which can be correlated with better permeability and production in the Eocene reservoirs.

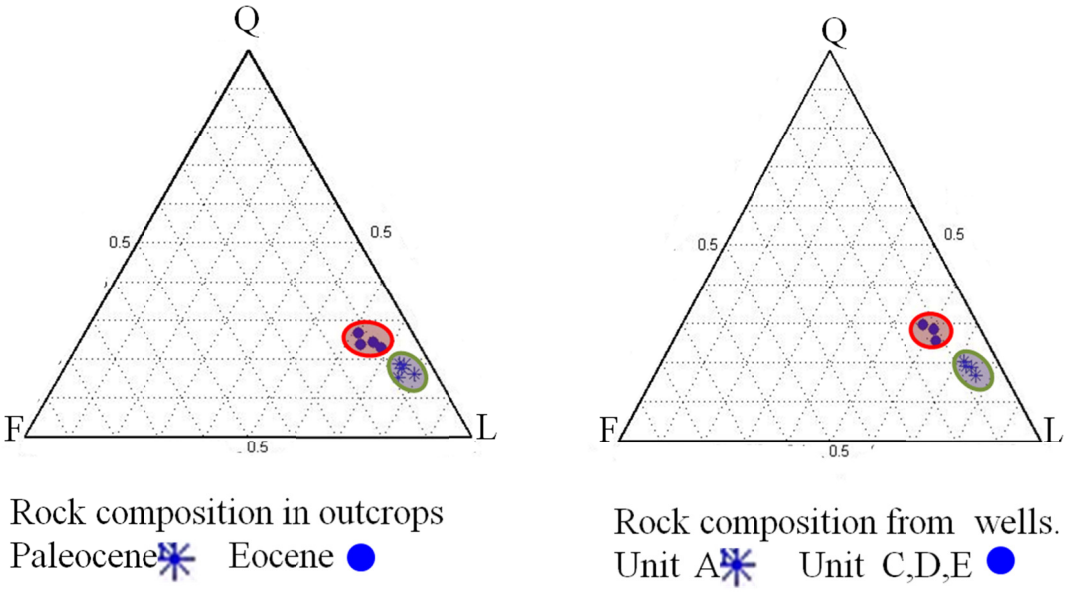

Figure 34: Rock composition determined from petrographic study and plotted against QFL ternery diagram, illustrates relative change in mineralogical composition in Paleocene and Eocene outcrops and core sections

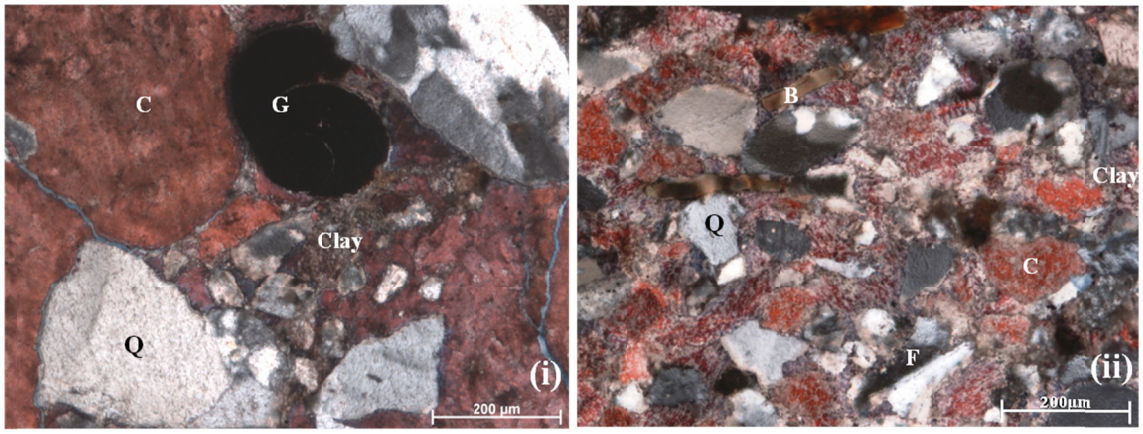

Figure 35: Photomicrograph from (i) stratigraphic unit A (Late Paleocene) and (ii) unit C (Early Eocene) from the same well. The sections are stained with alizarin red-S. Note the decrease in grain size, increase in quartz and improvement in sorting from (i) to (ii). Q= quartz; F= Feldsper; B= Biotite; C= Carbonate rock fragments; G= Gastropode fossil fragment within a carbonate rock fragment.

CALIBRATION WITH FACTS AND EVENTS OUTSIDE THE STUDY AREA

Within my study area in the northern part of the Chicontepec basin, sedimentary units in the Eocene are thicker than the Paleocene sections. It can be inferred from Diaz (2008) that sedimentary thickness of Paleocene units gets progressively thinner and Eocene strata become much thicker from the north to the southern part of the basin. The upper part of the Paleocene unit is absent or very thin in southern parts of the basin which can be attributed to the combined effect of erosion and nondeposition. So the basal sequence of the Chicontepec, equivalent to TA 2.1 (Haq et al., 1987) has negligible presence towards the southern part of basin. The energy of the axial flow complex might have reduced towards the south and at places was eroded by multiple axis perpendicular erosive flows during the Eocene.

As mentioned in my depositional history model, a major tectonic event began near the Paleocene-Eocene boundary. Along with increasing the sediment accommodation zone and sedimentation rate, this event dramatically changed the depositional pattern of the basin. After analyzing the sedimentation rate and sediment accumulation plot from multiple wells extending from north to south of the basin, Diaz (2008) proposed that this tectonic event occurred first in the northern wells compared to the wells to the south, indicating a progressive advance of the deformation front from north to south. This assumption conforms to the fact that wells in the southern part of the Chicontepec basin have younger reservoir units compared to the northern wells and some of those younger units are correlatable with non reservoir shaly units above the reservoir zone in the northern part. As for example, sequence equivalent to TA 3.1 (fig 19), which is s non reservoir in the northern part, represents a reservoir unit in some wells in the south.

The Chicontepec subsurface production area becomes progressively narrower from north to south (Basin width ~ 34Km in the northern end to ~17 km in the southern end) (Figure 1 and 12). Similar to the northern part, the most productive oil fields in the southern part are also located in the eastern side of the basin. But the reservoir units are thicker in the Eocene section in the southern part due to the proximity to the provenance. Seismic and core studies indicate that the mass transport complex facies is much more abundant in the reservoir units of the southern region as compared to the northern region; this may be attributed to the proximity of the reservoir units to the SMO.

Bitter (1993) showed that the average mineralogical composition of the Chicontepec outcrop rocks in the southern part of basin is $Q_{54}F_5$ L_{41}, which is

significantly different from Paleocene and Eocene outcrop rocks in the northern part of the basin ($Q_{22}F_7L_{71}$ and $Q_{31}F_{10}L_{59}$, respectively). This is also indicative of a significant difference in composition in the subsurface rocks as well. There remains a minor contribution of the axial flow system in the sedimentary units in the south, whereas in the north, the axis parallel and axis perpendicular systems gave rise to a mixed depositional system from late Upper Paleocene to Early Eocene.

After calibrating these events from the literature, I can infer that the stratigraphic units equivalent to the global 3rd order sequences identified in the northern part of the basin, are also present in the rest of the basin but there are dramatic character changes within the units due to significant differences in relative distance of the reservoir zones from two major provenance areas as well as the influence of tectonic events. Unit A becomes progressively thinner towards the south, and in some places, was completely eroded by the Eocene events. The composition, character and thickness of the other stratigraphic units (Units B-E) are also different in the southern part of the basin as compared to their northern counterparts. Moreover, there is a couple of additional younger Late Early Eocene to Early Middle Eocene reservoir units in the southern part of the basin. Finer clastic deposition dominated in equivalent sequences in the northern productive areas.

SUMMARY AND CONCLUSIONS

In summary, I propose a new model for the depositional history of the Chicontepec Formation in the northern part of the Chicontepec foredeep. The Chicontepec reservoir zone can be divided regionally into five stratigraphic units with six

regionally extensive shale layers or condensed sections, which are correlated with global 3rd order sequences (Haq et al., 1987) from Mid Paleocene to Early Eocene. These units can be calibrated to other parts of the basin but with significant changes in character. These units or sequences show progressive changes in deepwater patterns from Lower to Upper Chicontepec. A major axial channel system controlled the deepwater deposition during the Upper Paleocene Lower to Middle Chicontepec. The depositions in the basal Chicontepec sequence created a smooth gradient from the Sierra Madre Oriental fold thrust belt (SMO) to the middle part of the basin. A significant change in depositional pattern of the basin began in late Upper Paleocene period mainly due to the effect of a major tectonic pulse and a dramatic increase in basin axis-perpendicular flow from the SMO. A minor axial system remained active resulting in complex interaction with an axis-perpendicular system from the upper part of Late Paleocene to early Eocene strata. Contribution of sediment flows from east to west was minimal to the overall sedimentary column. These turbidite sequence assemblages grades into a predominantly shaly non reservoir sequence near Early-Mid Eocene boundary. Reservoir quality improves from stratigraphic units in Paleocene to stratigraphic units in Eocene specifically in the eastern part of the basin with more sediment from the SMO deposited with improved sorting and with higher mineralogical maturity.

REFERRENCES

Abbaszadeh, M., T. Shimamoto, F. M. Sandria, D. H. Zamora Guerrero and F. Rodriguez de la Garza, 2003, Integrated Geostatistical Reservoir Characterization of Turbidite Sandstone Deposits in Chicontepec Basin, Gulf of Mexico: Proceedings of the Society of Petroleum Engineers Annual Technical Conference and Exhibition, October 5-8, Denver, Colorado, U.S.A.,15p, SPE paper 84052.

Alzaga-Ruiz, H., M. Lopez, F. Roure, and M. Seranne, 2009, Interactions between the Laramide Foreland and the passive margin of the Gulf of Mexico: Tectonics and sedimentation in the Golden Lane area,Veracruz State, Mexico: Marine and Petroleum Geology, v. 26, p. 951-973.

Barker, G., and W.A. Berggren, 1977, Paleocene and Early Eocene of the Rio Grande and Tampico embayments: foraminiferal biostratigraphy and paleoecology: Marine micropaleontology, V. 2, p. 67-103.

Bermúdez, J. C., J. Araujo–Mendieta, M. Cruz–Hernández, H. Salazar–Soto, S. Brizuela–Mundo, S. Ferral–Ortega, and O. Salas–Ramírez, 2006, Diagenetic history of the turbiditic litharenites of the Chicontepec Formation, northern Veracruz: Controls on the secondary porosity for hydrocarbon emplacement: Gulf Coast Association of Geological Societies Transactions, v. 56, p. 65–72.

Bitter, M.R., 1993, The sedimentation and provenance of Chicontepec sandstones with implications for uplift of the Sierra Madre Oriental and Teziutlán Massif, East-Central Mexico, Proceedings 13th Annual SEPM Gulf Coast Section Reservoir Conference, Houston, p. 155-172.

Bitter, M. R., 1983, Sedimentation and petrology of the Chicontepec Formation, Tampico-Misantla Basin, Eastern Mexico: M.Sc. thesis, University of Kansas, Lawrence, 117 p.

Busch, D.A., 1992, Chicontepec Field–Mexico, Tampico–Misantla Basin, in Foster, N.H., and Beaumont, A.A., eds., Stratigraphic Traps III: AAPG Treatise of Petroleum Geology, Atlas of Oil and Gas Fields, p. 113–128.

Busch, D.A., and S.A. Govela, 1978, Stratigraphy and structure of Chicontepec turbidites, southeastern Tampico–Misantla Basin: AAPG Bulletin, v. 62, no. 2, p. 235–246.

Calavan, C. W. and T. R. Garfield, West Africa Deep-Water Developments: Subsurface Learning's: Proceedings of the Offshore Technology Conference, Houston, Texas, USA, p 1-6, SPE paper 16571.

Cantu Chapa, A., 1985, Is there a Chicontepec paleocanyon in the Paleocene of eastern Mexico?: Journal of Petroleum Geology, v. 8, no. 4, p. 423–434.

Carrillo, B. J., 1980, Paleocanones Terciarios de la Planicie Costera del Golfo de Mexico: Bol. Asociation Mexicana de Geologos Petroleros Boletin, v 32(1), p. 1419-1447.

Cheatwood, C. J., and Guzmán, A. E., 2002. Comparison of reservoir properties and development history – Spraberry Trend Field, west Texas and Chicontepec Field, Mexico, Proceedings SPE International Petroleum Conference and Exhibition, Villahermosa, Mexico, 19p, SPE Paper 74407.

Chopra, S., and K. J. Marfurt, 2008, Seismic attributes for stratigraphic feature characterization: Proceedings of the 78th Annual International Meeting of the SEG, Las Vegas, Nevada, U.S.A; Expanded Abstracts, p. 1590-1594.

Covault, J.A., S. M. Hubbard, S. A. Graham, R. Hinsch and H.Linzer, 2009, Turbidite-reservoir architecture in complex foredeep-margin and wedge-top depocenters, Tertiary Molasse foreland basin system, Austria: Marine and Petroleum Geology, v 26, p. 379- 396

Cossey, S. P. J., 2008, Debrites in the Chicontepec Formation, Tetlahuatl, Mexico in Nilsen, T. H., Shew R. D., Steffens, G. S., and Studlick, J. R. J., eds., Atlas of Deep-Water Outcrops, AAPG Studies in Geology 56, p. 231-234.

Cossey, S. P. J., 2006, Slumps and debrites in Paleocene Chicontepec Formation, Mexico: Implications for subsurface identification: American Association of Petroleum Geologists, Abstracts with Program, Annual Convention, April 9-12, CD-ROM publication.

Cossey, S. P. J. and D. V. Nieuwenhuise, 2011, A New Depositional Model for the Chicontepec Basin, Onshore Eastern Mexico: American Association of Petroleum Geologists, Abstracts with Program, Annual Convention, April 10-13, CD-ROM publication.

Cuevas, S. F., 1980, Exploración petrolera en sedimentos terrígenos: 35.° Reunión a nivel de expertos de ARPEL, Nuevos Conceptos Geológicos en Exploración Petrolera, México, v. 1, 14 p.

De Ruig, M.J. and S.M. Hubbard, 2006, Seismic facies and reservoir characteristics of a deep–marine channel belt in the Molasse foreland basin, Puchkirchen Formation, Austria: AAPG Bull., v. 90, 735–752.

Diaz Cadenas, G. E., Sequence stratigraphy of Chicontepec play, Tampico–Misantla basin, Mexico: MS thesis at University of Oklahoma.

Haq, B. U., J. Hardenbol, and P. R. Vail, 1987, Chronology of fluctuating sea levels since the Triassic: Science, v. 235, p. 1156-1166.

Horbury, A. D., S. Hall, F. Gonzalez-P., D. Rodrıguez-F., A. Reyes-F., P. Ortiz-G., M. Martinez-M., and G. Quintanilla-R., 2003, Tectonic sequence stratigraphy of the western margin of the Gulf of Mexico in the late Mesozoic and Cenozoic: Less passive than previously imagined, in C. Bartolini, R. T. Buffler, and J. Blickwede, eds., The Circum-Gulf of Mexico and the Caribbean: Hydrocarbon habitats, basin formation, and plate tectonics: AAPG Memoir 79, p. 184–245.

Kallweit, R.S., and L.C. Wood, 1982, Geophysics, v. 47, no. 7, p. 1035-1046.

Mai, H., K. J. Marfurt, and S. Chávez-Pérez , 2009, Coherence and volumetric curvatures and their spatial relationship to faults and folds, an example from Chicontepec basin, Mexico: Proceedings of the 78th Annual International Meeting of the SEG, Houston, Texas, U.S.A; Expanded Abstracts,p. 1063-1066

Morán -Zenteno, D., 1994, Geology of the Mexican Republic: AAPG Studies in Geology, no. 39, 160 p.

Paleo-data Inc., 2009, Biostratigraphic chart, Gulf Basin: USA-Neogene.

Pena, V., S Chávez–Pérez, M. Vázquez-García, and K.J. Marfurt, 2009, Impact of shallow volcanics on seismic data quality in Chicontepec Basin, Mexico: The Leading Edge, v. 28, p. 674-679.

Perez, M. J. D., 1967, Estudio del Yacimiento San Andres. Inst. Mex. del Petróleo, Rama de Expl.

Pickering, K. T. and J Corrigidor, 2005, Mass–transport complexes (mtcs) and tectonic control on basin–floor submarine fans, Middle Eocene, South Spanish pyrenees: Journal of Sedimentary Research, v. 75, p 761–783.

Plink-Bjorklund, P., D. Mellere, and R. J. Steel, 2001, Turbidite variability and architecture of sand-prone, deep-water slopes: Eocene clinoforms in the Central Basin, Spitsbergen: Journal of Sedimentary Research, v. 71, p. 895– 912.

Porter, M. L., A. R. G. Sprague, M. D. Sullivan, D. C. Jennette, R. T. Beaubouef,T. R. Garfield, C. Rossen, D. K. Sickafoose, G. N. Jensen, S. J. Friedmann,and D. C. Mohrig,2006,Stratigraphic organization and predictability of mixed coarse- and fine-grained lithofacies successions in a lower Miocene deep-water slope-channel system, Angola Block 15, in P. M. Harris and L. J. Weber, eds., Giant hydrocarbon reservoirs of the world: From Rocks to reservoir haracterization and modeling: AAPG Memoir 88/SEPM Special Publication, p. 281–305.

Prior, D. B., B. D. Bornhold, and M. W. Johns, 1986, Active sand transport along a fjord-bottom channel, Bute inlet, British Columbia: Geology, v. 14, p. 581– 584.

Ricci Lucchi, F., 1990, Turbidites in foreland and on thrust basins of the northern Apennnines: Paleogeography, Paleoclimatology, Paleoecology, v 77, p 51–66.

Romero Otero, G.A., Deepwater sedimentary processes in an active margin, Magdalena submarine fan, offshore Colombia: PhD dissertation at University of Oklahoma.

Saller, A. H., J. T. Noah, A. P. Ruzuar, and R. Schneider, 2004, Linked lowstand delta to basin-floor fan deposition, offshore Indonesia: An analog for deep-water reservoir systems: AAPG Bulletin, v. 88, p. 21–46.

Sarkar, S., K. J. Marfurt, R. M. Slatt, 2010, Generation of sea-level curves from depositional pattern as seen through seismic attributes-seismic geomorphology analysis of an MTC-rich shallow sediment column, northern Gulf of Mexico

Sinclair, H. D., 1997, Tectonostratigraphic model for underfilled peripheral foreland basins: An Alpine perspective: Geological Society of America Bulletin, v. 109, p. 324– 346.

Singh, H.K., S. De and A. maitra, 2004, An Integrated Approach to Decipher Depositional Model of Oligocene Basal Sand Pack and Hydrocarbon Entrapment in Ichapur Area, Bengal Basin: Proceedings of the 5th Conference and Exhibition on Petroleum Geophysics, Hyderabad, India, p 804-809.

Sprague, A.R.G., T.R.Garfield, F.J. Goulding, R.T. Beaubouef, M.D. Sullivan, C.Rossen, K.M.Campion, D.K.Sickafoose, V. Abreu, M. E. Schellpeper, G.N. Jensen, D.C. Jennette, C. Pirmez, B.T. Dixon, D. Ying, J. Ardill, D.C. Mohrig, M.L. Porter, M.E. Farrell, and D. Mellere, 2005, Integrated slope channel depositional models: the key to successful prediction of reservoir presence and quality in offshore West Africa: Proceedings of the E-Exitep, Veracruz, Mexico, 13p.

Takahashi, S. , M. Abbaszadeh, K. Ohno and H.S. Soto, 2006, Integrated Reservoir Modeling for Evaluating Field Development Options in Agua Fria, Coapechaca and Tajin Fields of Chicontepec Basin: Pcoceedings of the First International Oil Conference and Exhibition in Mexico, 31 August-2 September 2006, Cancun, Mexico, p. 1-14, SPE paper 103974.

Thornburg, T. M., L. D. Kulm, and D. M. Hussong, 1990, Submarine-fan development in the southern Chile trench: A dynamic interplay of tectonics and sedimentation: Geological Society of America Bulletin, v. 102, p. 1658–1680.

Weimer, P. and Slatt R.M., 2007, Introduction to the Petroleum Geology of Deepwater Settings, AAPG Studies in Geology 57, p. 816.

Widess, M.B., 1973, How thin is a thin bed, Geophysics, v. 38, no. 6, p. 1176-1180.

Zeng, H., 2011, Frequency dependency of seismic facies and seismic sedimentology:Proceedings of the 30th Annual GCSSEPM Foundation Bob F. Perkins Research Conference, December 5-8, 2010, Houston, Texas, p. 11-21.

Zeng, H., W.A. Ambrose and E. Villalta, 2001, Seismic sedimentology and regional depositional systems in Mioceno Norte, Lake Maracaibo, Venezuela: The Leading Edge, v. 20, p. 1260-1269.

Chapter 3

Seismic reservoir characterization in the northern part of the Chicontepec Basin, Mexico

ABSTRACT

The Chicontepec Formation in East Central Mexico is comprised of complex unconventional reservoirs consisting of low permeability disconnected turbidite reservoir facies. Hydraulic fracturing both increases permeability and joins these otherwise tight reservoirs. I use a recently acquired 3D seismic survey and well control to divide the Chicontepec reservoir interval in the northern part of the basin into five stratigraphic units, equivalent to global 3rd order seismic sequences. By combining well log and core information with principles of seismic geomorphology, I am able to map deepwater facies within these stratigraphic units that result from the complex interaction of flows from different directions. Correlating these stratigraphic units to producing and non-producing wells provides the link between rock properties and Chicontepec reservoirs that can be delineated from surface seismic data. The final product is a prestack inversion-driven map of stacked pay that correlates to currently producing wells and indicates potential untapped targets.

INTRODUCTION

The sandstones in the Chicontepec Formation were deposited within a foredeep basin deepwater system during the Upper Paleocene and Early-Middle Eocene periods. The elongated foredeep basin is known as the Chicontepec foredeep, which was formed in front of the Sierra Madre Oriental fold and thrust belt during the Late Cretaceous to Early Tertiary Laramide orogeny in east-central Mexico. The foredeep is bounded on the east by the Golden Lane atoll Cretaceous carbonate platform (Figure 1).

The Chicontepec play is characterized by a complex depositional history, which can be attributed to the interplay of several factors, including multiple provenances, tectonic activity and associated differential rate of subsidence and sediment accumulation within the foredeep. The deposits are rich in carbonate fragments eroded from nearby Jurassic and Cretaceous carbonate rocks spread throughout the region. Other than carbonate rock fragments, the major constituent is quartz along with feldspars and some clay (Figure 2). The Chicontepec sandstones have an average quartz, feldspar and rock fragment composition of $Q_{29}F_{13}R_{58}$ in the Northern part of the Chicontepec basin (Bermudez et al., 2006). After the depositional events, the Chicontepec sandstone was subjected to extensive complex diagenetic processes (Bermudez et al., 2006) as well as Tertiary volcanic activity. The extensive carbonate cementation seen in the Chicontepec rocks is due to the presence of carbonate rock fragments as a major constituent.

The Chicontepec reservoirs have very low porosity (0.5%-11%) and permeability (.001– 5 mD). Factors contributing to this low porosity and permeability of the reservoir include poor sorting, predominance of carbonate rock fragments, and extensive diagenesis. Due to this poor reservoir quality, only 0.1% of the original oil in place, equal

to 140 million barrels of oil–equivalent, had been recovered by 2002 (Cheatwood and Guzman, 2002). Currently, production from the Chicontepec Formation in the Tampico-Misantla basin occurs from some 50 fields scattered throughout the basin at depths ranging between 800 and 2,400 meters (Cossey, 2008).

The Chicontepec Formation and tight gas reservoirs in general do not exhibit a significant seismic 'Direct Hydrocarbon Indicator' (DHI). In addition to the very low porosity and permeability of the reservoirs, the absence of free gas and the presence of major amounts of carbonate give rise to reservoirs that are relatively fluid insensitive, with almost no AVO effect (Figure 3). I concentrate my study in the northern part of the Chicontepec foredeep where prestack and poststack seismic data over a ~700 km^2 area (Figure 1) along with well logs and production from oil fields situated in the eastern part of the survey were available. The seismic dataset is plagued by multiple shallow volcanic bodies which give rise to both velocity pull-up, and interbed multiples. Extrusive volcanic mounds, swamps and populated areas limit surface access, resulting in locally low fold data (Figure 4). As a result of these limitations to seismic data quality and the complex sediment stacking pattern, seismic data have played a minimal role in guiding the dense drilling program. Pemex had a 1000 new well drilling program in 2009 (Donnelly, 2009) mostly guided by pattern drilling. Such challenges have been faced by other tight sandstone reservoirs as well. The tight gas reservoirs in Wamsutter field, Wyoming also went through similar pattern drilling program until recently when the advancements in Geosciences contributed towards the higher production rate and recovery in recent years (e.g. Tobin et al., 2010, Geetan et al., 2011)

In this paper I present a simple and effective way to characterize the complex unconventional Chicontepec reservoirs by integrating acoustic and elastic rock properties within a stratigraphic framework to better map the distribution of the potential reservoir units. I begin by building a geologic framework and delineating facies patterns for the Chicontepec reservoirs within the Amatitlan 3D survey area. Next, I analyze the petrophysical properties from the well logs and identify the set of properties that provide the best distinction between reservoir and non- reservoir sections within the stratigraphic units. Then I use the 3D seismic data to map the distribution of the best reservoir properties in three dimensional space. After pre-conditioning the seismic gathers I obtain rock properties using prestack angle dependent inversion, and map the potential reservoir bodies within each stratigraphic unit within my facies distribution framework. Finally, I compare the zones that have potential reservoirs from multiple stratigraphic units to the available production data to highgrade areas of greater productivity.

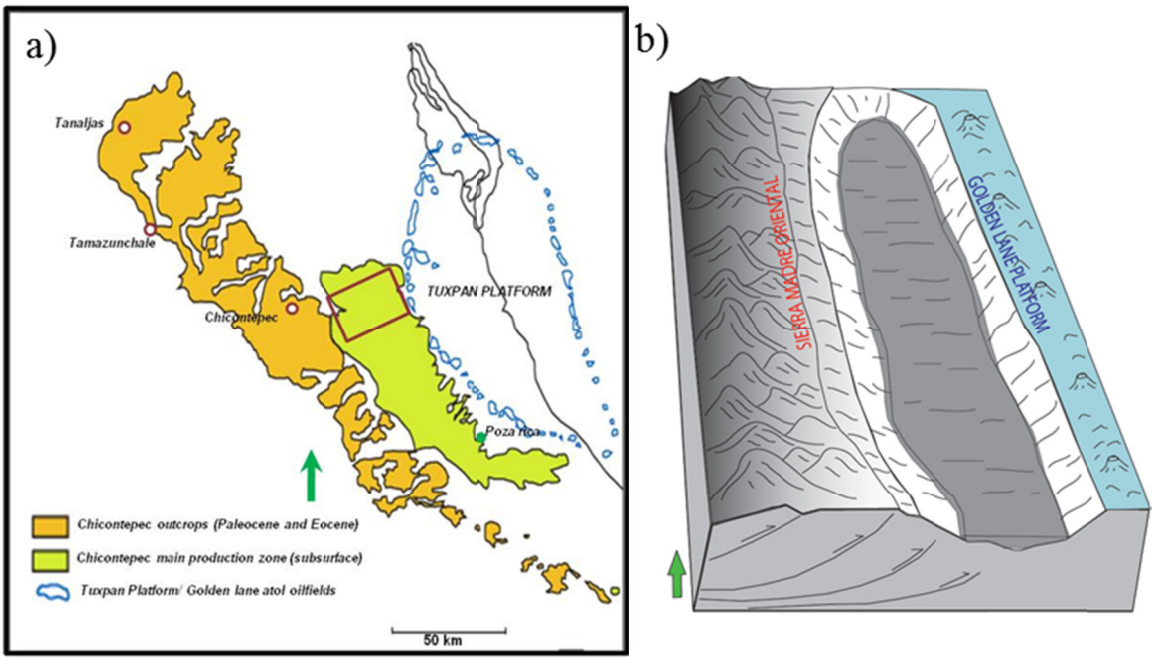

Figure 1. (a) Location map of the Chicontepec foredeep in East-Central Mexico (Modified after Bermudez et al., 2006). The orange area indicates the foothill region of the Sierra Madre Oriental fold thrust belt. The red rectangle is the outline of the 3D seismic coverage within the northern part of the Chicontepec basin where this study is concentrated. (b) Schematic diagram showing the Chicontepec foredeep forming an elongated trough between the Sierra Madre Oriental and the Golden Lane (Tuxpan) platform.

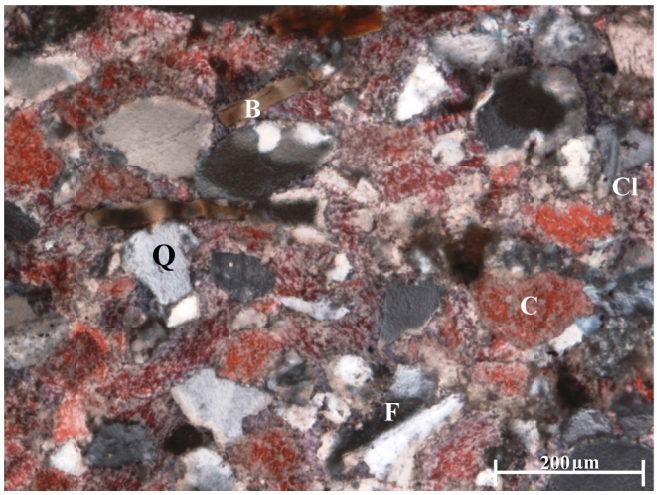

Figure 2. Photomicrograph of a Chicontepec Sandstone. The section is stained with alizarin red-S. Q= quartz, F= Feldspar, B= Biotite, C= Carbonate rock fragments, and Cl= Clay.

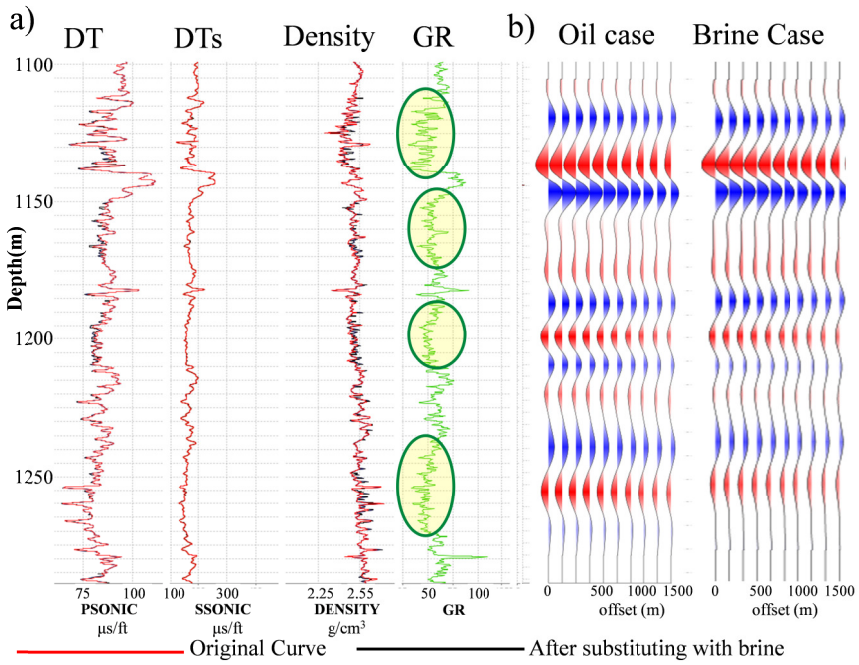

Figure 3. (a) Green ellipses in the gamma ray log show the oil-bearing reservoir intervals. Using Gassman substitution, oil has been replaced with brine. Red and black curves correspond to Psonic, Ssonic and density logs before and after substituting with brine. Note that the P-wave sonic (DT) and density curves do not show any distinct differences before and after fluid substitution, such that the modeled AVO responses in (b) are very similar.

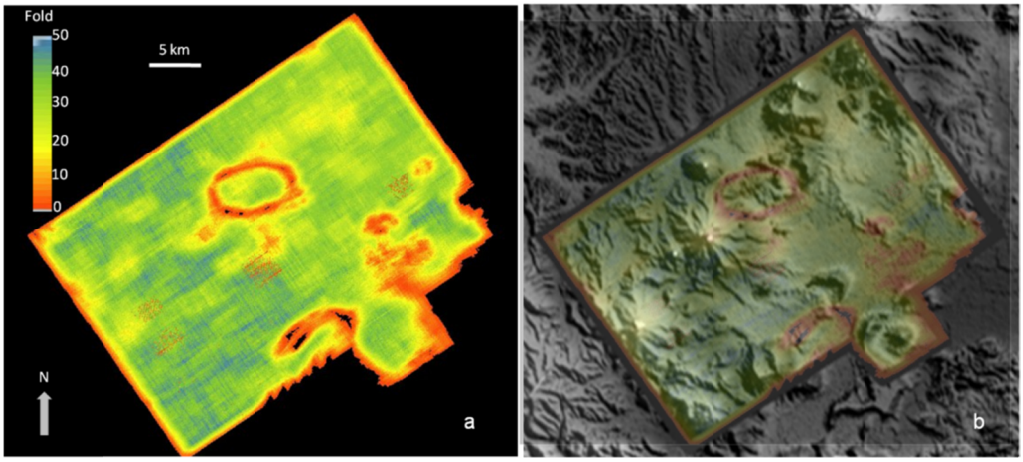

Figure 4. (a) Seismic fold map of the Amatitlan seismic survey. (b) Digital elevation map blended with the seismic fold map. Several extrusive volcanic mounds can be observed throughout the survey area. (Modified from Pena et al., 2009).

STRATIGRAPHIC FRAMEWORK

In a recent paper (Chapter 2 of this dissertation) I developed the stratigraphic framework in the northern part of the Chicontepec foredeep by integrating outcrop information with well log correlation, chronostratigraphic calibration, seismic geomorphology and core interpretation. The Chicontepec reservoir section has been subdivided into five stratigraphic units equivalent to global 3rd order sequences of Haq et al. (1987) (Figure 5). Deepwater facies distribution patterns within those stratigraphic units show two major flow directions that provide the sediments within the Chicontepec foredeep (Figure 6). The basin axis-parallel system consists of multiple channels and amalgamated channel systems dominated the Upper Paleocene basal Chicontepec sequence, or unit A. The basin axis-perpendicular channel-fan systems and mass transport complexes originated from the Sierra Madre Oriental fold thrust belt (SMO) as well as rivers or canyons passing through the SMO. Basin subsidence and sediment accumulation from the basin axis-perpendicular system was closely related to the tectonic activity that continued from Late Upper Paleocene to Early Eocene time. The basin axis-perpendicular system dominated the Early Eocene stratigraphic units, although the presence of axial flows gave rise to mixed depositional systems in several zones. The influence of axial channel systems progressively weakened towards the top of the Chicontepec strata. Within the uppermost zones of the Chicontepec reservoirs, especially in unit E (equivalent to 3rd order global sequence TA 2.9 of Haq et al., 1987), the proportion of finer clastics or clays increase giving rise to poorer reservoirs. This stratigraphic system derived from this integrated study is different from the existing

Chicontepec depositional concepts (e.g., Bush and Govela, 1978; Cheatwood and Guzman, 2002; Abbaszadeh et al., 2003).

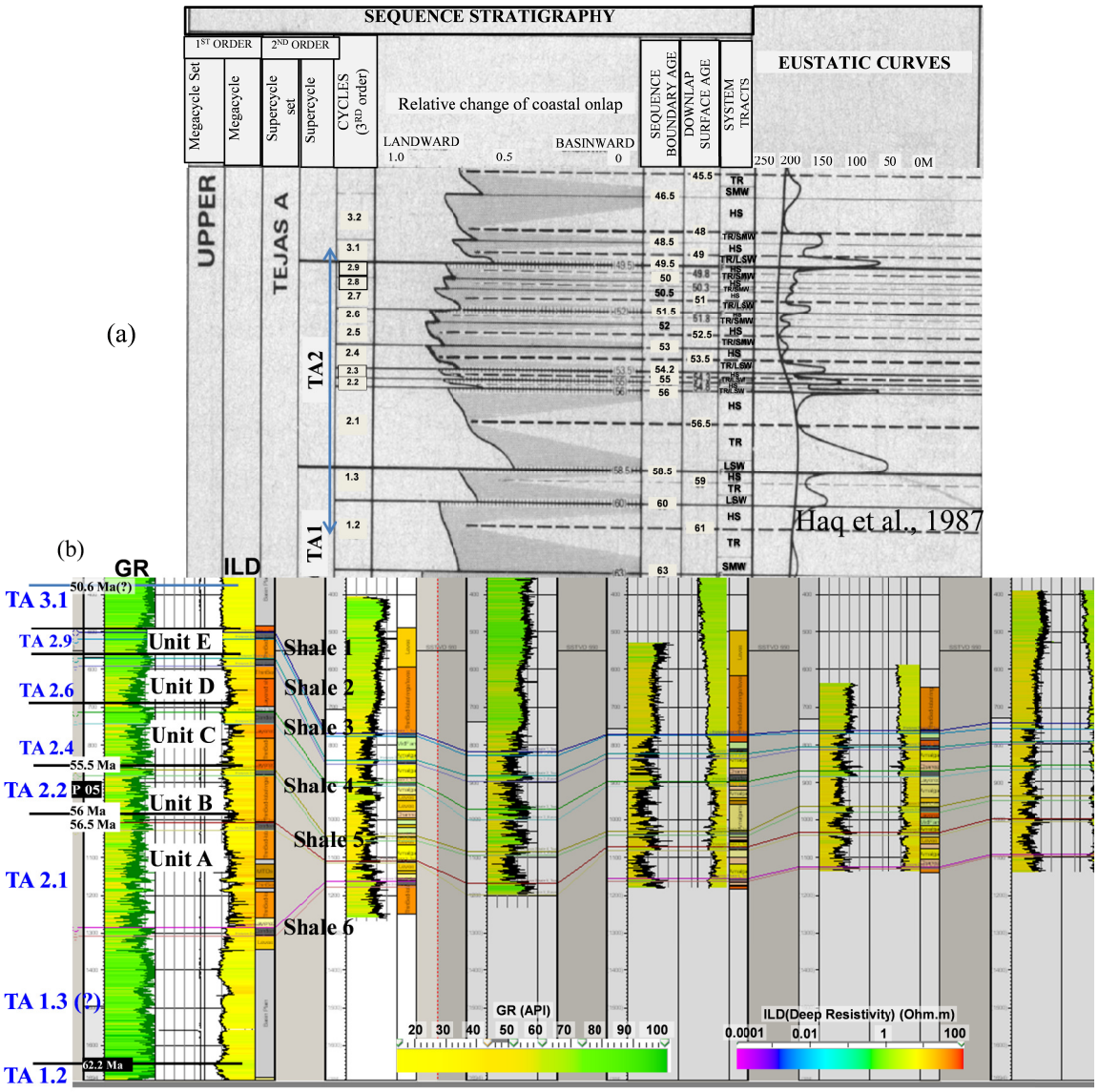

Figure 5. (a) Eustatic curves and global 3rd order sequences for the Upper Paleocene-Early Eocene (Haq et al., 1987). (b) Six regionally extensive shale layers and possible condensed sections identified from stratigraphic correlation that divides the Chicontepec reservoir section into five stratigraphic units labeled A-E. Using biostratigraphic records, the stratigraphic units can be correlated with global sequences TA 2.1, TA 2.2, TA 2.4, TA 2.6 and TA 2.9.

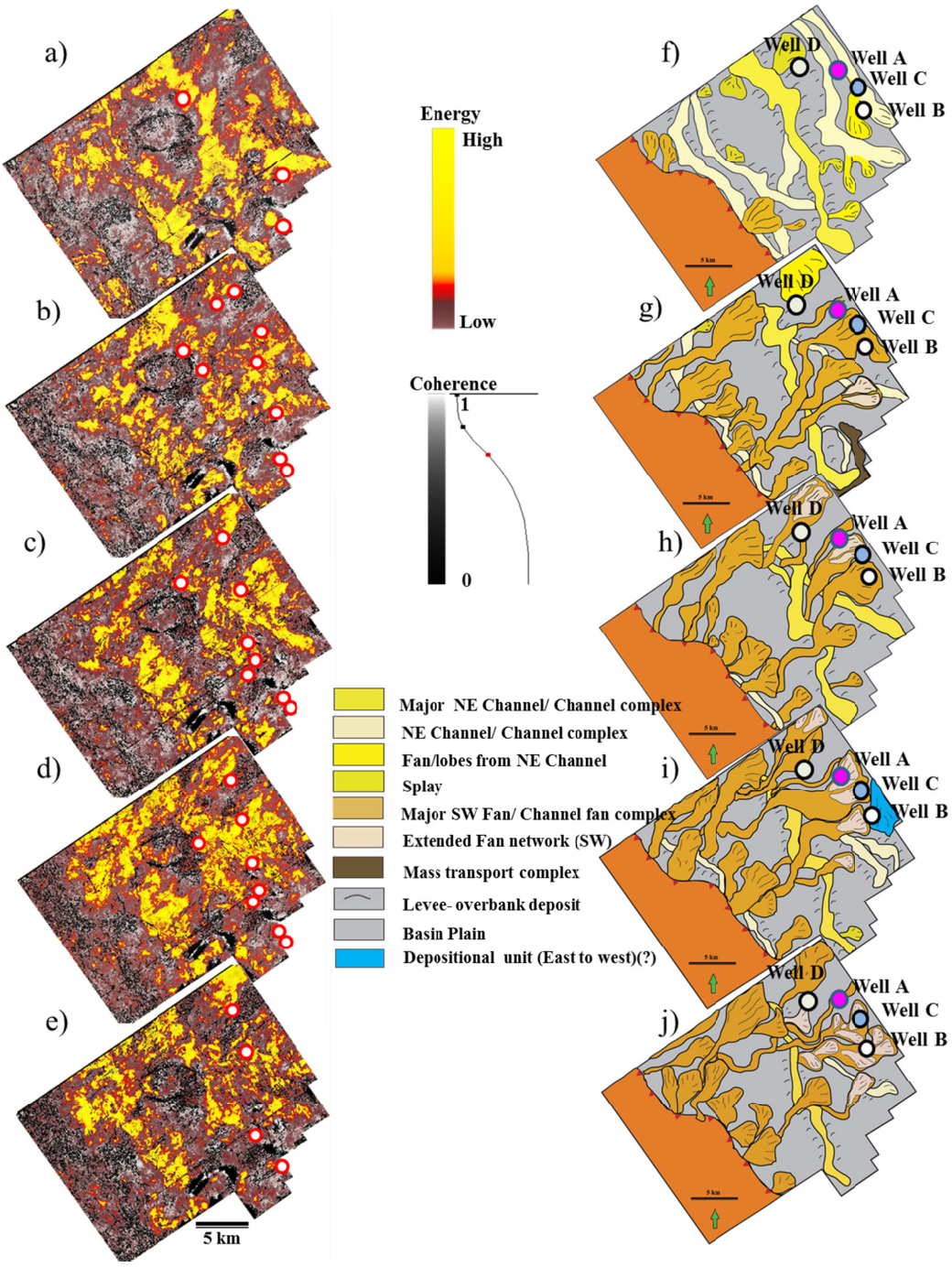

Figure 6. (a)-(e): Stratal slices along stratigraphic units A-E through coherent energy corendered with coherence volumes. Core locations used during interpretation indicated by white circles. (f)-(j) represent turbidite facies pattern within unit A-E (corresponding to Figures a-e) based on seismic geomorphology combined with well control. Well A-D are location of the wells shown in the following section in Figures 7, 8, 9, 13, 14, 23.

PETROPHYSICAL ANALYSIS

Petrophysical properties from well logs provide the basis to define rock types, reservoir zones and mechanical properties that can be later correlated to inverted surface seismic data showing their distribution in 3D space. Along with the petrophysical properties obtained directly from the well logs (Table 1), I also analyzed derived rock properties such as Lame's parameters of rigidity, μ, and incompressibility, λ, Young's Modulus, E, and Poisson's ratio, ν. Crossplots between these rock properties provide qualitative correlation of rock properties measurable from surface seismic data to good and poor reservoir rocks as well as shales. Although the reservoir zone is insensitive to fluid product (Figure 3), rock properties do allow to differentiate between shale and sandstone and between relatively porous and non porous cemented sandstone. Most important, since all wells need to be hydraulically fractured, a primary objective is to correlate rock type as measured by production to logs and surface seismic measurements. In the following sections I discuss the most important petrophysical properties and their application in reservoir delineation.

Table 1. List of well logs analyzed for the petrophysical analysis.

Total Wells	Gamma ray	Density	P wave sonic	S wave sonic	Neutron porosity	Permeability	Core	Deep resistivity	Wells with all logs
100	80	35	51	11	20	35	11	25	3

Gamma ray

Gamma ray logs clearly demarcate the shale zones in between the reservoir units (Figure 7a), with a shale cut off of GR<55 for the best reservoir intervals. Carbonate rock fragments are a major constituent of this system. Since the gamma ray count of

carbonates are very low, gamma ray logs alone are insufficient to identifying good reservoir.

V_P/ V_S ratio

V_P/ V_S ratio has been successfully used to classify tight sand reservoirs (e.g., Rojas et al., 2005; Close et al., 2010; Valentin and Tatham, 2010). The V_P/ V_S ratio shows moderate to high correlation with Gamma ray within a particular well and it also defines the reservoir zones (Figure 7b). In more carbonate rich reservoir intervals, the V_P/ V_S ratio better delineates the reservoir zone than gamma ray. Across the study area, the best productive reservoir zones fall within a V_P/ V_S ratio of 1.7-1.94.

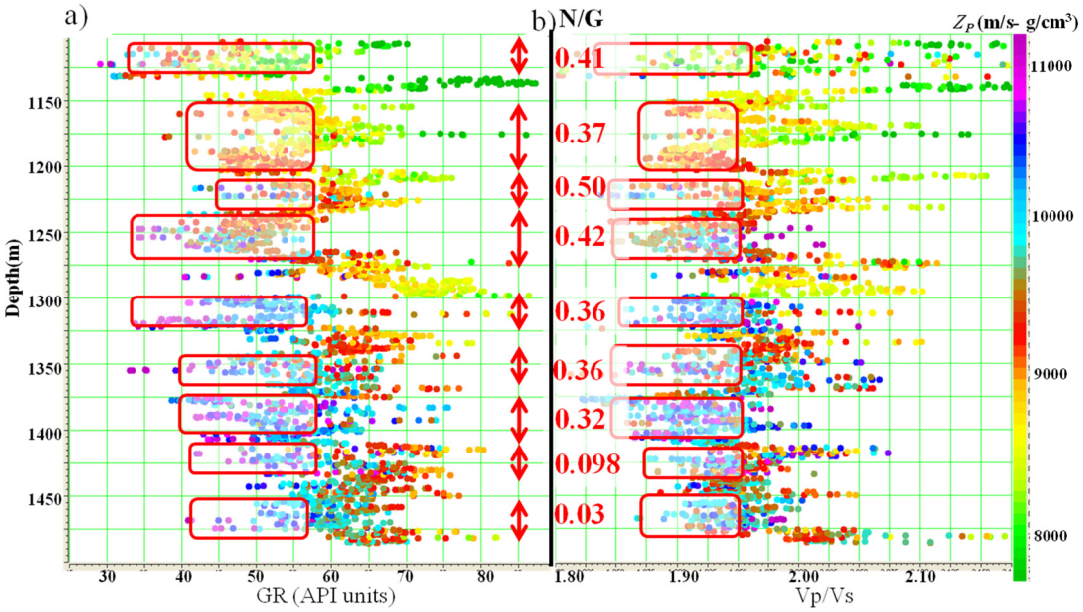

Figure 7. (a) Depth vs. gamma ray and (b) depth vs. V_P/V_S plot, colored by P-Impedance, Z_P, for well A. Net/ Gross (N/G) ratios from post-drill information from each of the reservoir units shown in red. Note the better definition of the reservoir units by relatively low values of gamma ray and V_P/V_S ratio in those reservoir units. The reservoir zones below 1400 meters have low N/G ratio (less than 0.1) due to very low porosity and permeability. Higher impedance zones predominantly correspond to higher carbonate content.

μ (rigidity), λ (incompressibility) and λρ-μρ crossplots

Goodway et al. (1997) showed the value of μ (rigidity) and λ (incompressibility) in the identification of reservoir zones. λ indicates sensitivity to pore fluids while μ and λ together serve as a lithology indicator. μ and λ can be calculated from the V_P, V_S and density logs from the following equations

$$\mu = \rho V_s^2 \ , \qquad (1)$$

$$\text{and } \lambda = \rho V_p^2 - 2\rho V_s^2. \qquad (2)$$

A primary objective is to obtain rock properties from seismic inversion. Debski and Tarantola (1995) and Gray and Andersen (2000) show that AVO inversion can accurately estimate two parameters $\lambda\rho$ and $\mu\rho$. The products $\lambda\rho$ and $\mu\rho$ can be accurately estimated from prestack seismic gathers, and provide the same lithology discrimination as λ and μ.

Computing $\mu\rho$ and $\lambda\rho$ in several wells across the Chicontepec play from conventional logs shows $\mu\rho$ to be an excellent indicator of the calcilithite reservoir rocks (terminology from Folk, 1965) within the Chicontepec Formation (Figure 8), since μ is directly related to the matrix composition. In contrast, the Chicontepec reservoirs are very tight and contain oil (mostly with no free gas), λ, is relatively insensitive to the reservoir zone (Figure 9).

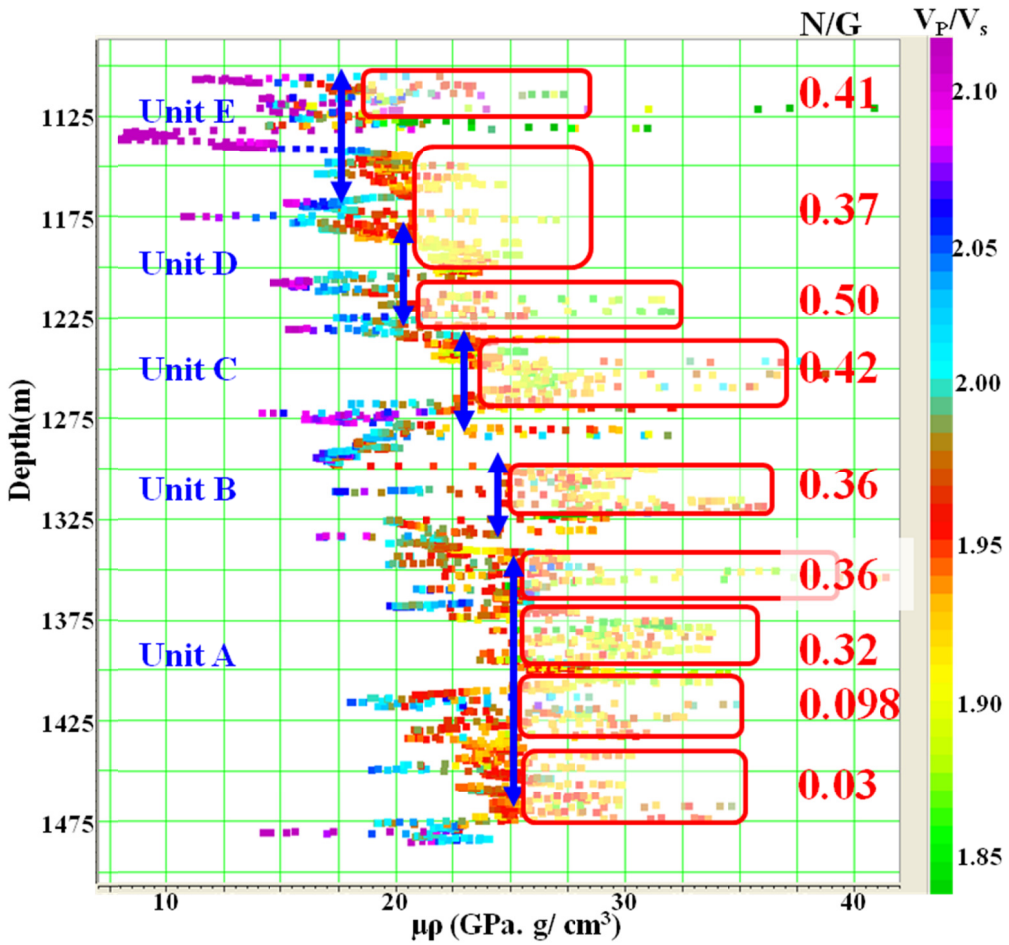

Figure 8. $\mu\rho$ vs. depth colored by V_P/V_S ratio plot from the well A shown in Figure 7. Blue arrows indicate the stratigraphic units shown in Figures 5 and 6 and gradual decrease in the $\mu\rho$ boundary values from lower stratigraphic units to upper stratigraphic units for reservoir delineation. Red rectangles indicate the reservoir units and their N/G ratio (from post-drill information) within the stratigraphic units.

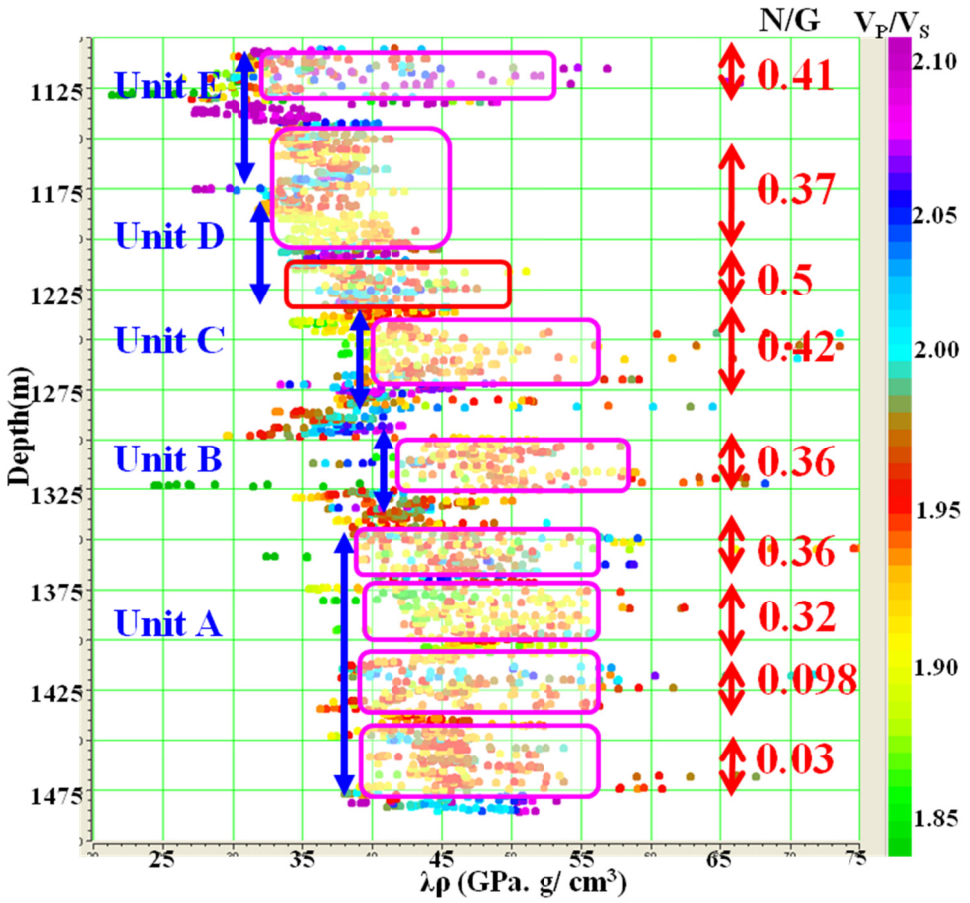

Figure 9. $\lambda\rho$ vs. depth plot from the same well as Figures 7 and 8, colored with V_P/V_S ratio. Blue arrows indicate the stratigraphic units within Chicontepec reservoir zone as shown in Figures 5 and 6 and the changing boundary values of $\lambda\rho$ from bottom to top stratigraphic units. Magenta rectangles indicate the reservoir units and their N/G ratio (from post-drill information) within the stratigraphic units.

The two seismically measurable properties that best describe the productive zones within the Chicontepec reservoir interval are $\mu\rho$ and V_P/V_S. Crossplots between $\mu\rho$ and V_P/V_S ratio from ten wells from different fields, reveal the different trends of reservoir and non-reservoir rocks within the Chicontepec reservoir zone (Figure 10). The range of $\mu\rho$ for delineating productive intervals varies between different stratigraphic units and shows an overall decrease in the mean value from lower to upper stratigraphic units (e.g.

Figure 8). This value varies between 18-34 GPa*g/cm^3 for unit E; 22-38 GPa*g/cm^3 for unit D; 23-42 GPa*g/cm^3 for unit C, 25-45 GPa*g/cm^{3}for unit B, and 26-46 GPa*g/cm^{3}for unit A. The $\lambda\rho$ vs. V_P/V_S crossplots from the same wells also show demarcation between reservoir and non-reservoir zones (Figure 11). The $\lambda\rho$ value for the productive reservoir zones varies between 38-56 GPa*g/cm^3 for stratigraphic unit A, 44-58 for unit B, 42-56 for unit C, and 33-53 for units D and E. The mean value of $\lambda\rho$ shows a decreasing trend from unit A to Unit E. My analysis indicate that a few high carbonate prone poor reservoir areas can be eliminated for values of $\lambda\rho > 58$ GPa*g/cm^3, where $V_P/V_S < 1.94$ (Figure 12). Most of these areas also fall within acceptable range of $\mu\rho$ for the reservoir zone (18-46 GPa*g/cm^3). To qualitatively delineate the most productive zones using the boundary values for these three parameters ($\lambda\rho$, $\mu\rho$ and V_P/V_S ratio) provide the best result. Since, $\frac{\lambda\rho}{\mu\rho} = \frac{V_P^2}{V_S^2} - 2$; the V_P/V_S ratio can be directly correlated to the points within $\lambda\rho$- $\mu\rho$ space. Plotting the points in $\lambda\rho$- $\mu\rho$ space and coloring with the gamma ray values provide a broad idea about the reservoir zone and we can demarcate the points with the boundary values discussed above (Figure 12). Within a stratigraphic unit, the better reservoir zones show higher $\mu\rho$ and lower $\lambda\rho$. To conceptualize the effect of the three major constituents of the rocks; calcite and quartz, and feldspar within the $\lambda\rho$- $\mu\rho$ space, their values are plotted alongside the points from the reservoir zones. This plot indicates an overall trend toward calcite, which conforms to the fact that calcite rock fragments and cement is the dominant constituent of these rocks. However, at the same time the best reservoir zones have a trend toward quartz abundance. Laboratory analyses of core samples indicate that porosity in the Chicontepec reservoirs is inversely

proportional to the calcite percentage in the rock, whereas decrease in calcite/quartz ratio can be correlated with higher porosity within the rock (Figure 13).

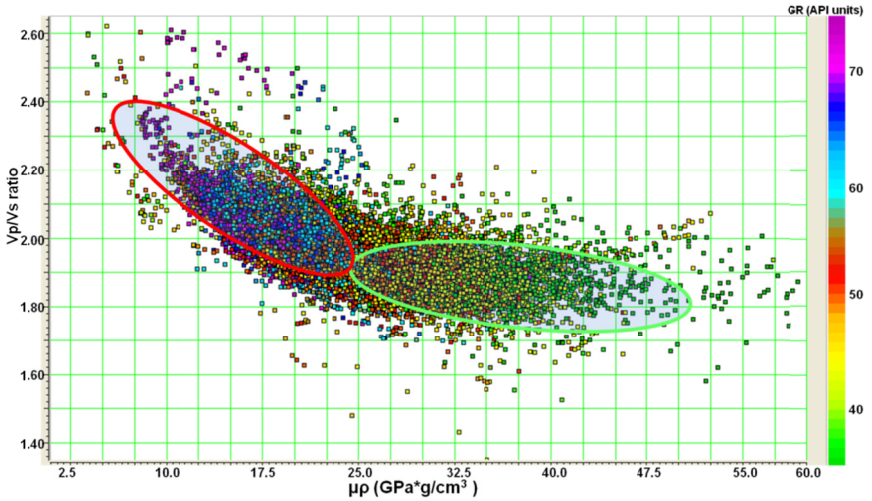

Figure 10. Crossplot between $\mu\rho$ and V_P/V_S ratio from 10 wells across the northern Chicontepec basin, colored by gamma ray. Green ellipse indicates reservoir rocks (lower gamma ray values) and red ellipse indicates non productive rocks (higher gamma ray values). Note the trend of the points within green and red ellipses have different slopes.

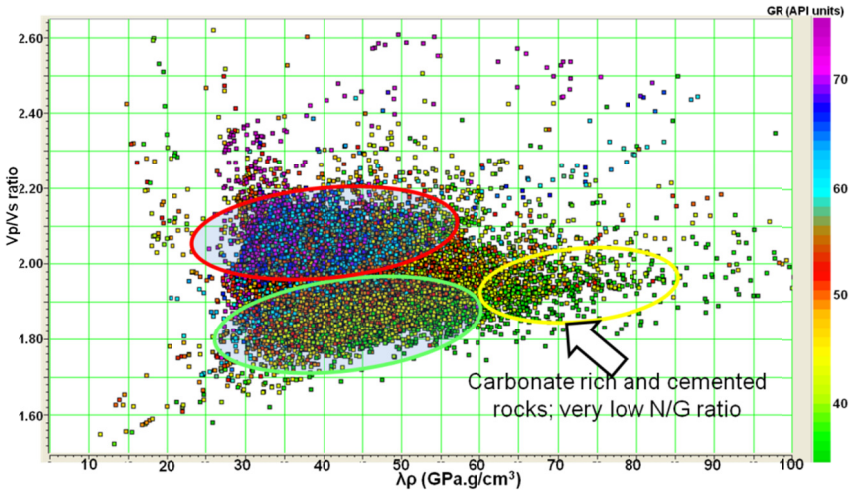

Figure 11. Crossplot between $\lambda\rho$ and V_P/V_S ratio from 10 wells across the northern Chicontepec basin, colored by gamma ray. Green ellipse indicates values from the reservoir units while the red ellipse defines the points from non-productive units. Low gamma ray points within the yellow ellipse are from very low N/G ratio carbonate rich cemented rocks have a value of $\lambda\rho$ > 60 GPa.g/cm^3.

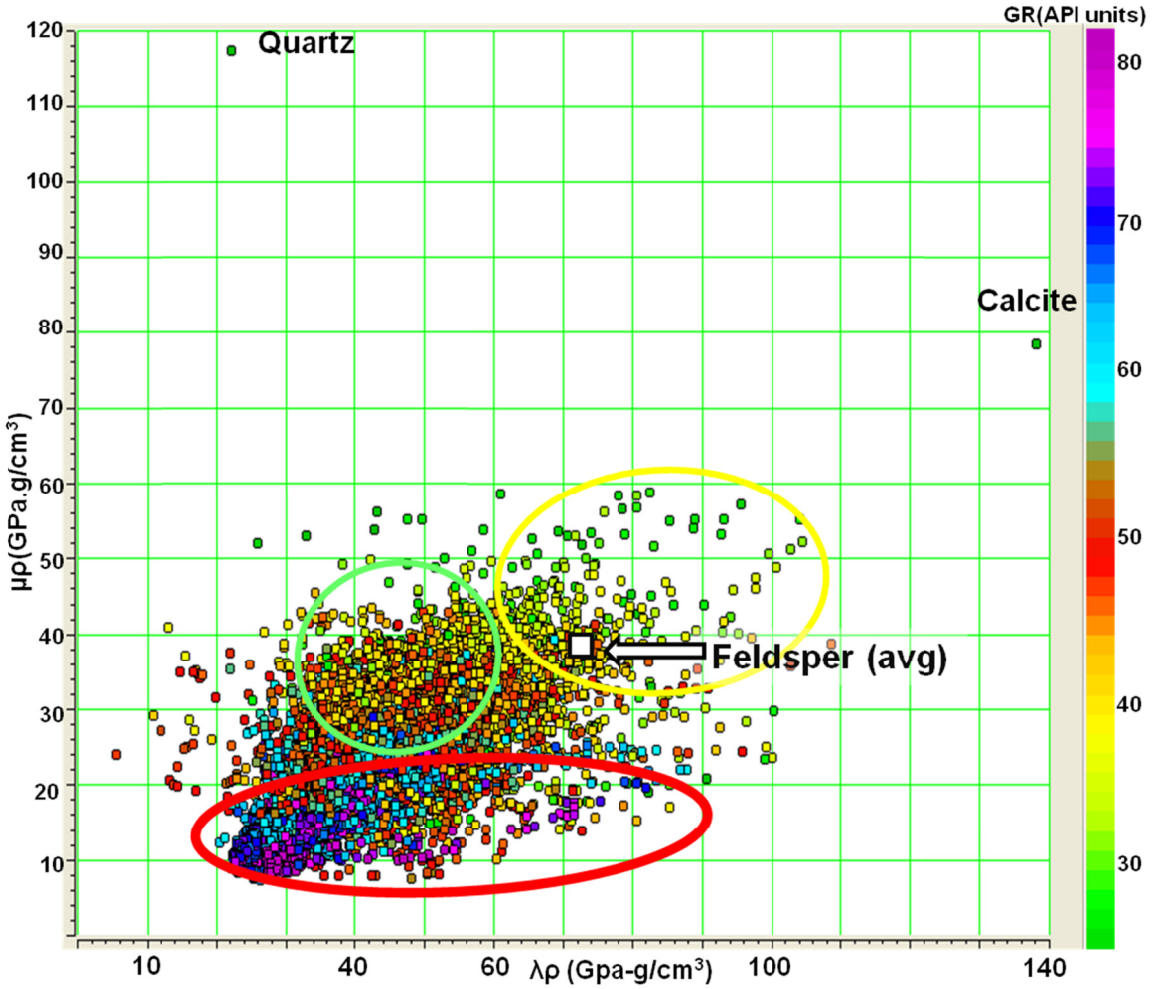

Figure 12. ***λρ-μρ*** **crossplot colored by gamma ray, from the points within the Chicontepec reservoir interval from multiple wells across the field along with values for pure quartz and calcite and feldspar (average). Plagioclase feldspar plots at** ***μρ*****=67,** ***λρ*****=154. The green ellipse includes the points from good productive zones. The red ellipse indicates shaly zones while the yellow ellipse indicates highly cemented and carbonate rich poor sandstone reservoir units.**

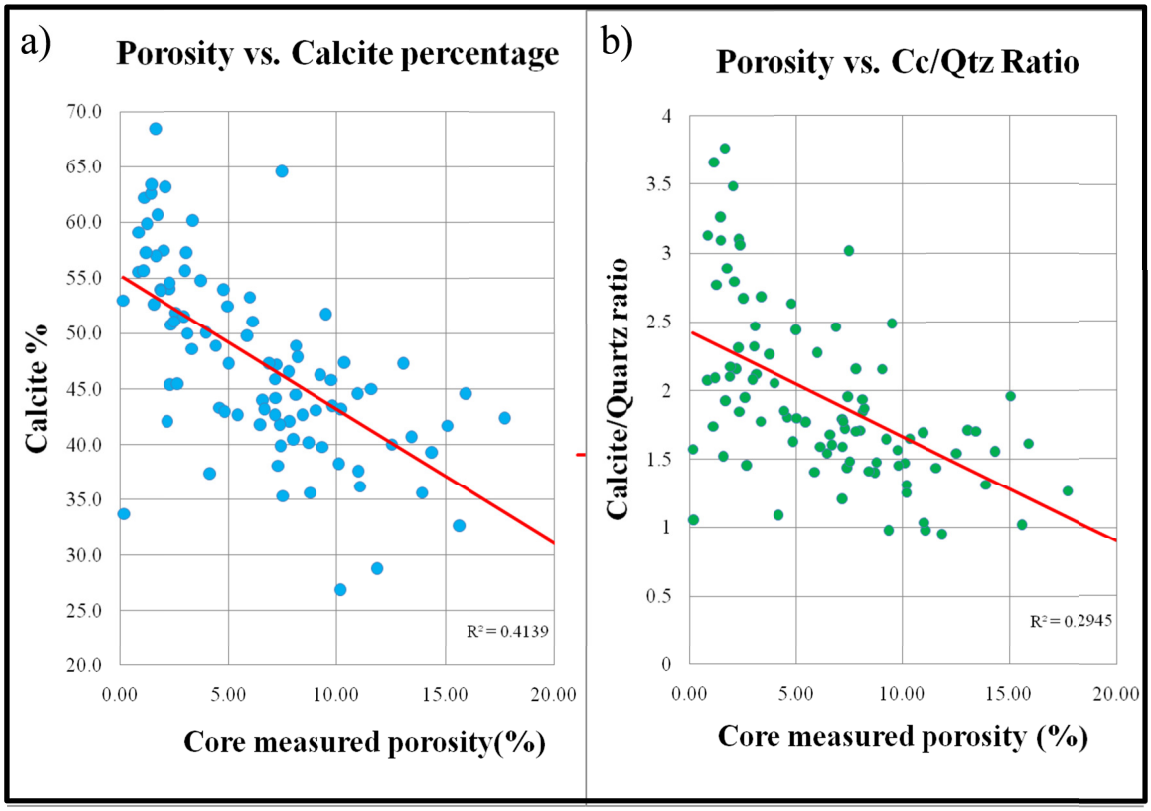

Figure 13. (a) Crossplot between core measured porosity and calcite weight percent within Chicontepec reservoir rocks from multiple wells in the study area. (b) Crossplot between core measured porosity shown in (a) against calcite/quartz ratio within the rocks measured from conventional core samples. Note the low porosity areas correspond to the higher calcite and high calcite/quartz ratio. Porosity increases with decrease in calcite content in (a), whereas in (b) lower quartz/calcite ratio exhibit higher porosity trend.

Neutron porosity

Since a neutron porosity log is a measure of hydrogen concentration (response primarily comes from the pore fluids of the formation), it shows high values in shales and clay rich areas within the reservoir zones in the Chicontepec Formation (Figure 14a) mainly due to bound water rather than effective porosity. Neutron porosity is also sensitive to water-filled, non-connected intragranular pores from the carbonate rock

fragments. Nevertheless, neutron porosity is one of the best tools to estimate the relative porosities within the Chicontepec reservoir units, and correlates reasonably well with the reservoir facies demarcated by $\mu\rho$ and V_P/V_S ratio, where it distinguishes between reservoir and non-reservoir areas (Figure 14b). Neutron porosity values range between 5% and 30% for the potential productive facies.

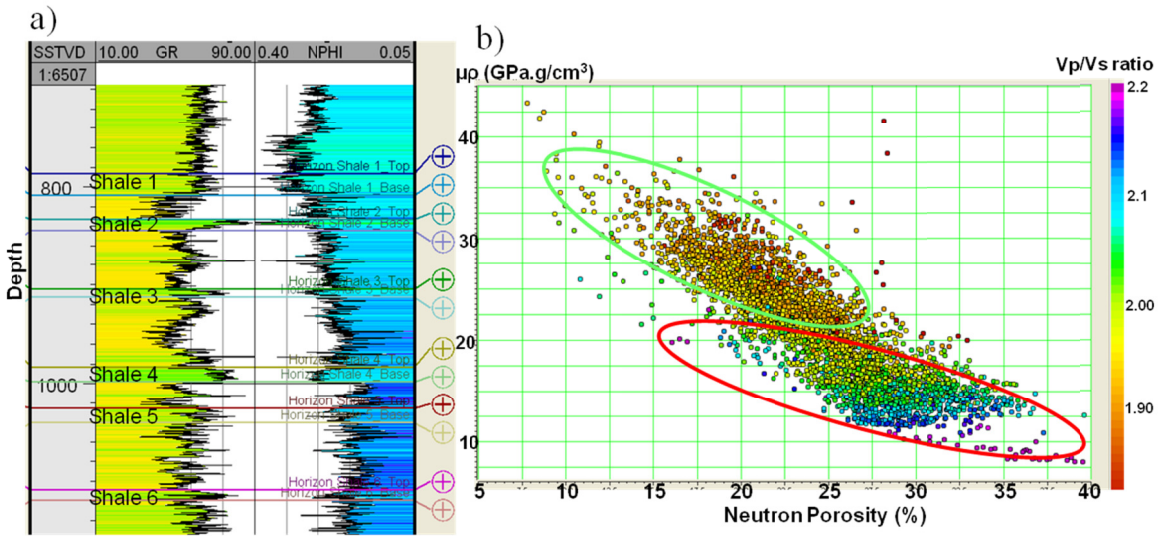

Figure 14. (a) Gamma ray and neutron porosity (NPHI) logs in the Chicontepec reservoir interval from Well A. (b) $\mu\rho$ plotted against neutron porosity and colored with V_P/V_S ratio from wells A,B,C shown in Figure 6. The red ellipse represent non-reservoir shaly zone and the green ellipse include the points from productive zones.

The zones marked in Figure 12 for best, poor and non reservoir rocks is further supported by a $\lambda\rho$- $\mu\rho$ crossplot from three of the wells in Figure 12 (well A, B, C in Figure 6) colored with Neutron porosity (%, Figure 15) and permeability (mD, Figure 16). The shaly non-reservoir zones show highest neutron porosity and lowest permeability. The good reservoir rocks represented by green ellipse in Figures 15 and 16 show moderate neutron porosity and 80% of the points fall within 0.1-0.6 mD

permeability values. Poor reservoir rocks marked by yellow ellipse in Figures 15 and 16 show lowest Neutron porosity and very low permeability.

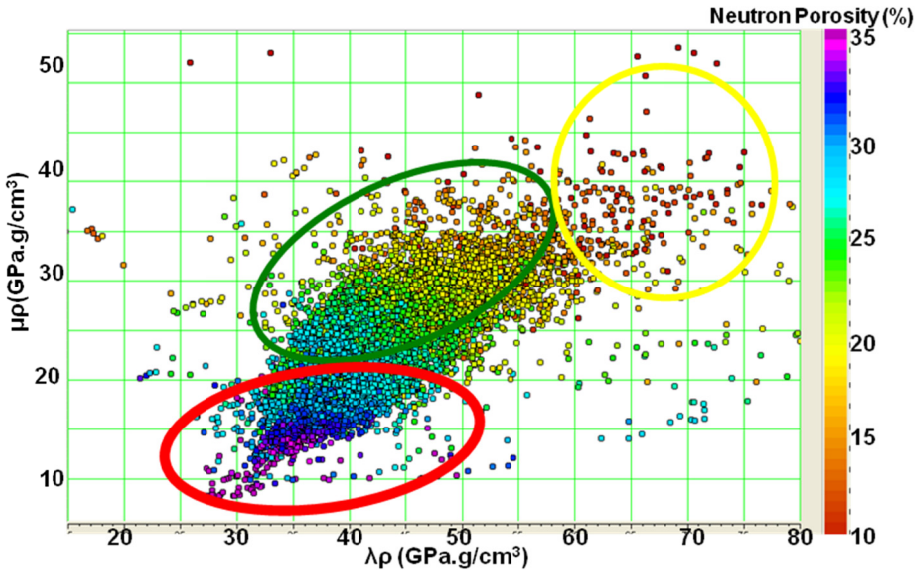

Figure 15: Points from 3 wells used in Figure 12 within the reservoir zone are plotted in the *λρ-μρ* space, colored with neutron porosity (%) values. The good, poor and non reservoir zones shown by green, yellow and red ellipses correspond to the zones indicated in Figure 12.

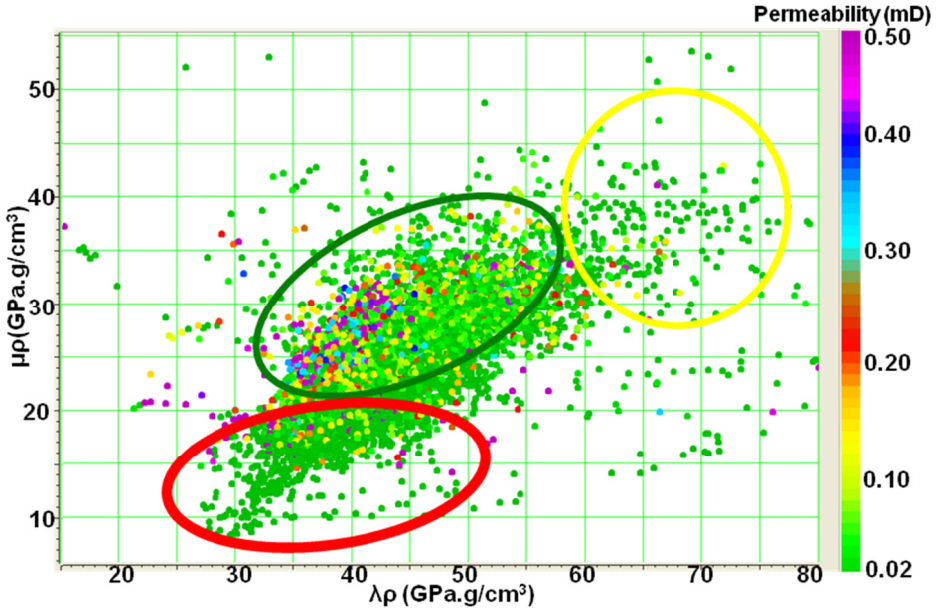

Figure 16: *λρ-μρ* crossplot from Figure 15 colored with log permeability values. Note the good correlation between points within green, red and yellow ellipses in Figure 15.

Dividing the $\lambda\rho$- $\mu\rho$ crossplot in Figure 16 within the stratigraphic units supports the $\mu\rho$ values corresponding to the productive zones within those units.

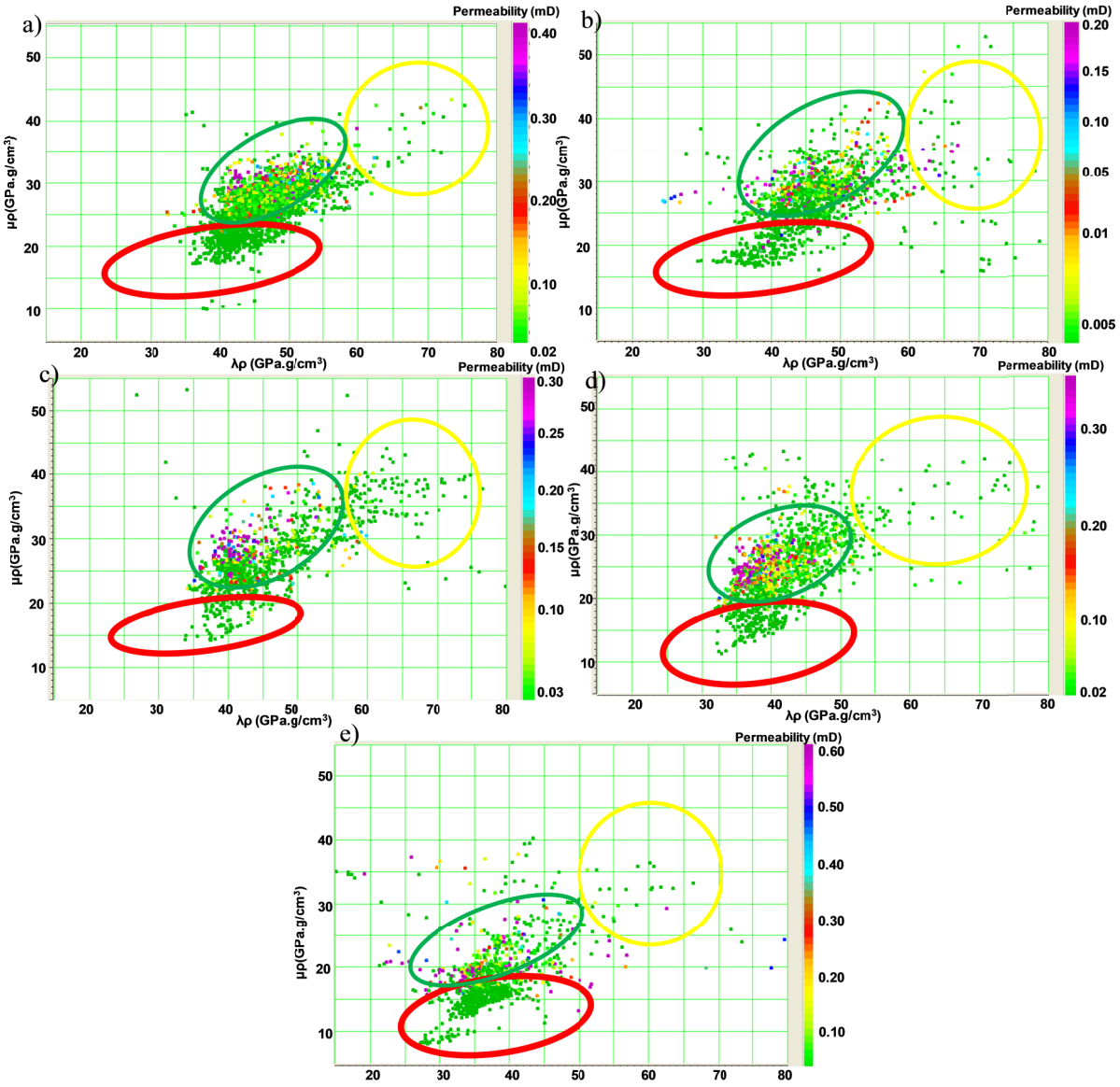

Figure 17. (a)- (e) Represent $\lambda\rho$-$\mu\rho$ crossplot corresponding to stratigraphic units A-E respectively colored by log permeability values from the same wells as in Figure 16. Green ellipse in each of the Figure shows ranges of $\mu\rho$ values corresponding to the stratigraphic unit for better reservoir zones. Red and yellow ellipses in each of the figures demarcate shaly non reservoir and highly cemented poor reservoir zones respectively.

Young's modulus and Poisson's ratio

Oil production from tight Chicontepec reservoirs requires extensive hydraulic fracturing and stimulation. The Chicontepec rocks are assumed to be homogeneous, isotropic and elastic. Along with the in situ stress field, the rock mechanics and fracability are generally defined by Young's Modulus, *E*, and Poisson's ratio, *v*. A range of values *E* and *v* defines the more "fracable" reservoir zones for tight sand and shale gas reservoirs (e.g. Grigg, 2004).

Young's Modulus, *E*, is a measure of elastic stiffness and is used by drilling engineers to design the wellbore stability and mechanical strength of the reservoir rocks. So, pre-drill prediction of *E* is extremely important for safe and successful well design as well as defining the limits for hydraulic fracturing. Higher Young's Modulus, *E*, indicates higher mechanical stiffness which in turn can be positively correlated with fracability.

Poisson's ratio, *v*, measurement is directly related to the in situ stress as well as applied stress. The relationship between the vertical maximum matrix stress (σ_V) and the horizontal stresses (where the horizontal stresses are considered to be equal) is given by $\sigma_{Hmax} = \sigma_{Hmin} = \left(\frac{v}{1-v}\right)\sigma_V$. Poisson's ratio for petroleum reservoirs ranges from 0.10 to 0.35 (Daniel and Dowell, 1980). *E* and *v* values for quartz are respectively 95.75 GPa and 0.08, whereas those values for calcite are respectively 76.5 GPa and 0.32. An increase in quartz and a decrease in calcite corresponding to an increase the Young's modulus and decrease Poisson's ratio improves the quality of the Chicontepec reservoir. Quartz is much more fracable than calcite such that better reservoir zones within the Chicontepec reservoir have a higher quartz content.

E and v can be related to μ (rigidity) by

$$\frac{E}{1+v} = 2\mu \qquad (3)$$

which indicates that μ is directly proportional to E and inversely proportional to v. Poisson's ratio ,v, is a function of the V_P/V_S ratio by the following equation

$$v = 0.5\frac{(\frac{Vp}{Vs})^2-2}{(\frac{Vp}{Vs})^2-1} \qquad (4)$$

Reservoir intervals of V_P/V_S: 1.7-1.94 correspond to v values between 0.27- 0.31 and E values 30-50. Thus, petrophysical analysis indicates that best reservoir zones of Chicontepec Sandstone are among the most suitable rocks for hydraulic fracturing. Crossplotting E vs. v and demarcates the best fracable zones within the reservoir (Figure 18).

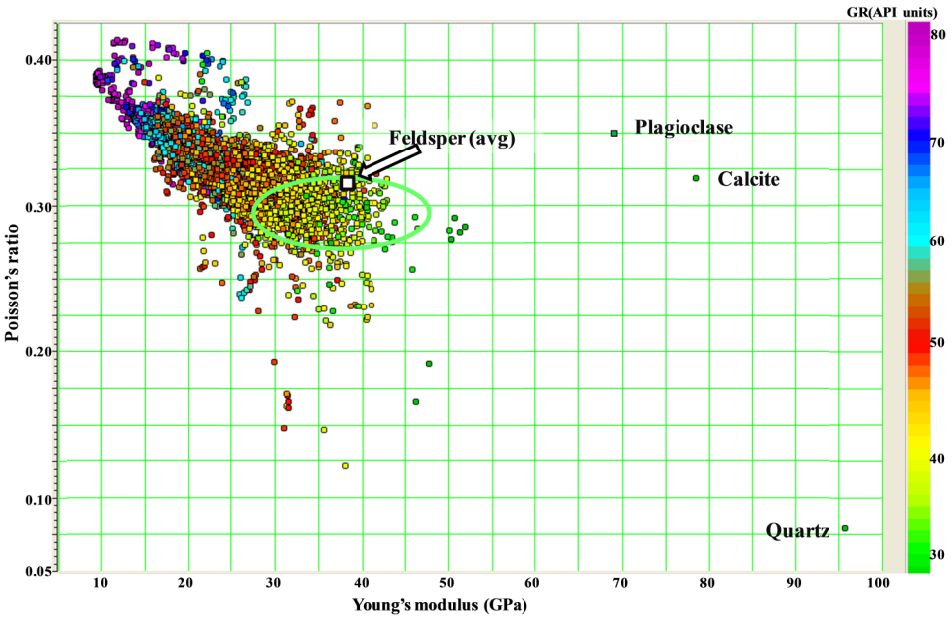

Figure 18: E vs. v crossplot colored by gamma ray from well A, B, and C along with the corresponding values of pure quartz, calcite, plagioclase feldspar and average feldspar. Green ellipse indicates reservoir rocks in wells A, B and C and falls within the productive reservoir zone shown in Figure 12. This zone also correlates to more fracable units (e.g. Grigg, 2004).

In summary, petrophysical analysis indicate that the Chicontepec reservoir section can be divided into relatively better reservoir, poor reservoir and shaly non reservoir zones which is clearly defined in the $\lambda\rho$- $\mu\rho$ space. Highly cemented poor reservoir zones correspond to high calcite and high calcite to quartz ratio within the rock. The best reservoir definition can be obtained from $\mu\rho$ and V_P/V_S ratio along with $\lambda\rho$ values, where a unique range of $\mu\rho$ and $\lambda\rho$ values characterizes each stratigraphic unit within the reservoir zone. Range of high E and moderate v values indicating potential 'fracable' zones (e.g., Grigg, 2004) correspond to the relatively better reservoir areas defined from the petrophysical analysis.

SEISMIC DATA ANALYSIS

Preconditioning seismic gathers

NMO correction and flattening of gathers

A basic assumption of AVO and angle dependent inversions is that the reflectors within a gather have been properly corrected for velocity such that they appear to be "flat". The original data were prestack time migrated using a Kirchhoff algorithm at 50 m offset bins ranging between 50 and 3000 m. The original migration velocities were then removed (Figure 19b). I then analyzed velocities on a 375 m x 375 m grid to provide a "residual" velocity analysis (Figures 19a and c) to flatten the gathers.

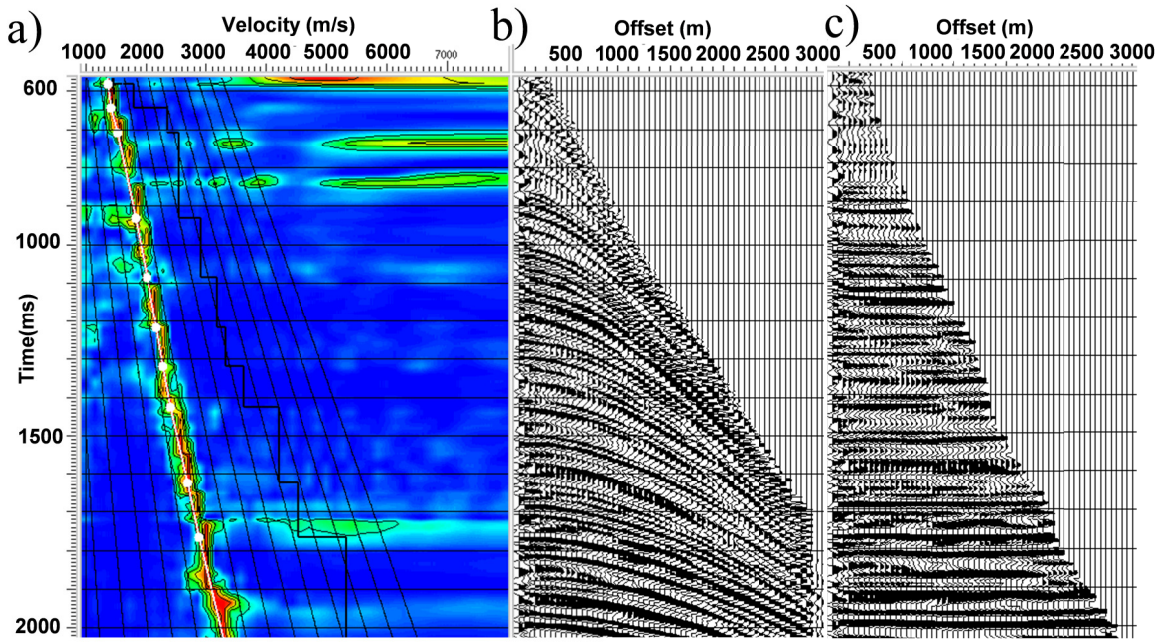

Figure 19. (a) A representative common reflection point gather illustrating (a) velocity analysis of a CMP gather (b) before and (c) after the NMO correction. A 30% stretch mute is applied to the flattened gathers.

After the residual velocity analysis, the frequency content and the signal-to-noise ratio of the dataset improved in many places within the Chicontepec interval compared to the original prestack time-migrated data. Residual velocity analysis results in better vertical and lateral definition of reservoir units as seen by seismic amplitude as well as computed attributes (Figure 20).

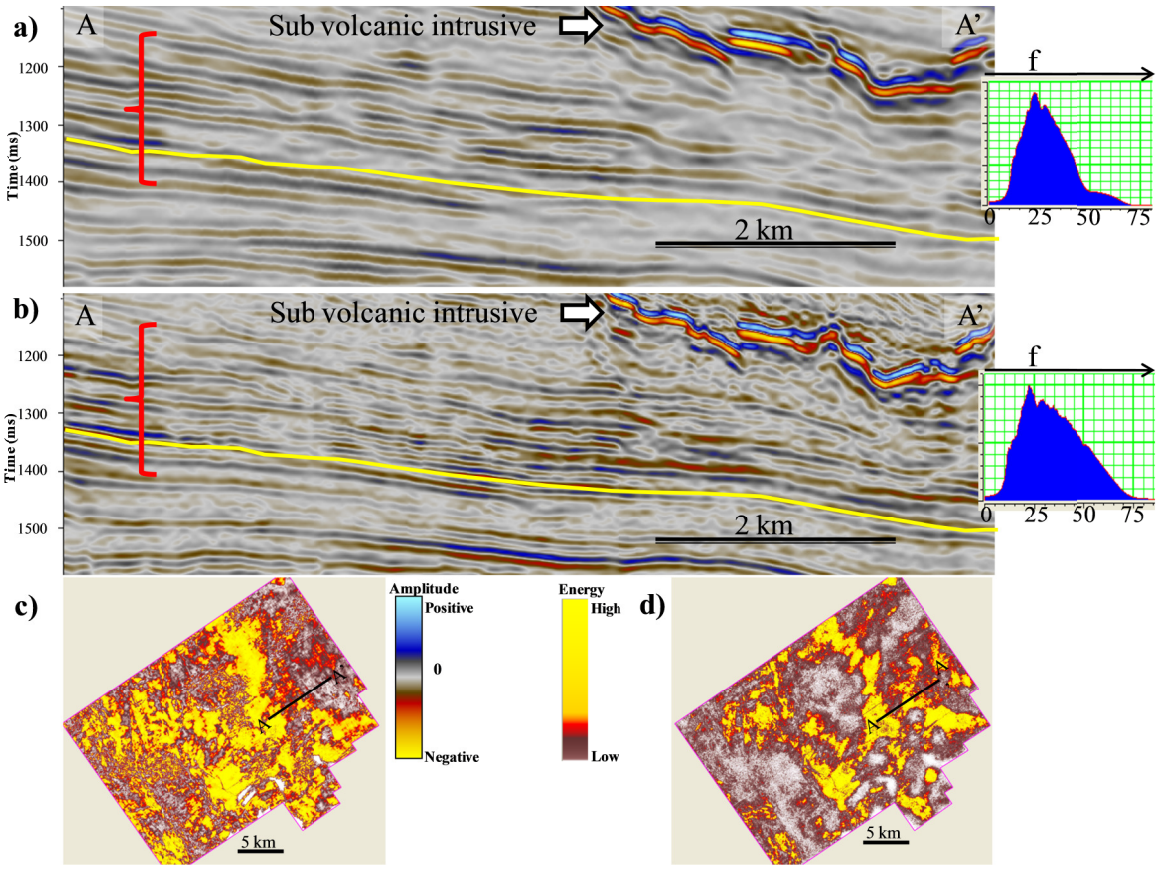

Figure 20. Example of (a) original prestack time migrated vertical seismic amplitude section and (b) the same section after performing residual velocity analysis. Note the improved stratal definition within the Chicontepec interval demarcated by red bracket and also below the shallow volcanic body. The frequency spectra corresponding to each volume indicates significant frequency enhancement. (c) and (d) represents equivalent coherent energy slices along the yellow horizon in (a) and (b).

Prestack structure oriented filtering

After flattening, I applied structure oriented filtering on each of the prestack time-migrated common offset gathers using a workflow described by Kwiatkowski and Marfurt (2011) (Figure 21). This approach uses a consistent estimate of reflector dip and coherence computed from the stacked volumes used for each common offset volume. For these data a 20% alpha trimmed mean filter reflector dip was used to filter the data of relatively high coherence, thereby preserving low coherence lateral discontinuities.

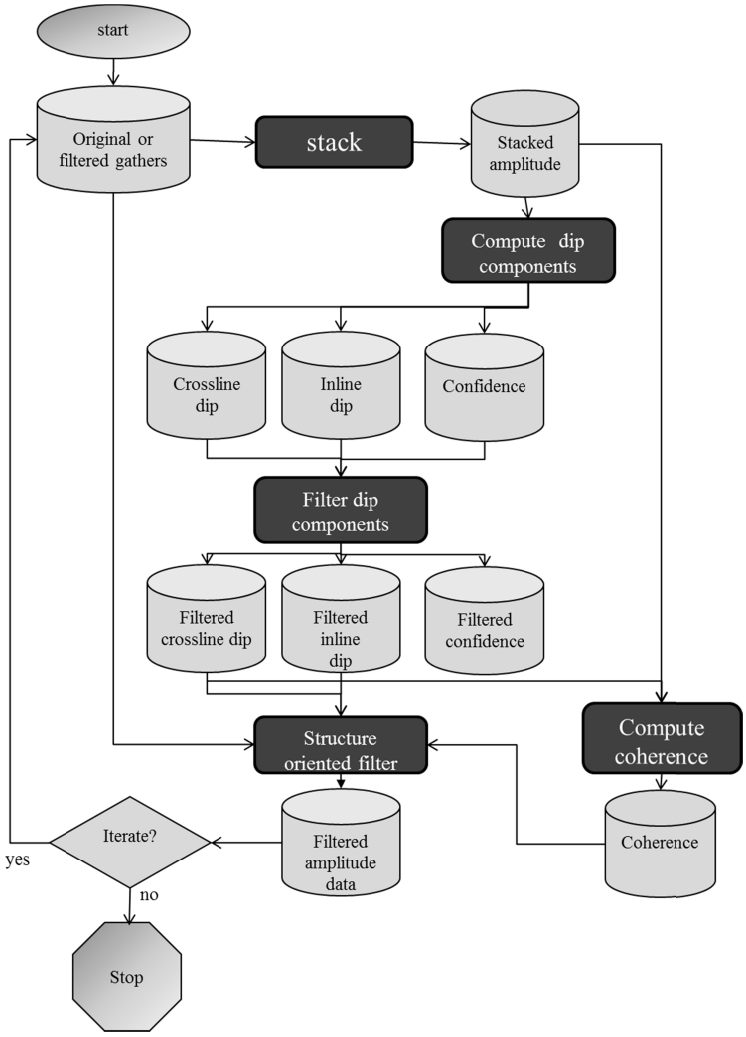

Figure 21. Prestack structure oriented filtering steps for preconditioning of seismic gathers (after Kwiatkowski and Marfurt, 2011).

The result is a signal-enhanced common reflection point gathers suitable for prestack inversion analysis (Figure 22).

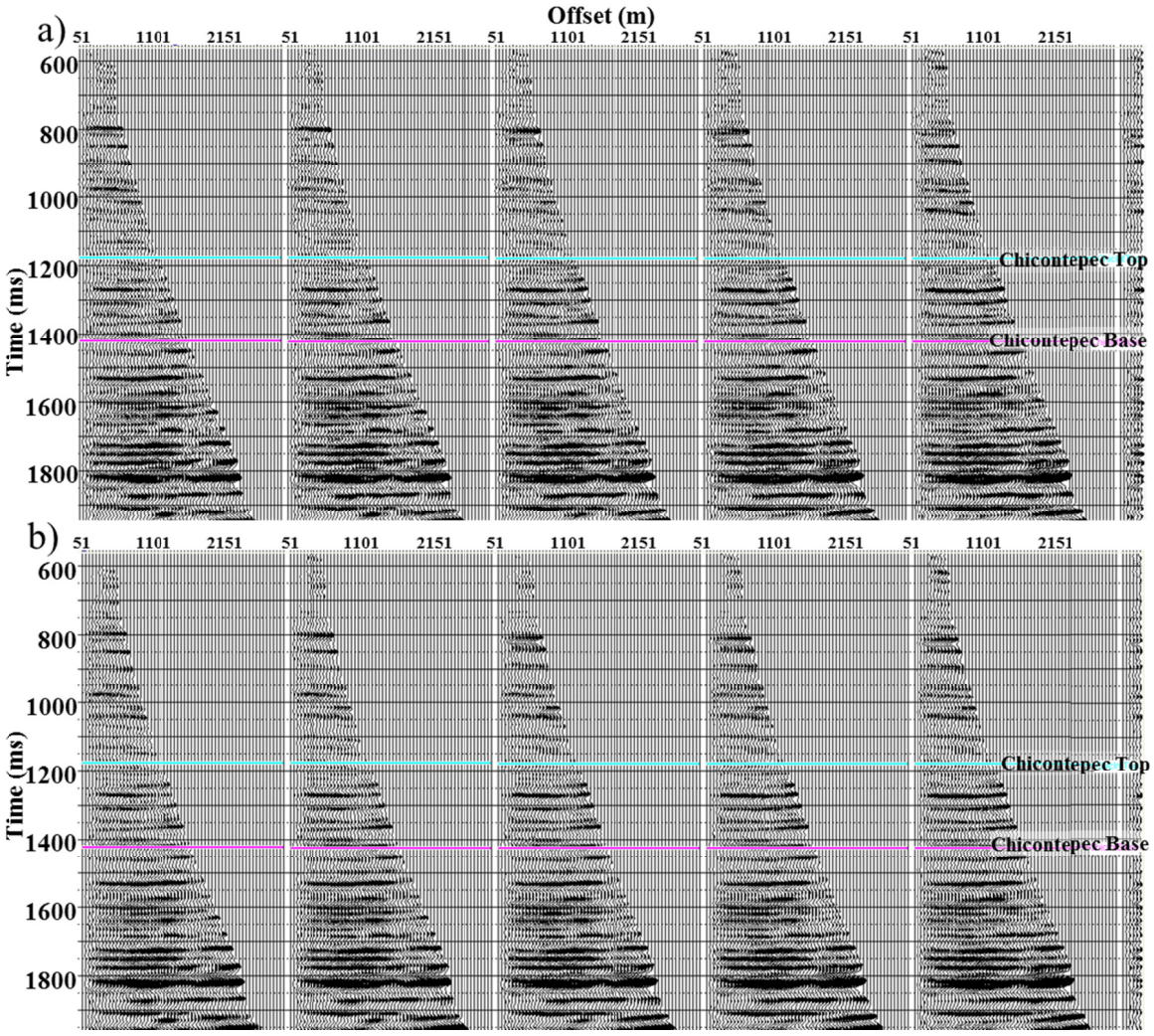

Figure 22. Migrated CRP gathers (a) before and (b) after applying prestack structure oriented filtering to common offset volumes. Note the cleaner data within the Chicontepec reservoir zone marked by the cyan and magenta horizons.

Simultaneous angle-dependent inversion

Analysis of the petrophysical properties of the Chicontepec reservoir rocks revealed that the best properties for delineating prospective intervals within the

Chicontepec reservoirs are the rigidity, μ, and the V_P/V_S ratio, and the best, poor and non reservoir zones separate out nicely in the $\lambda\rho$-$\mu\rho$ space. To estimate these properties from surface seismic data, I performed simultaneous angle-dependent inversion (Hampson et al., 2005) on the preconditioned prestack CRP gathers. This inversion technique is based on Fatti et al.'s (1994) modification of Aki and Richard's (1980) approximation of the Zeoppritz equations. Goodway et al. (1997) have shown this approximation to be successful in extracting P- and S-wave impedance reflectivities from prestack CMP (common midpoint) gathers. The inversion process involved following five steps:

i) selecting tie wells across the seismic survey,

ii) angle gather generation,

iii) extracting wavelets and well seismic tie,

iv) modeling the low frequency component of Z_P and Z_S from well logs and seismic horizons,

v) inverting the seismic data,

Selecting tie wells across the seismic survey

I selected 20 wells representing both good and bad production across the seismic survey to tie the seismic data and provide the low frequency Z_P and Z_S components not measured by the seismic experiment. Ideally each of the wells has shear wave (or dipole sonic) as well as compressional wave logs. Since all the wells did not have dipole sonic information, I had to estimate the shear wave properties for those wells through correlation techniques. The popularly used Castagna's equation (analyzed from water saturated and dry elastic silicate sedimentary rocks) to estimate S- wave information from

P-wave information is not applicable to the highly cemented and carbonate rock fragment-rich Chicontepec rocks. Therefore, I derived a relationship between P and S wave slowness (Figure 23) from multiple wells with dipole sonic logs across the northern part of the Chicontepec basin.

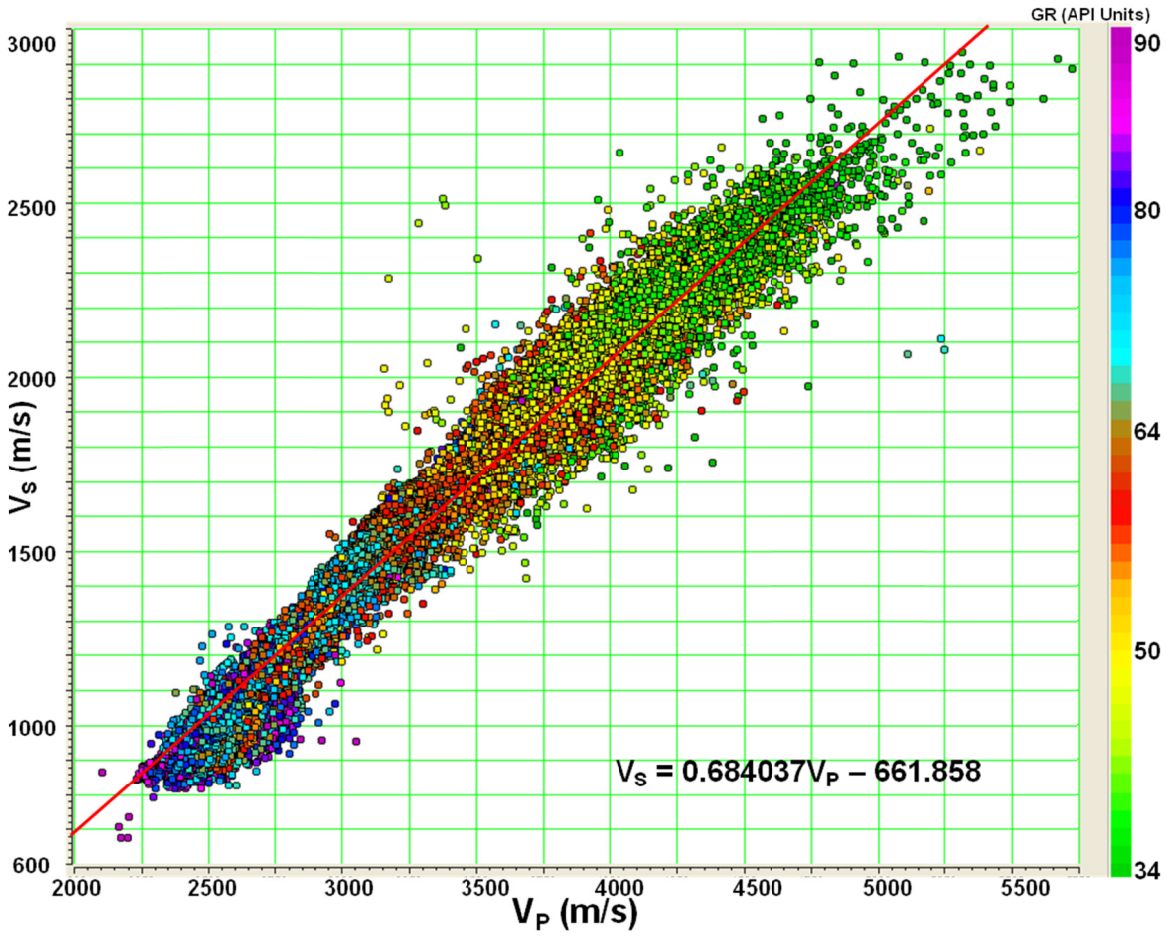

Figure 23. Estimating the relationship between V_P and V_S for the Chicontepec basin from well control in order to predict dipole sonic logs where they do not exist.

Angle gather generation

Aki and Richards (1980) showed that PP and PS reflectivity behaves linearly as a function of $\sin^2\theta$. Fatti et al. (1994) recast the Aki and Richards equations to estimate P- and S-wave impedances. Hampson et al. (2005) used Fatti et al.'s (1994) equation to

extend the principles of model-based poststack inversion (Russell and Hampson, 1991) to prestack domain and proposed the methodology for simultaneous prestack inversion. I used the RMS velocity volume obtained from the residual velocity analysis to convert the gathers from offset to angle domain.

Extracting wavelets and well correlation

Angle-dependent wavelets were extracted for each of three limited angle gathers (near angle stack: 0-11°, mid angle stack: 12-22° and far angle stack: 23-33°, Figure 24) by tying the seismic gathers to the wells with synthetic seismograms. The wells tie well within the Chicontepec interval with correlation coefficients .73 -.95 (Figure 25).

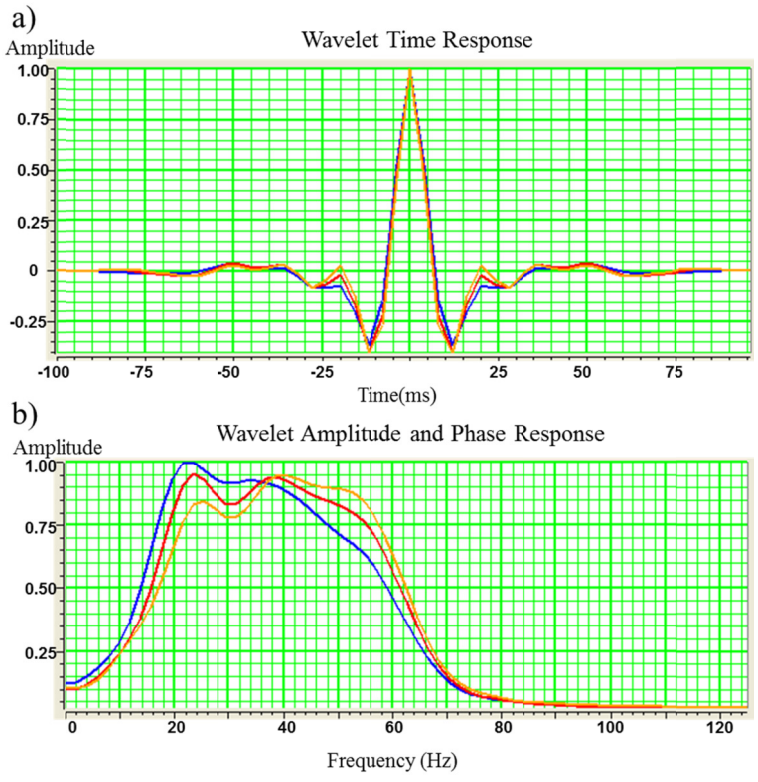

Figure 24. Angle dependent statistical wavelets extracted from the angle gathers (within the Chicontepec reservoir interval) and their corresponding frequency spectra. Orange: Near angles (0-11°); Red: Mid angles (12-22°); Blue: Far angles (23-33°).

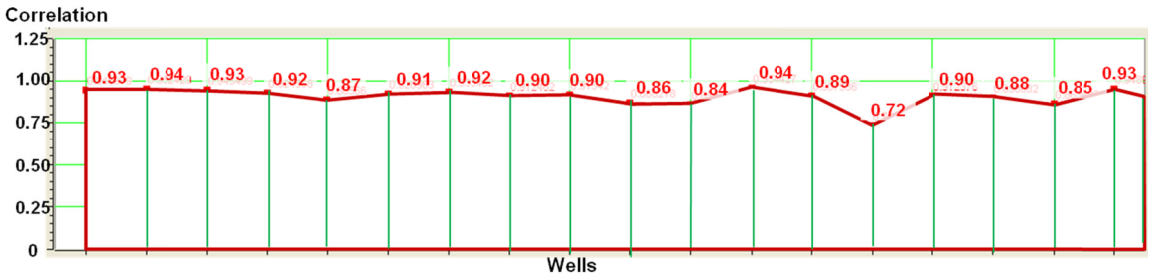

Figure 25. High correlation (R^2 = .90) between the synthetics in the initial model for the prestack inversion and the original angle gathers within the Chicontepec reservoir interval.

Low frequency modeling

The low frequency (< 15 Hz) model for Z_p and Z_s are obtained from the well logs and picked seismic horizons through a krigging process. The low frequency model for Z_s corresponding to line AA' is shown in Figure 26.

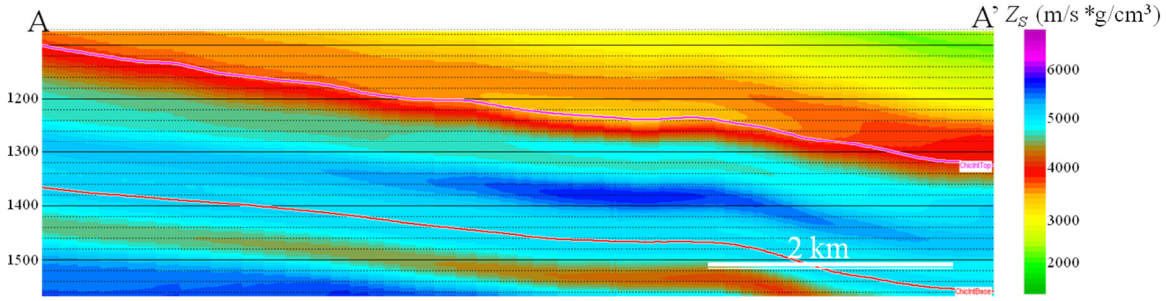

Figure 26. Low frequency model for ZS corresponding to Line AA' shown in Figure 20

Results

Simultaneous inversion was performed on the prestack gathers resulted in P-impedance (Z_p), S-impedance (Z_s) as well as (a less reliable) density volumes. To quality control the inversion process, traces from the inversion volumes were compared at random well locations (both used and unused in the background construction model), which indicated a good match between the original logs and inverted traces for Z_p, Z_s, V_P/V_S, and density (Figure 27). This quality check indicates that the inverted volumes can be

used for rock properties analysis throughout the volume. Figure 28 shows vertical slices along AA' through the Z_P and Z_S volumes corresponding to figures 26 and 20.

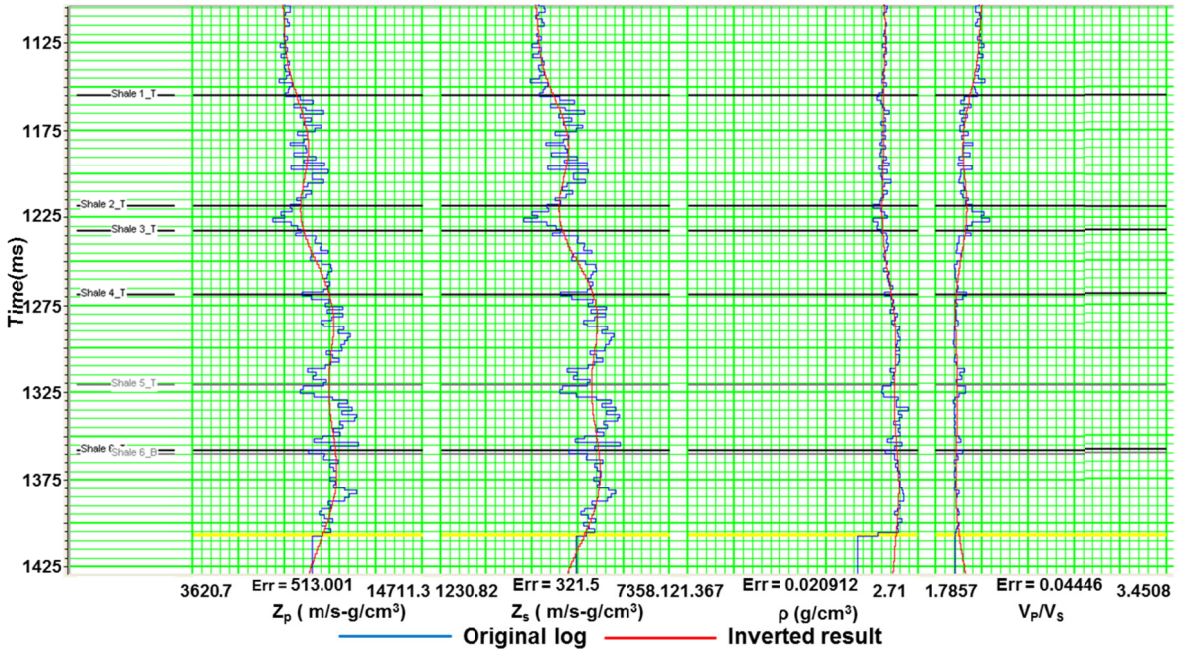

Figure 27. Comparison between original well logs and traces from the inverted property cubes generated from simultaneous prestack inversion, at a well D.

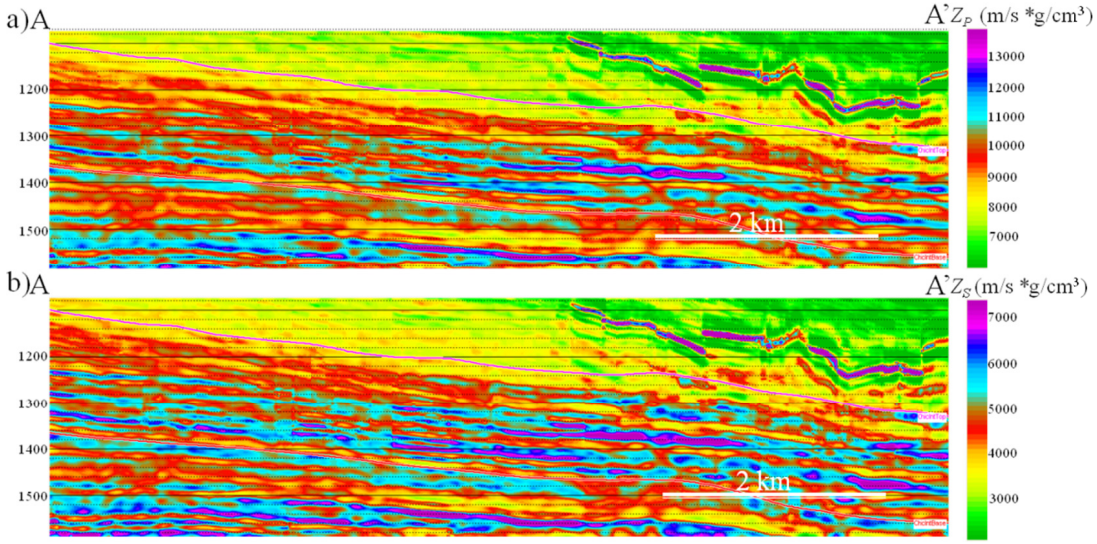

Figure 28. Vertical slices along AA' through the Z_P and Z_S volumes.

INTERPRETATION

Volumetric prediction of rock type

The previous well log rock properties analysis (Figure 12) showed that the productive zones within the Chicontepec interval fell within a specific range of computing $\mu\rho$, $\lambda\rho$ and V_P/V_S values. Computing $\mu\rho$ and $\lambda\rho$ cubes from Z_p and Z_s:

$$\mu\rho = Z_s^2 \qquad (5)$$

$$\lambda\rho = Z_p^2 - 2Z_s^2 \qquad (6).$$

The data points from these computed volumes show a similar distribution in $\lambda\rho$- $\mu\rho$ space (colored by two-way time) to the well data in Figure 12 within the Chicontepec Formation (Figure 29). This similarity is also an indicator for the quality of the inversion process.

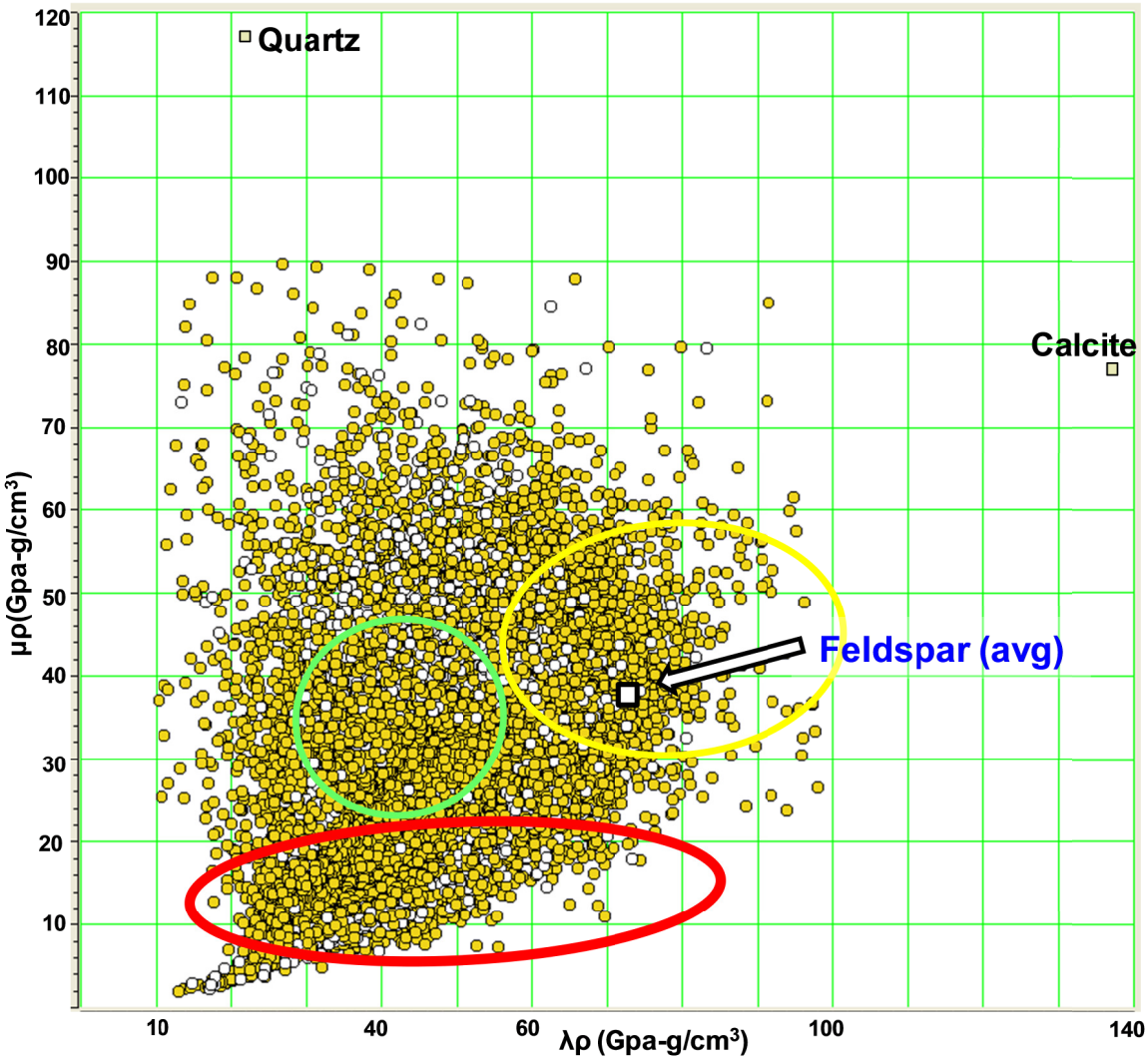

Figure 29. Seismically estimated *λρ-μρ* crossplot from points within the Chicontepec reservoir interval plotted using the same scale as in Figure 12 with the values of pure quartz, calcite and average feldspar. The lithology polygons from Figure 12 have been transferred to this crossplot.

Spatial correlation of rock type and facies distributions.

Through the use of 3D seismic visualization I can highlight voxels having $\lambda\rho$-$\mu\rho$ values corresponding to potential reservoir zones. Figure 30 and 31 shows each of the five stratigraphic units shown in Figures 5 and 6. I also correlated the seismic geomorphologic interpretation with the trends from seismic inversion results in Figure 32.

2D color bar technique for visualization

Transferring values from Figure 29, I analyzed the prospective areas within a stratigraphic unit along stratal slices, where $\lambda\rho$, $\mu\rho$ and V_P/V_S ratio values are plotted from the inverted rock property cubes. Using transparency applied to a 2D color bar I highlighted ranges in $\lambda\rho$-$\mu\rho$ space I analyzed from the petrophysical analysis which corresponds with the V_P/V_S ratio range determined for the good reservoir zone (1.7-1.94)(Figures 30, 31).

The changes in color in the 2D hue-lightness color bar generated for this analysis indicate the change in $\lambda\rho$ values, whereas the intensity of a particular color is represented by an increasing $\mu\rho$ value (Figures 30, 31). As each stratigraphic unit is characterized by a unique set of $\lambda\rho$ and $\mu\rho$ values, the prospective zone is visualized by making the non-prospective areas corresponding to the rest of the values transparent. Figure 30a shows the 2D color bar used for analyzing the points from Chicontepec reservoir interval in $\lambda\rho$-$\mu\rho$ space, where the grayed area represents the transparency applied to the values that fall outside the interest zone corresponding to the potential prospective units for unit A. The product is a potential pay zone map corresponding to the stratal slice from unit A (Figure

30b). Figure 31 shows the transparency applied color bars corresponding to the stratal slices from stratigraphic units B-E and the potential pay zone maps.

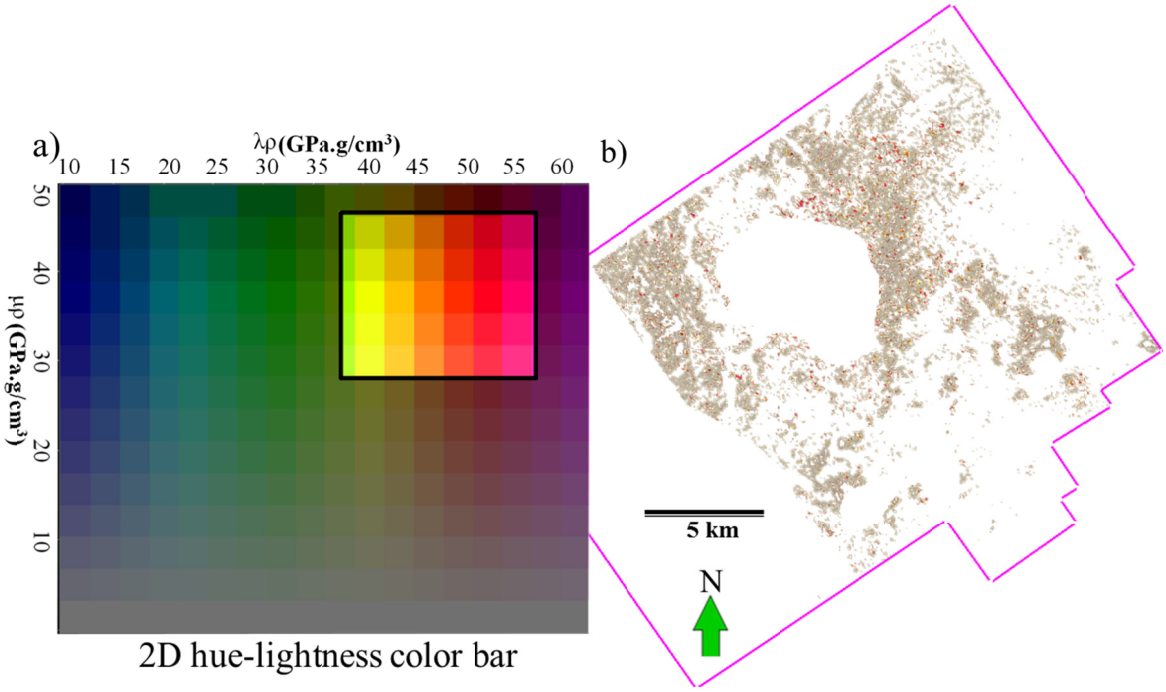

Figure 30. (a) The 2D hue-lightness color bar used for analyzing the points from Chicontepec reservoir interval in the *λρ-μρ* space. Grayed zone indicates the areas corresponding to the values outside the interest zone in *λρ-μρ* space defined for stratigraphic unit A. (b) Potential pay zone map on a stratigraphic unit A stratal slice through the *λρ-μρ* volume using the transparency applied 2D color bar in (a).

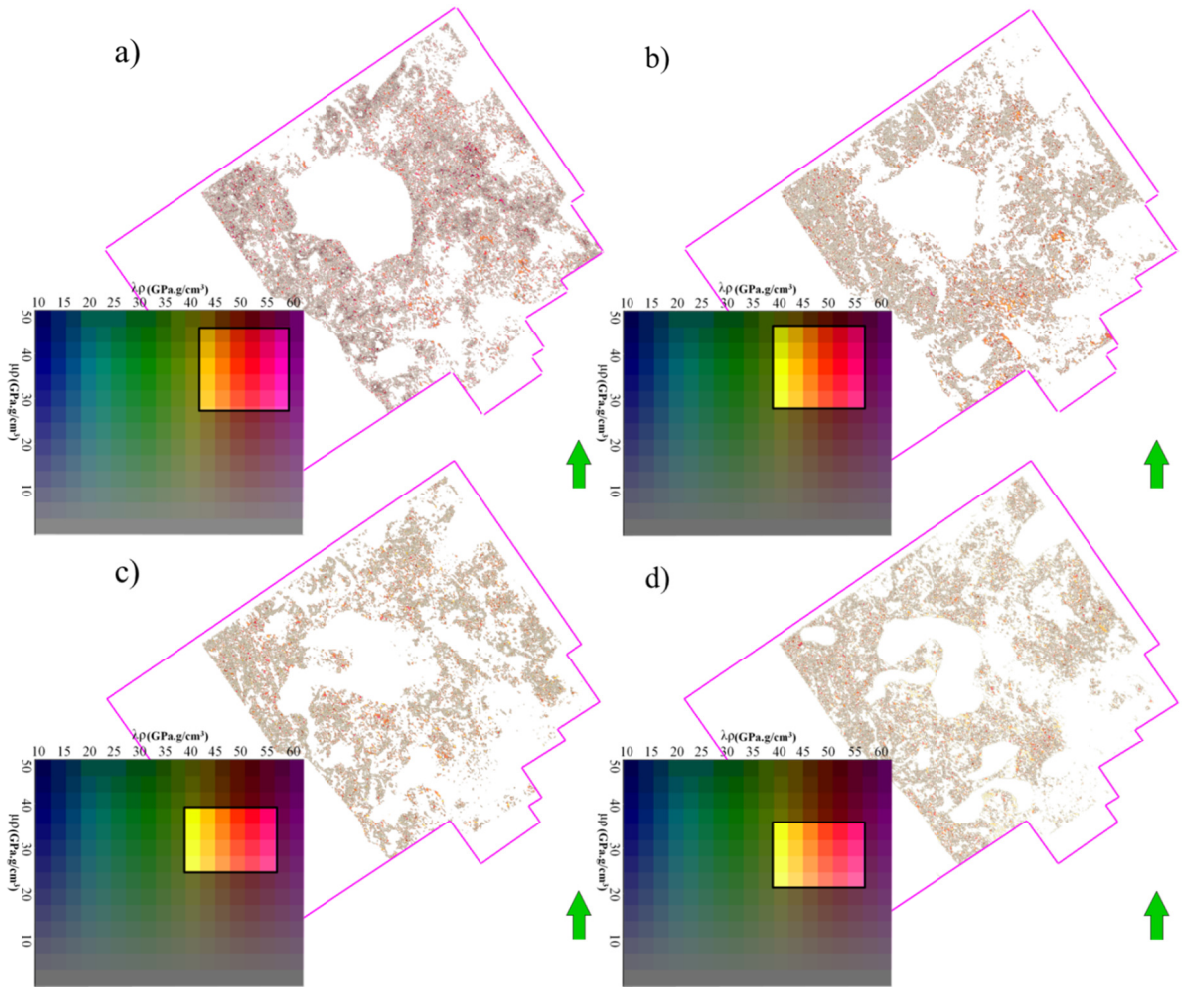

Figure 31: (a)-(d) Represent the potential pay zone map respectively for stratigraphic units B-E obtained from the prestack inversion driven *λρ-μρ* volumes and using the transparency applied 2D color bar. The grayed area in the color bars in (a)-(d), represent the zones that made transparent to display the prospective areas.

The stratal slices used in Figures 30 and 31 are the same slices used in Figure 6 for stratigraphic analysis. I superimposed the potential pay zone maps for the stratigraphic units A-E from Figure 30 and 31 on the facies distribution maps in Figure 6 to relate the potential reservoir distribution with respect to the interpreted deepwater architectural elements (Figure 32). The reasonably good correlation of the potential pay zones with the turbidite facies units validates both the stratigraphic analysis and the reservoir characterization process. Some of the architectural elements show lack of continuity of reservoir zone across them indicating to the character of the Chicontepec reservoirs spread as several small fields with little lateral continuity. One of the possible reasons is lateral variation in carbonate, clay content and cementation due to complex interaction of several flows from different directions.

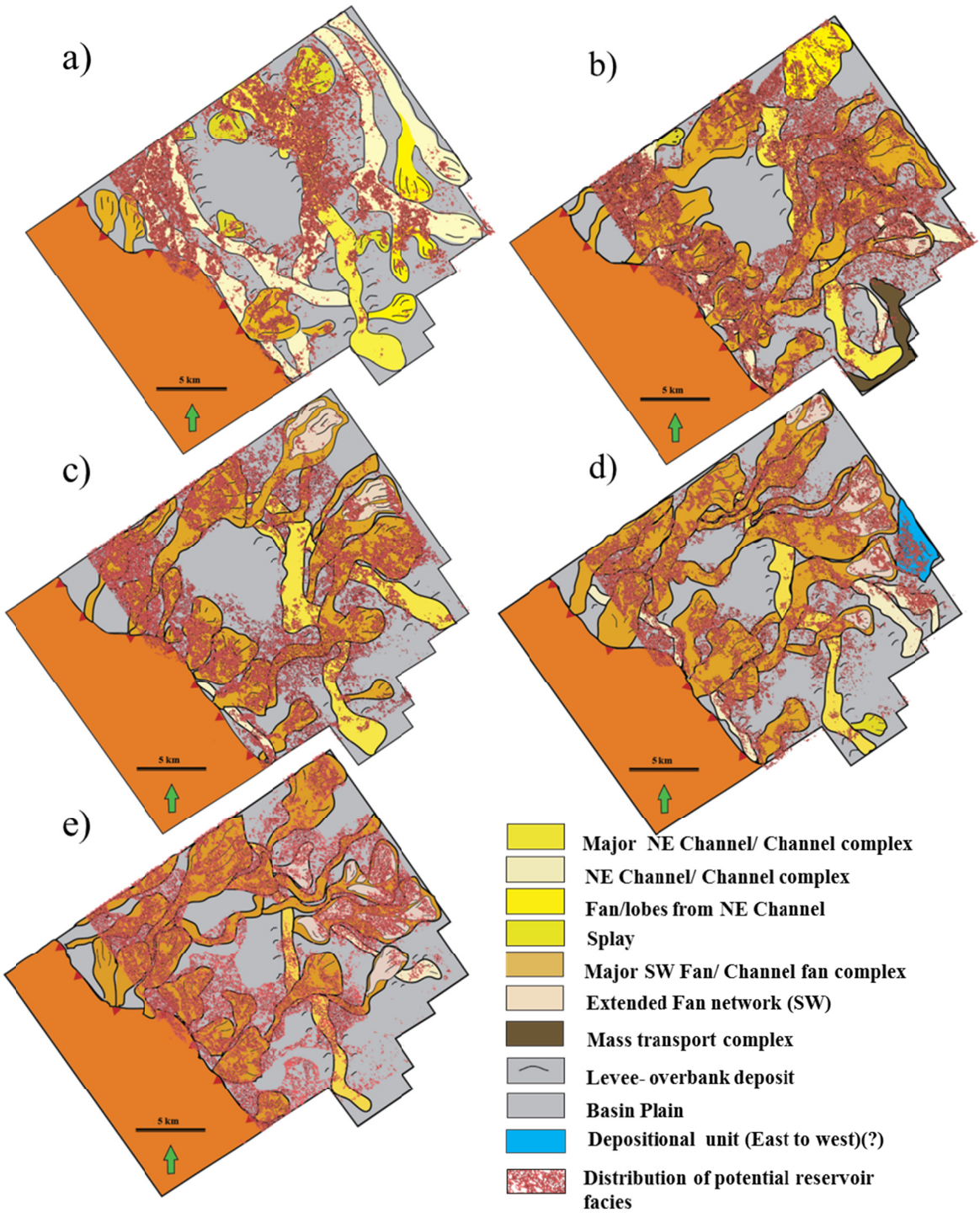

Figure 32. (a)-(e) Distribution of potential good reservoir facies (shown in red points) from Figures 29 and 30 plotted using transparency against the interpreted deepwater facies distribution maps along stratigraphic units A-E shown in Figure 6.

Correlation with production

The best way to evaluate the prospective zones interpreted from the seismic reservoir characterization process is to compare with the cumulative production data available. I drew polygons on each stratal slice shown in Figure 30 and 31 encompassing the potential pay zones. Polygons corresponding to each stratigraphic unit are represented by a unique color. Figure 33 shows areas in green where at least four polygons from the different stratigraphic zones overlap. These zones should coincide with better cumulative production areas. where I have available production information. Since the wells started operating between 1969 and 2008, a good estimate of production is the cumulative production of first six months; plotted as yellow circles, where the radius of the circle is directly proportional to first six months production.

Note the overlap of the green polygons with the first six months of relative cumulative production. The majority of the areas, with well information coincide with the wells with better production (Figure 34).

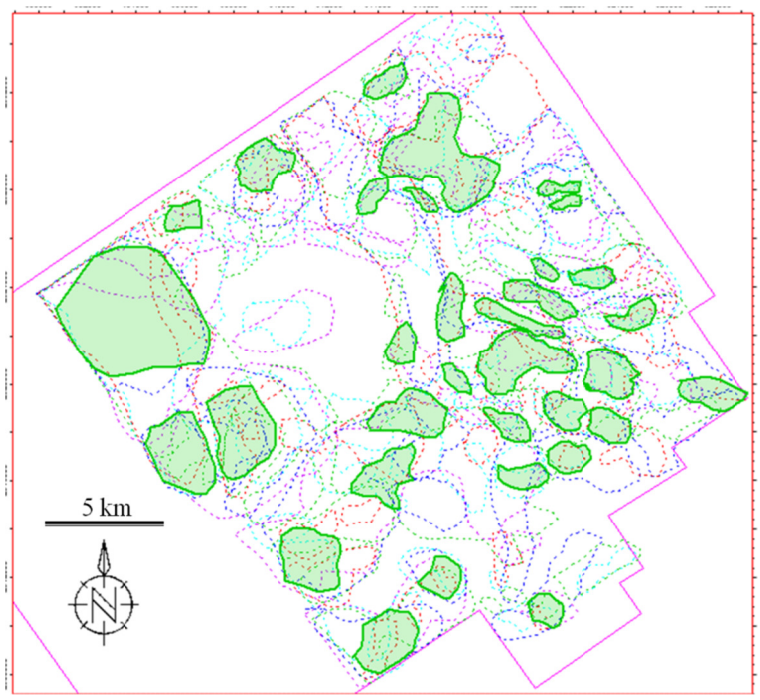

Figure 33. Potential stacked pay obtained by projecting prospective polygons from all the stratigraphic units. Green polygons indicate at least four levels of stacked pay.

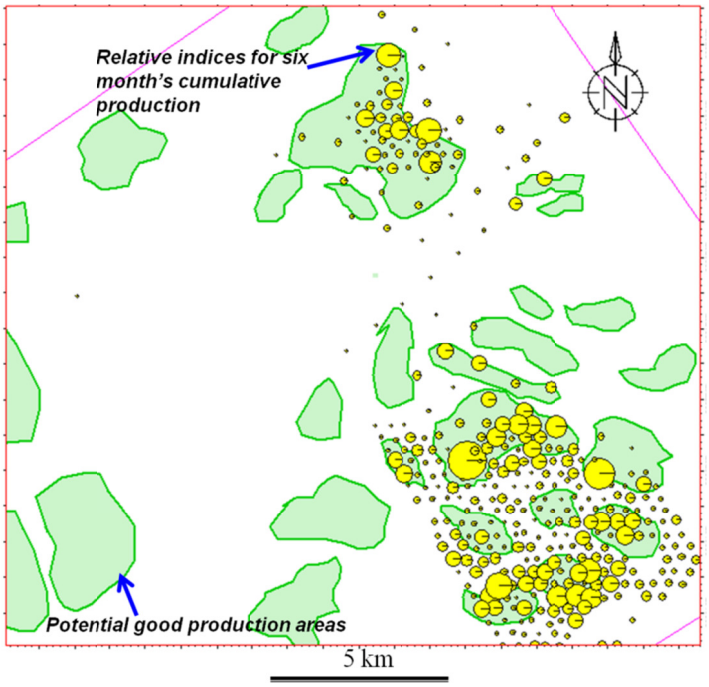

Figure 34. Zoomed area of predicted pay shown in Figure 33 plotted against six month's cumulative production. (Scaled production shown due to data sensitivity). Magenta lines indicate survey boundary.

CONCLUSIONS

Seismic reservoir characterization has potential to significantly improve the understanding of the complex, tight and mineralogically immature Chicontepec oil reservoirs. A similar methodology can be adopted for other tight reservoirs as well. Integration of seismic geomorphology with stratigraphic correlation constrained by chronostratigraphic records showed the Chicontepec interval in the northern part of the Chicontepec basin to consist of five stratigraphic units, equivalent to 3rd order global stratigraphic sequences. The deepwater patterns within these stratigraphic units revealed complex interaction between axis-parallel and axis-perpendicular flow within the elongated foreland basin. Petrophysical analysis indicates the productive interval within a small window in $\lambda\rho$- $\mu\rho$ space, corresponding to rock types with good fracability. Residual velocity analysis and application of structure-oriented filtering was key to improving both vertical resolution and the signal-to-noise ratio of the prestack gathers. Calibration of prestack simultaneous inversion $\lambda\rho$-$\mu\rho$, V_P/V_S volumes with the petrophysical analysis provides a volumetric estimation of rock type, which allowed the differentiation of shales and highly cemented sandstone from the less cemented reservoir sandstone. Further linkage of these rock types with the seismic geomorphology and facies distribution maps provide a means to extrapolate currently-productive areas beyond the well control. The final product is a predicted stacked pay map showing four or more potential reservoir units that can be used statistically to reduce risk and update statistics with more drilling.

REFERENCES

Abbaszadeh, M., T. Shimamoto, F. M. Sandria, D. H. Zamora Guerrero and F. Rodriguez de la Garza, 2003, Integrated Geostatistical Reservoir Characterization of Turbidite Sandstone Deposits in Chicontepec Basin, Gulf of Mexico: Proceedings of the Society of Petroleum Engineers Annual Technical Conference and Exhibition, October 5-8, Denver, Colorado, U.S.A.,15p, SPE paper 84052.

Aki, K., and P.G. Richards, 1980, Quantitative seismology: Theory and methods:**1**,W.H. Freeman and Company.

Bermúdez, J. C., J. Araujo–Mendieta, M. Cruz–Hernández, H. Salazar–Soto, S. Brizuela–Mundo, S. Ferral–Ortega, and O. Salas–Ramírez, 2006, Diagenetic history of the turbiditic litharenites of the Chicontepec Formation, northern Veracruz: Controls on the secondary porosity for hydrocarbon emplacement: Gulf Coast Association of Geological Societies Transactions, **56**, 65–72.

Busch, D.A., and S.A. Govela, 1978, Stratigraphy and structure of Chicontepec turbidites, southeastern Tampico–Misantla Basin: AAPG Bulletin, **62**, 2, 235–246.

Cheatwood, C. J., and Guzmán, A. E., 2002. Comparison of reservoir properties and development history – Spraberry Trend Field, west Texas and Chicontepec Field, Mexico, Proceedings SPE International Petroleum Conference and Exhibition, Villahermosa, Mexico, 19p, SPE Paper 74407.

Close, D., S. Stirling, D. Cho, and F. Horn, 2010, Tight Gas Geophysics: AVO Inversion for Reservoir Characterization: CSEG Recorder, **35**, 28-35.

Cossey, S. P. J., 2008, Debrites in the Chicontepec Formation, Tetlahuatl, Mexico in Nilsen, T. H., Shew R. D., Steffens, G. S., and Studlick, J. R. J., eds., Atlas of Deep-Water Outcrops, AAPG Studies in Geology **56**, 231-234.

Daniel, G and J. H. Dowell, 1980, Fundamentals of fracturing: Proceedings of the SPE Cotton Valley symposium, 8p. SPE Paper 9064-MS.

Debski, W. and A. Tarantola, 1995, Information on elastic parameters obtained from the amplitudes of reflected waves: Geophysics, **60**, 1426-1436.

Donnelly, J., 2009, Mexico's Challenge: Journal of Petroleum Technology, **62**, 16.

Fatti, J.L., G.C. Smith, P.J. Vail, P.J. Strauss, and P.R. Levitt, 1994, Detection of gas in sandstone reservoirs using AVO analysis: a 3D Seismic Case History Using the Geostack Technique: Geophysics, **59**, 1362-1376.

Folk, R.L., 1965, Petrology of Sedimentary Rocks: Hemphill Publishing Company.

Geetan, R., B. Hornby and R. Wardhana, 2011, Seismic Technologies for Unconventional Reservoir Characterization: Wamsutter Field Case Study: American Association of

Petroleum Geologists, Abstracts with Program, Annual Convention, April 10-13, CD-ROM publication.

Goodway, B., T. Chen, , and J. Downton, 1997, Improved AVO fluid detection and lithology discrimination using Lame petrophysical parameters; "λρ ", "μρ", & "λ/μ fluid stack", from P and S inversions: 67th Annual international Meeting of the SEG; Expanded Abstracts, 183-186.

Gray, F., D., and E. C. Andersen, 2000, Case histories: Inversion for rock properties: Proceedings of the EAGE 62nd Conference and Technical Exposition, 4p.

Grigg M., 2004, Emphasis on mineralogy and basin stress for gas shale exploration: SPE meeting on Gas Shale Technology Exchange.

Hampson, D. P., B. H. Russell, and B. Bankhead, 2005,Simultaneous inversion of pre-stack seismic data: Proceedings of the 75th Annual international Meeting of the SEG; Expanded Abstracts, 1,633-1,637.

Haq, B. U., J. Hardenbol, and P. R. Vail, 1987, Chronology of fluctuating sea levels since the Triassic: Science, **235**, 1156-1166.

Kwiatkowski, J. T., and K.J. Marfurt, 2011, Data conditioning of legacy pre-stack time migrated gathers from the Mid-Continent: Abstract volume of the AAPG Mid Continent Section Meeting.

Pena, V., S Chávez–Pérez, M. Vázquez-García, and K.J. Marfurt, 2009, Impact of shallow volcanics on seismic data quality in Chicontepec Basin, Mexico: The Leading Edge, **28**, 674-679.

Rojas, E., T.L. Davis, M. Batzle, and M. Prasad, 2005, Vp-Vs ratio sensitivity to pressure, fluid, and lithology changes in tight gas sandstones: 75th Annual international Meeting of the SEG; Expanded Abstracts, 1401-1404.

Russell, B.H., and D.P. Hampson, 1991, "A comparison of post-stack seismic inversion methods": 61st Annual international Meeting of the SEG; Expanded Abstracts, 876-878.

Takahashi, S. , M. Abbaszadeh, K. Ohno and H.S. Soto, 2006, Integrated Reservoir Modeling for Evaluating Field Development Options in Agua Fria, Coapechaca and Tajin Fields of Chicontepec Basin: Pcoceedings of the First International Oil Conference and Exhibition in Mexico, 31 August-2 September 2006, Cancun, Mexico, 14p, SPE paper 103974.

Tobin, R.C., T. Mcclain, R.B. Lieber, A. Pzkan, L.A. Banfield, A.M.E. Marchand and L.E. Mcrae, 2010, Reservoir quality modeling of tight-gas sands in Wamsutter field: Integration of diagenesis, petroleum systems, and production data: AAPG Bulletin, **94**, 1229-1266.

Valentin, D.A., and R.H. Tatham, 2010, Identifying Jurassic tight gas sands in the East Texas Basin with 3D-3C seismic data: 67th Annual international Meeting of the SEG; Expanded Abstracts, 1620-1624.

Chapter 4

Effect of Volcanic Bodies on Hydrocarbon Reservoirs in the North Eastern Part of the Chicontepec Foredeep, Mexico

ABSTRACT

Turbidites of the Chicontepec Formation developed in the elongated Chicontepec foredeep in front of the Sierra Madre Oriental fold and thrust belt during the Paleocene and Eocene. Intrusive and extrusive volcanic events in this convergent tectonic margin add to the complexity of these tight and complex turbidite reservoirs.

The majority of the shallow volcanic bodies in the north-eastern part of the foredeep are in close proximity to the Chicontepec reservoir units. In places, these intrusive and extrusive bodies hinder the reservoir characterization process. Reservoir analogues from the Chicontepec outcrops coupled with an integrated study of the subsurface dataset in the upper part of the reservoir reveals the high potential of these volcanic bodies to create a system of natural fractures in the adjacent sandstone reservoirs resulting in a dual porosity system in some areas.

INTRODUCTION

During the Late Cretaceous Laramide (Cordilleran) Orogeny, the Farallon (Pacific) plate began subducting under the North American plate resulting in island arc complexes along the western margin of Mexico (Morán -Zenteno, 1994; Alzaga-Ruiz et al., 2008). The north-eastward movement of the Farallon plate continued into the Latest Cretaceous and Early Paleocene period. This movement of the Farallon plate accreted and uplifted the Mesozoic sedimentary layers of the former passive margin of Gulf of Mexico forming the Sierra Madre Oriental fold and thrust belt. Tectonic pulses in the Sierra Madre Oriental continued until the Early Eocene (Alzaga-Ruiz et al., 2008). The Chicontepec foreland flexural basin developed in front of this thrust front, with syn-tectonic sedimentation within the foredeep. The Tuxpan platform is situated in the eastern part of the basin (Figure 1).

The Early Paleocene Velasco Formation provided the initial sedimentation within the Chicontepec Foredeep, which was followed by Upper Paleocene Lower Chicontepec deposition. A basin-axis-parallel amalgamated channel system was a major source of sediment in the Lower Chicontepec turbidites. A major tectonic pulse beginning during the late Upper Paleocene initiated syn-tectonic basin-axis-perpendicular sediment flows from the direction of the Sierra Madre Oriental. These basin-axis- perpendicular channel-fan systems were the major contributor to the Middle and Upper Chicontepec Formation. These Paleocene-Eocene turbidites represent tight hydrocarbon reservoirs (porosity: 1% – 10%; permeability: .001– 5 mD) which can be primarily attributed to the mineralogical immaturity of the sandstone and extensive diagenetic processes. In spite of their low

porosity and permeability, the Chicontepec Formation represents one of Mexico's most important hydrocarbon plays.

Tristán-González et al. (2009) summarized the volcanic activities in east- central Mexico from the Late Cretaceous to Miocene (Figure 2). Subduction volcanism dominated the volcanic processes until the culmination of the Laramide Orogeny during Late Eocene time followed by transitional volcanism from Late Eocene to Mid Oligocene, and finally, intraplate volcanism from Mid Oligocene to Mid Miocene (~20Ma).

The burial history chart from the adjacent Veracruz basin (Magoon et al., 2001), where petroleum generation occurred from Upper Jurassic source rocks similar to those in the Chicontepec play, shows that oil generation and migration started around 20 Ma and continued through the Miocene (Figure 3).

As part of a comprehensive reservoir characterization process in the northern part of the Chicontepec basin, my objective is to understand the effect of the Tertiary shallow volcanic bodies on the Chicontepec Sandstones, which form an integral part of the petroleum system. I begin by defining the igneous petroleum system followed by the study of volcanic rock outcrops and the changes in surrounding sedimentary rocks due to the influence of volcanic emplacement. Next, I study the changes in well log patterns within the volcanic bodies as well as within the underlying and overlying contact zones. Then, I use the observation from outcrops and logs to delineate potential prospective zones from volumetric seismic attributes and calibrate the analysis results with some reservoir information. Finally, I discuss and exhibit some petrophysical information

relating to a potential 'dual' porosity system created within the Chicontepec reservoirs as a result of the volcanic influence.

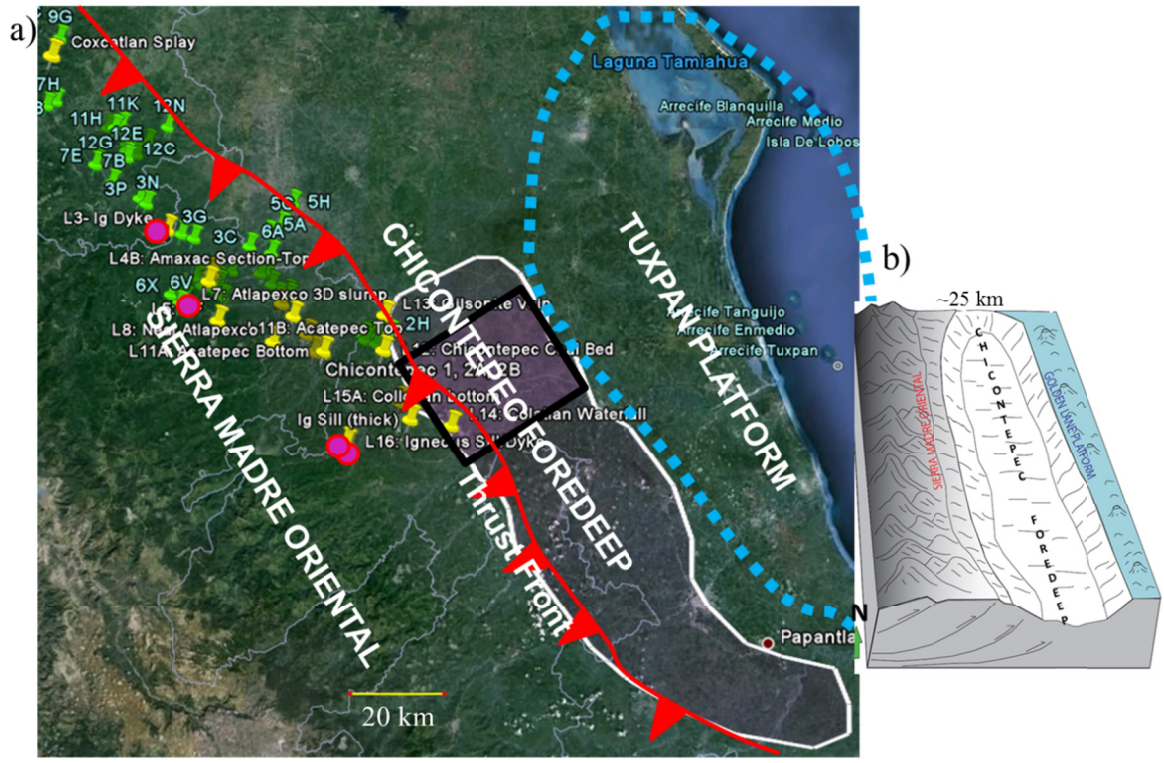

Figure 1. (a) Location of the Chicontepec Foredeep in between the Sierra Madre Oriental fold and thrust belt and the Tuxpan Platform. Yellow and green points indicate several outcrop locations exposing the Chicontepec Formation at the foothills of the Sierra Madre Oriental. Magenta circles show the Chicontepec outcrops with volcanic emplacements analyzed for this study. The white polygon represents the Chicontepec subsurface production area and the black rectangle indicates the outline of the Amatitlan 3D survey used in this study. (b) Schematic diagram of the Chicontepec Foredeep.

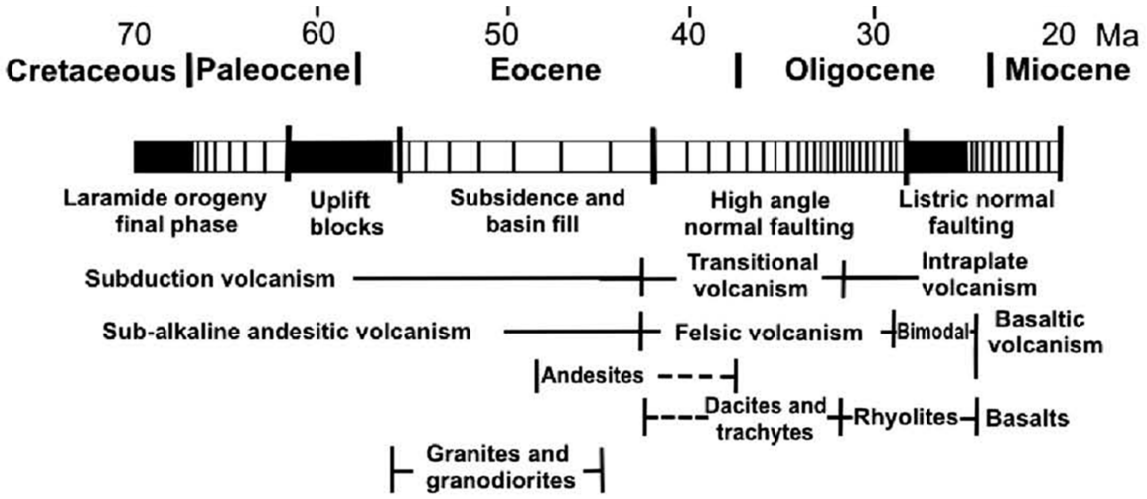

Figure 2. Summary of volcanic events in the Mesa Central in east-central Mexico for the time range between 60 and 20 Ma (after Aguirre-Díaz and McDowell, 1991, and Tristán-González et al., 2009).

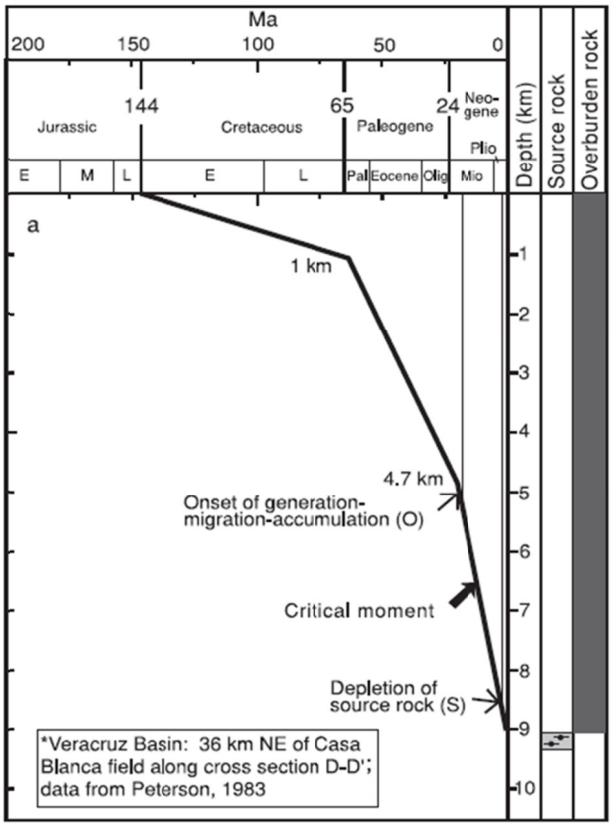

Figure 3. Burial history chart for the Upper Jurassic source rocks in the Veracruz basin (equivalent to the source rocks for the Chicontepec reservoirs). Note the onset of oil generation in the Early Miocene (after Magoon et al., 2001).

IGNEOUS PETROLEUM SYSTEMS

Delpino and Bermudez (2009) classified igneous petroleum systems into two types: Type I consist of igneous rock intruded into a potential source rock, while Type II consists of igneous body been emplaced into another type of sedimentary rock (Figure 4). Type II systems are further classified into three subtypes: IIA, IIB and IIC. Subtype IIA represents the kind of host rock which is originally a well known productive formation throughout a basin. Subtype IIB corresponds to a system in which the sills and laccoliths intrude into a tight formation and syn-intrusive fractures; hot hydrothermal solutions may improve the reservoir quality. In subtype IIC the feeders can act as a trap in the petroleum system. Using this classification, the volcanic bodies intruding the Chicontepec Formation fall into subtype IIB.

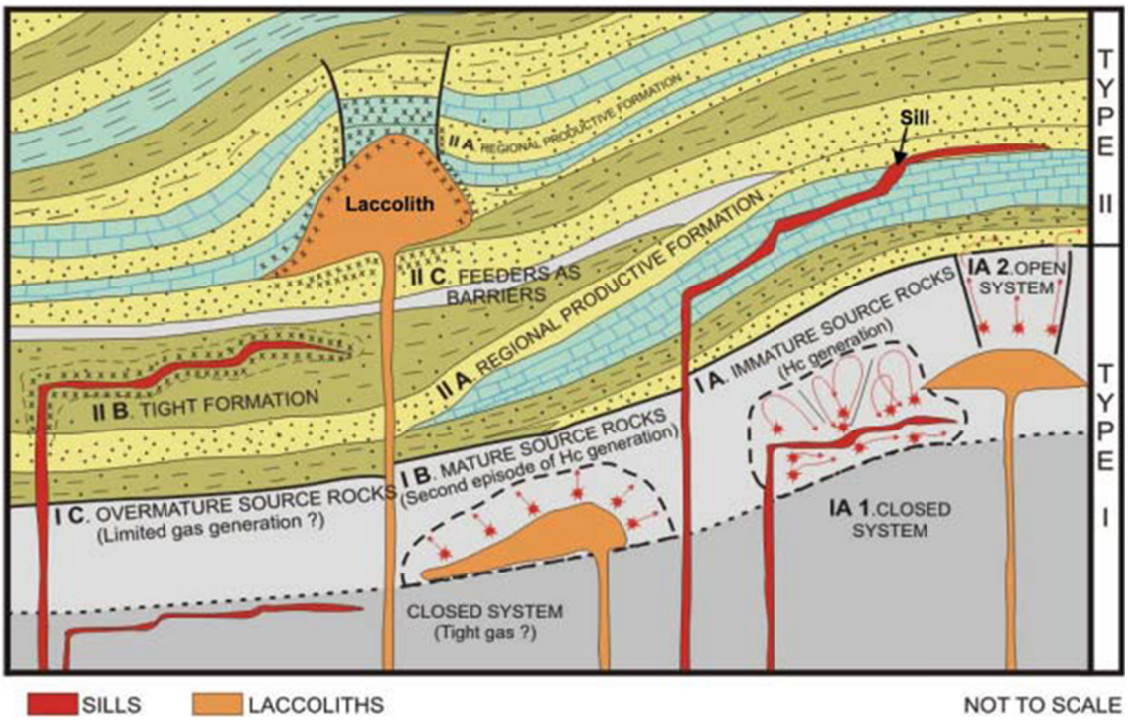

Figure 4. Classification of igneous petroleum systems (Delpino and Bermudez, 2009).

Volcanic bodies in the outcrops

I mapped shallow volcanic bodies including dykes, sills and basaltic lava flows in some of the outcrops exposed in the foothill regions of the Sierra Madre Oriental fold and thrust belt (Figure 5). The majority of the volcanic bodies are characterized by adjacent baked zones and diffused contacts with the underlying and overlying Chicontepec Sandstone. The baked zones are generally highly friable and fractured (Figure 5g). The strata adjacent to the subvolcanic intrusives in most cases exhibit enhancement of fracture intensity (Figure 6). This enhancement is more common in sandstones as compared to shales primarily due to the higher sand brittleness. In many cases the volcanic body itself is highly fractured (Figure 6c), implying its potential for reservoir rock under suitable conditions.

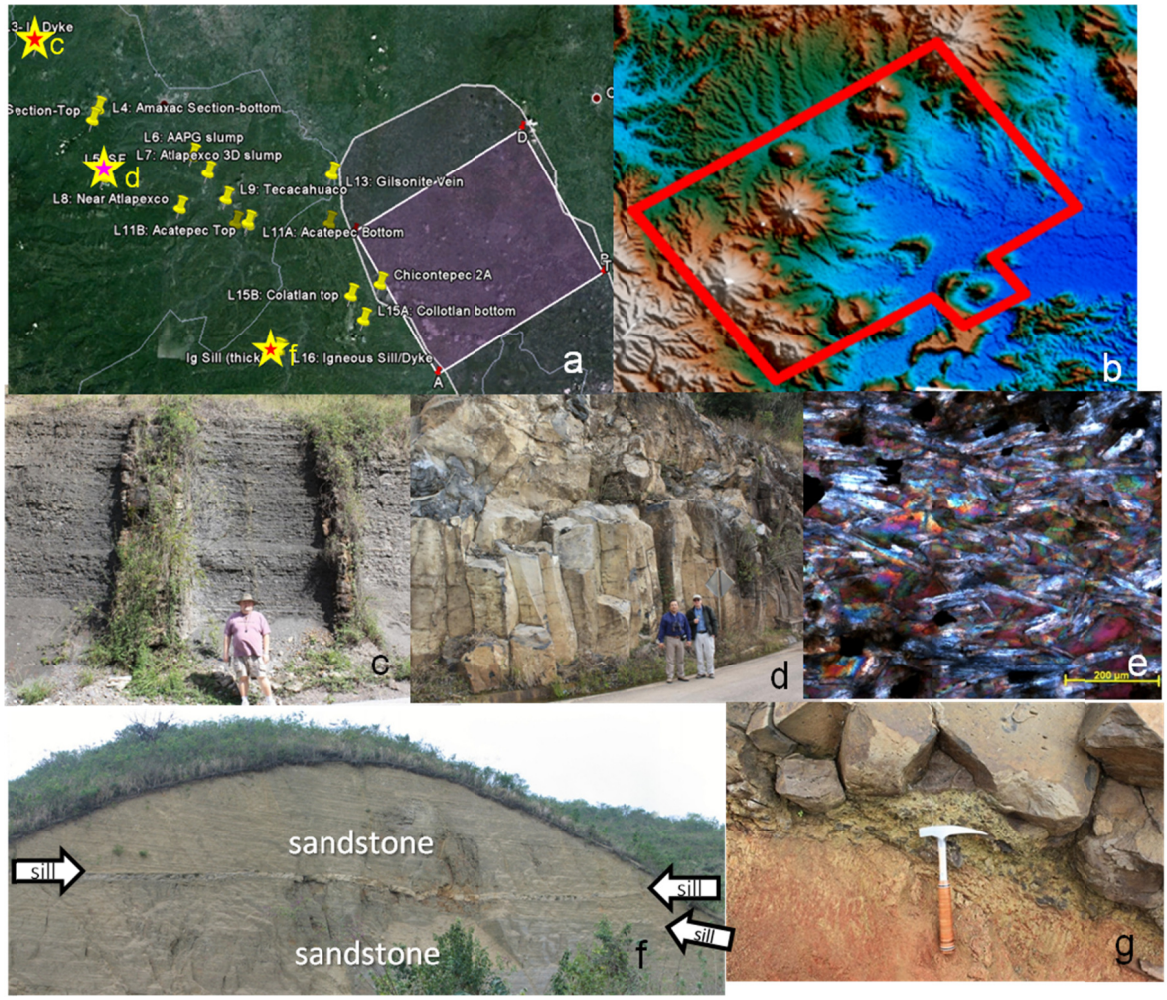

Figure 5. (a) Yellow polygons represent location of the igneous outcrops shown in (c), (d), (f) with respect to the Amatitlan 3D seismic survey. (b) Digital elevation map near the 3D survey (red polygon), exhibits several volcanic mounds. Outcrops of (c) Igneous dykes within a shaly formation, (d) basaltic lava flow showing columnar joints and (e) photomicrograph of the olivine basalt from the outcrop shown in (d). (f) Sills within the Chicontepec Formation. (g) Baked zone at the contact of the basalt outcrop (d) and the Chicontepec Formation.

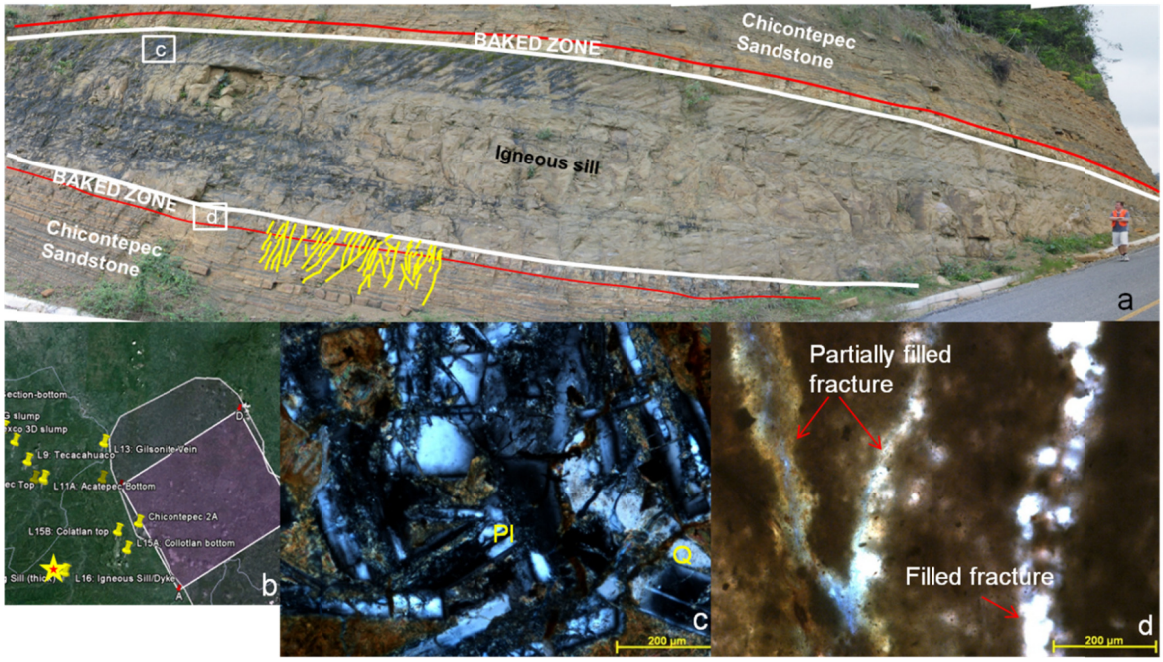

Figure 6. (a) An igneous sill emplaced within the Chicontepec Formation whose location is shown in (b). Yellow lines represent high fracture intensity within the baked zone and the adjacent sandstone. (c) and (d) show photomicrographs from the igneous sill and the baked zone from locations shown with white rectangles in (a). (c) Shows an andesitic rock rich with Plagioclase feldspar, which is highly fractured. (d) Represents the partially filled and filled (with calcite) fracture networks within the baked zone.

Well log pattern

Well log information from the volcanic bodies is very rare in the Chicontepec basin as the wells are generally planned to avoid these bodies. One of the wells that were drilled through such subvolcanic intrusives shows a sharp drop in gamma ray and an increase in resistivity at the contact zone between the sedimentary rock and the volcanic bodies (Figure 7). The most significant observation from this well log suite is the increase in permeability at both the contact zone at the top and bottom of the volcanic body. This observation conforms to the increase in fracture intensity near the volcanic-sedimentary

rock contact zone in some of the outcrops. Thus from both outcrops and well logs there is a significant potential for an increase in permeability due to enhancement of fracture intensity near the contact zones where the volcanic dykes and sills intrude through or are emplaced adjacent to the tight Chicontepec reservoir.

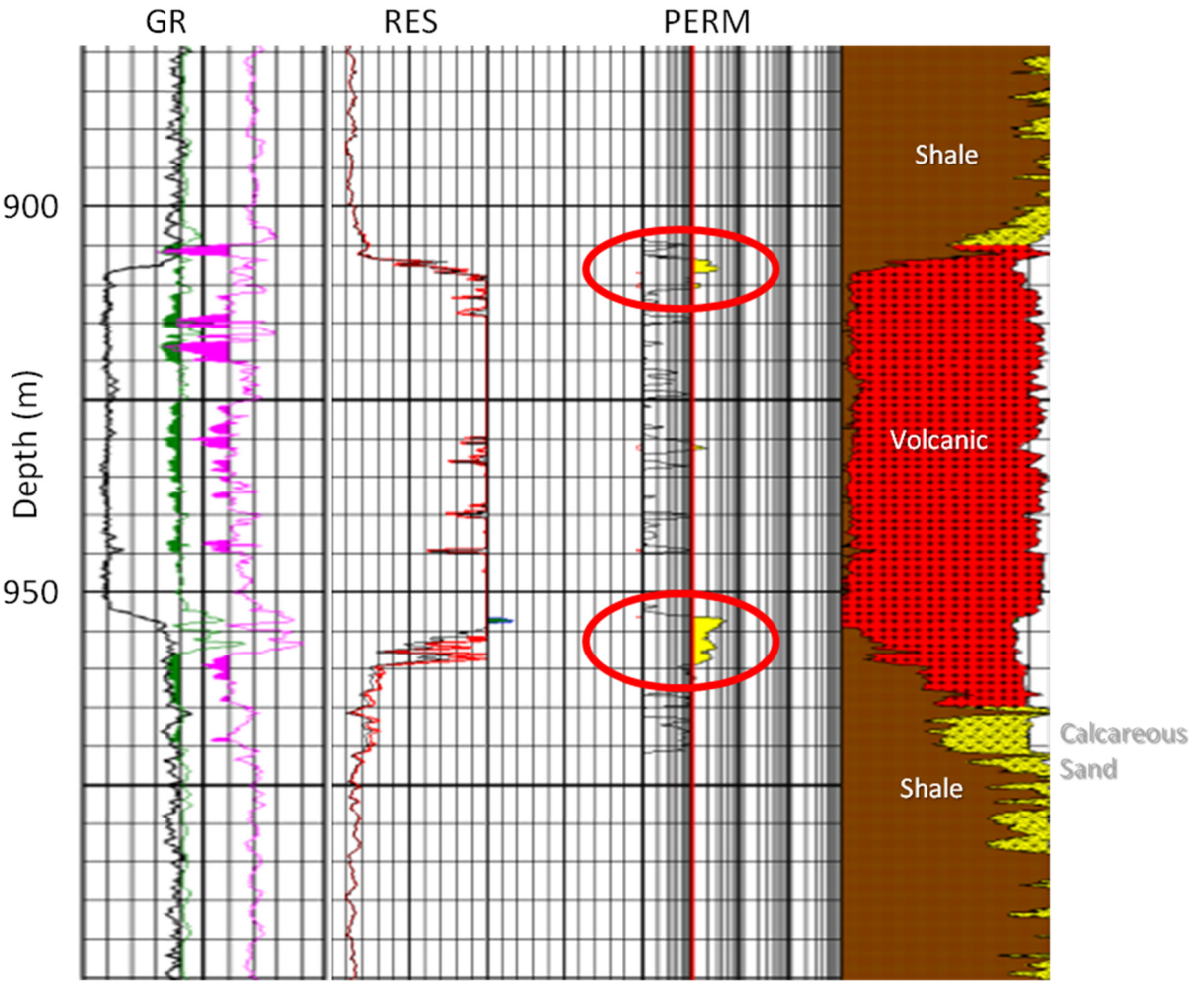

Figure 7. Well log pattern of a subvolcanic intrusive rock within the Chicontepec Formation. Note the increase in permeability (red ellipse) at the contact zone between the volcanic rock and the underlying and overlying Chicontepec Formation.

SEISMIC DATA ANALYSIS

Volcanic geobodies can be easily extracted from the seismic amplitude and derived RMS amplitude volumes as the density and velocity of these layers are significantly higher than those of the adjacent sandstone (Figures 8a and b). I interpreted each of the subvolcanic intrusive bodies near the Chicontepec interval (Figure 8c). In most places, the seismic amplitude immediately below the volcanic bodies could not be interpreted due to velocity pull up and interbed multiples generated by the volcanics. I denote the first reflector below the volcanic bodies that can be interpreted reasonably well throughout the seismic volume as horizon1 (Figure 9). This interpreted horizon is very close to the top of the Chicontepec reservoir zone, and is representative of the contact zone between the volcanics and the Chicontepec reservoir units in general.

Seismic attributes

The outcrop and well log study revealed the significant potential for increased fracture density at the contact zone of the sedimentary and volcanic layers. Likewise, the interpreted seismic attributes at the fracture intensive contact zones will likely represent highly fractured zones near the top of the Chicontepec reservoir strata.

Volumetric curvature attributes (Chopra and Marfurt, 2007) and corendered curvature and coherence attributes (Chopra and Marfurt, 2010) can be effectively used to delineate fracture prone zones along stratal and horizon slices. After computing the curvature and coherence attribute volumes from the Amatitlan 3D seismic volume, I analyzed them along the horizon slice corresponding to ‘horizon1’. Then I mapped the areas near the volcanic bodies where the most negative curvature (short wavelength)

attribute values coincide with the most incoherent values from the coherence attribute (Figure 10). I interpret these zones as potential enhanced fractured areas with improved permeability and reservoir net-to-gross (N/G) ratios. To validate this interpretation, I looked at the post drill reservoir information for the wells as indicated in Figure 10 within and outside the mapped zones. Comparison between the equivalent stratigraphic units towards the top of the reservoir zone among these wells show that the wells within the mapped volcanic influenced zones show relatively higher net-to-gross ratio than the wells outside the mapped zones (Figure 10).

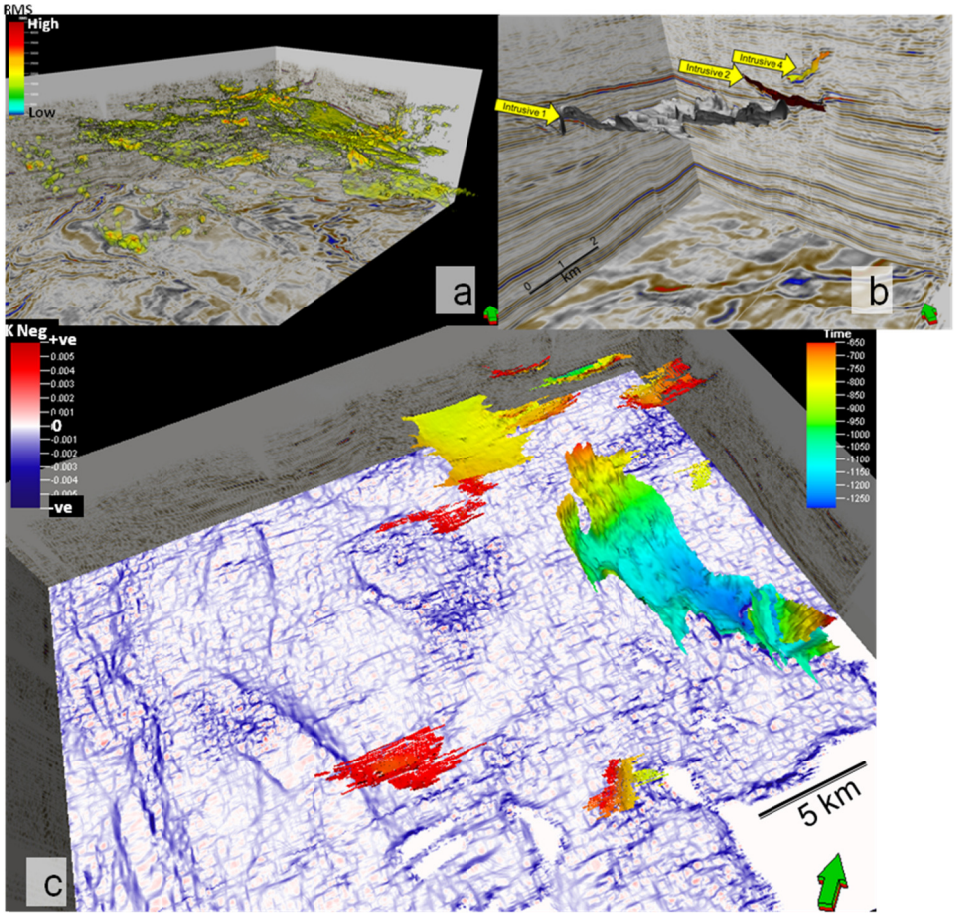

Figure 8. (a) Volcanic geobodies extracted from the RMS amplitude volume computed from the 3D seismic data. (b) and (c) exhibit the mapping and distribution of the subvolcanic intrusive rocks within the 3D seismic data.

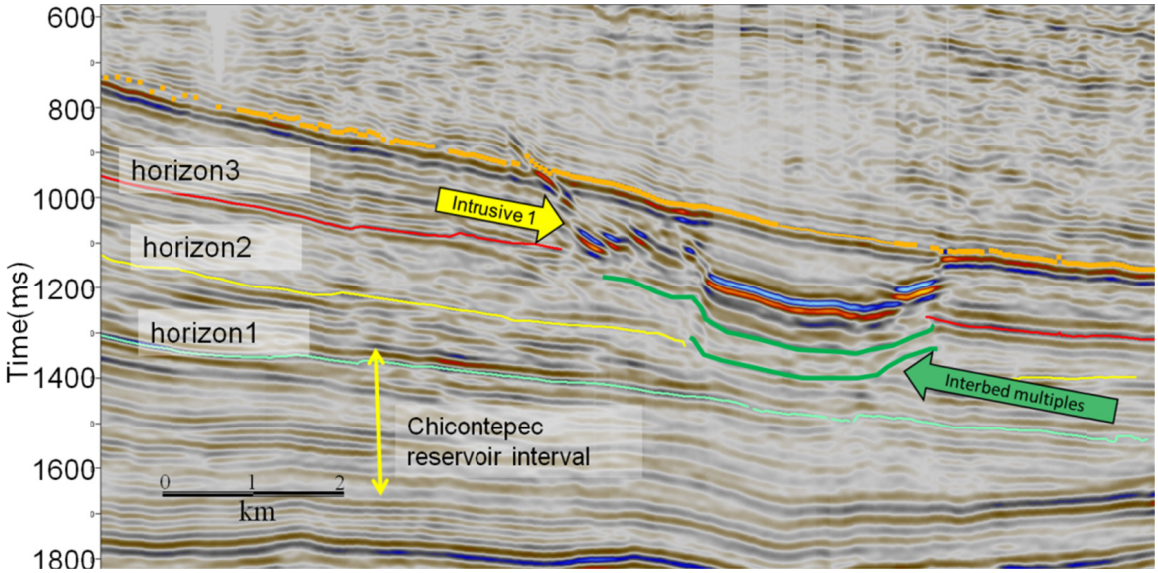

Figure 9. Interbed multiples below the volcanic body prevent the continuous interpretation of horizon 2 and horizon 3. Horizon 1 is the 1st horizon below the volcanic bodies which could be regionally interpreted with confidence.

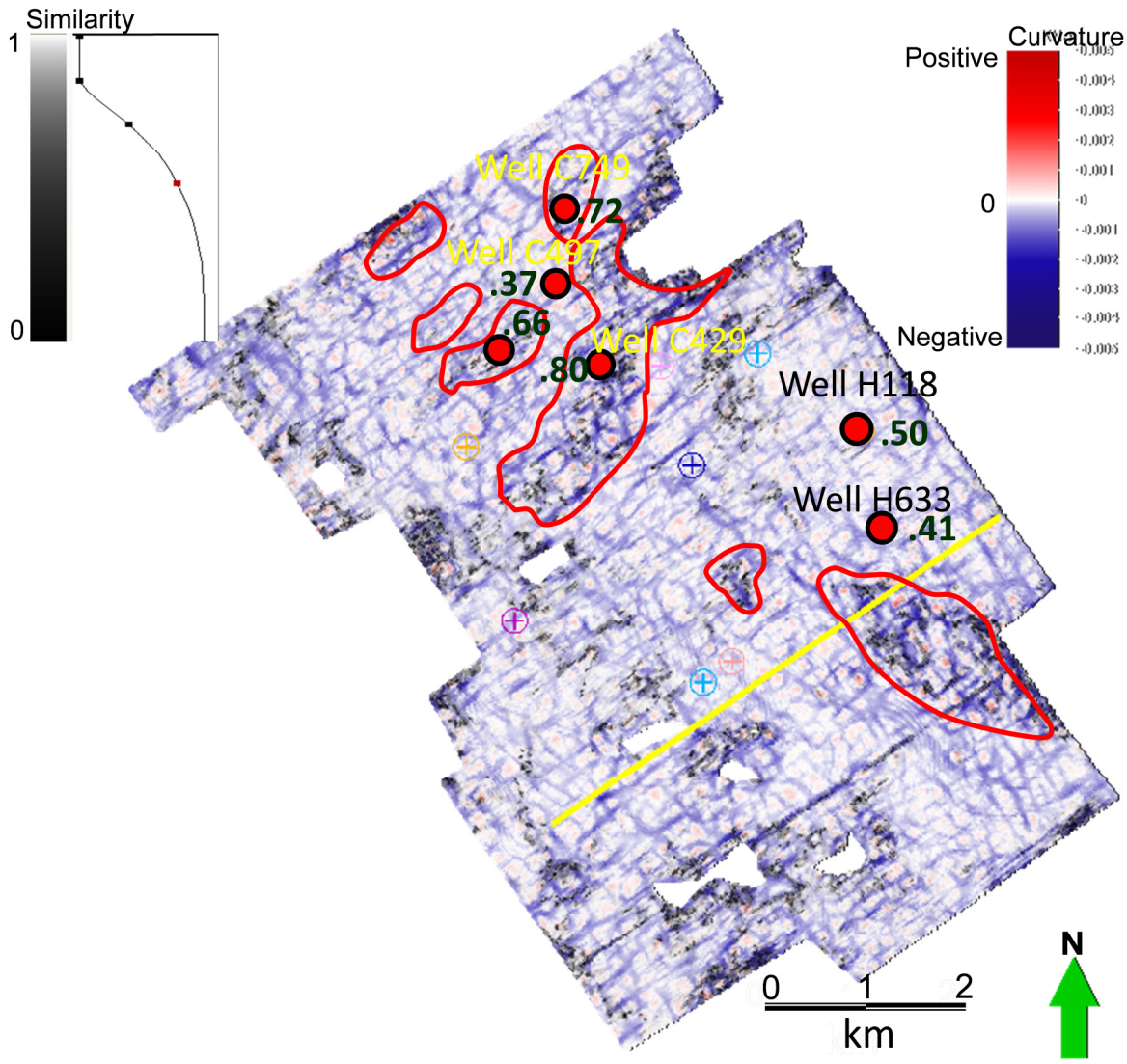

Figure 10. Horizon slice along horizon 1, through the corendered coherence and most negative curvature volumes. Red polygons represent the areas where the most incoherent values of the coherence attribute coincide with the lower values of most negative curvature attribute. Net-to-gross ratios are indicated from some wells within and outside the polygons from the equivalent stratigraphic units. Note the relatively higher numbers from the wells inside the polygons.

DUAL POROSITY CONCEPT

The Chicontepec sandstones have average quartz, feldspar and rock fragment composition of $Q_{29}F_{13}R_{58}$ in the northern part of the Chicontepec basin. 84% of these rock fragments are carbonate rock fragments eroded from Mesozoic carbonate rocks (Bermudez et al., 2006). Some of these carbonate rock fragments contain intragranular pores (pore space bound within a framework grain), primarily due to the internal chambers of fossil fragments within the rock. In photomicrographs, we can observe that the majority of these intragranular pores are isolated from the primary intergranular pores (pore space between the grains) (Figure 11). Consequently, although the intragranular pores are counted during the measurement of total effective porosity, they do not contribute to the permeability of the rock and mostly contain water. The quantity of intragranular porosity varies within the Chicontepec reservoir units, but the areas close to the Tuxpan platform have the potential to contain more intragranular pores due to their influence from this Mesozoic coral reef system.

However, if a natural fracture system is present, there is a strong potential that these intragranular pores are connected through the fracture network and incorporated in the secondary porosity, and in these cases the rock will have 'dual' porosity. To analyze this phenomenon, I examine the capillary pressure/ incremental mercury injection data from two wells: one within and one outside the mapped zones of seismically delineated areas of potential enhanced fracture intensity. The CM well within the mapped zone shows dominant dual porosity and the HM well, outside the mapped zone show dominant single porosity (Figure 12).

As the mercury injection process does not identify intragranular porosity, the wells outside the mapped zone have a dominant single porosity system consisting of intergranular porosity. At the same time, the well within the mapped zone, owing to enhanced fracture intensity from volcanic influence, has a secondary porosity system incorporating the intragranular pores. Thus the well within the mapped zone shows a dual porosity system from the incremental mercury injection data.

Comparing neutron porosity vs. permeability crossplots from two wells (Figure 13) from different sides of the mapped zone, I observed that the permeability in the well within the mapped zone shows a reasonably linear relationship with neutron porosity. On the other hand, the well outside the mapped zone does not show any such relationship. Since neutron porosity is a response from hydrogen ion concentration, it accounts for the intragranular porosity, where it is not connected by fractures. So, the neutron porosity from the well outside the mapped zone does not show any relationship with the permeability, whereas the well within the mapped zone shows a good neutron porosity-permeability relationship as both primary and secondary porosity within its 'dual' porosity system are related to permeability.

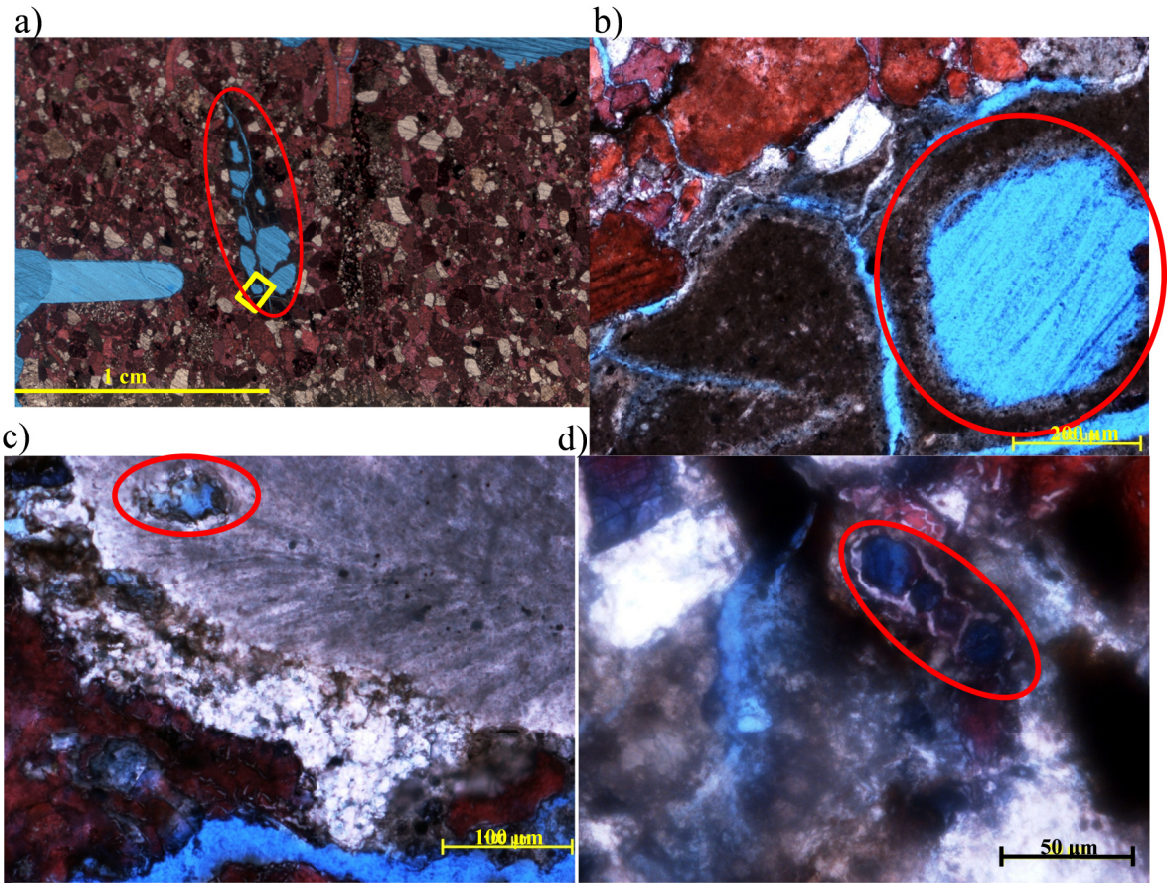

Figure 11. (a) Thin section scan from a reservoir section of the Chicontepec Formation, where the red ellipse encompass intragranular pores (filled by blue epoxy) from the internal chamber of a fossil fragment (the sections are stained with alizarin red-S). (b) Photomicrograph representing the yellow rectangle in (a), showing the isolated nature of the intragranular porosity from the adjacent intergranular porosity. Red ellipses in (c) and (d) exhibiting isolated intragranular porosities from other Chicontepec Sandstone samples.

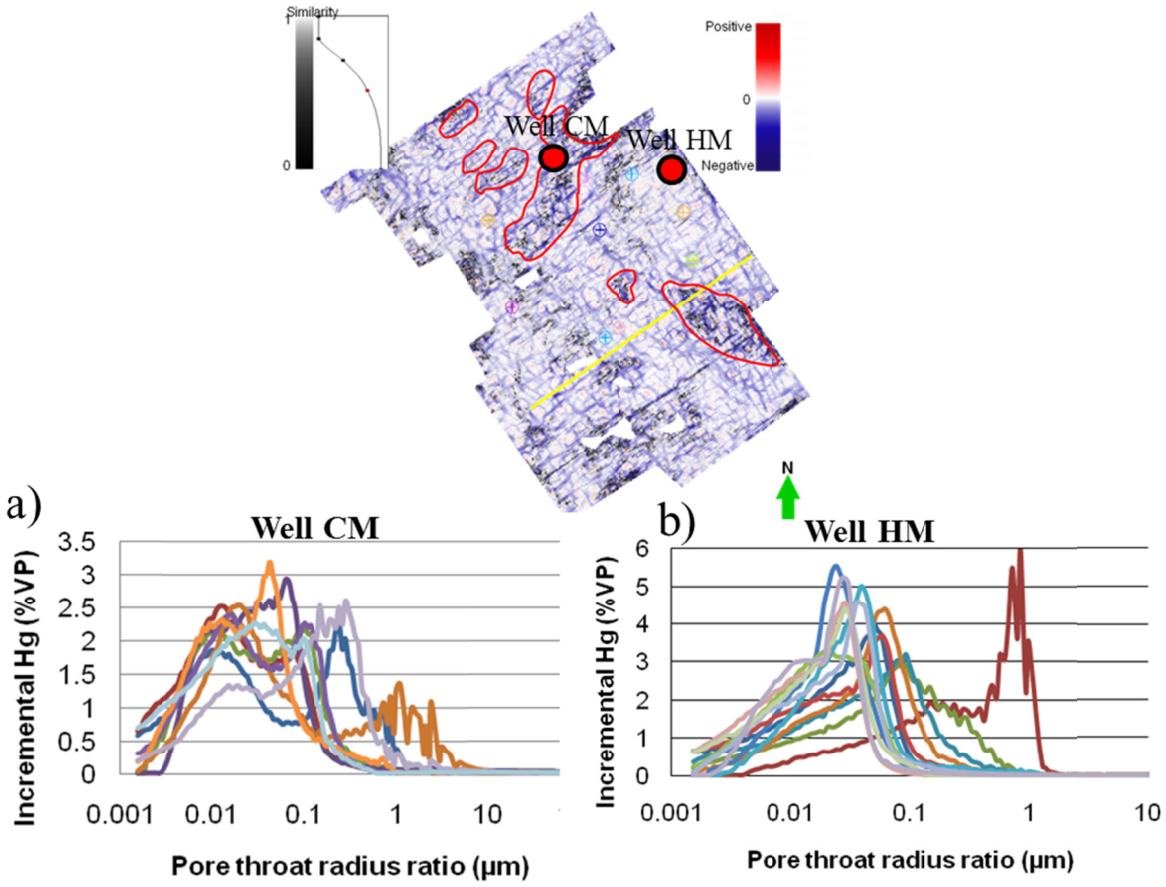

Figure 12. Plotting the incremental mercury injection values against the pore throat radius ratio from well CM, which falls inside one of the mapped polygons in Figure 10 and well HM, outside the polygons. The well CM shows a dominant dual porosity nature while well HM show dominant single porosity nature. Different colors represent different samples.

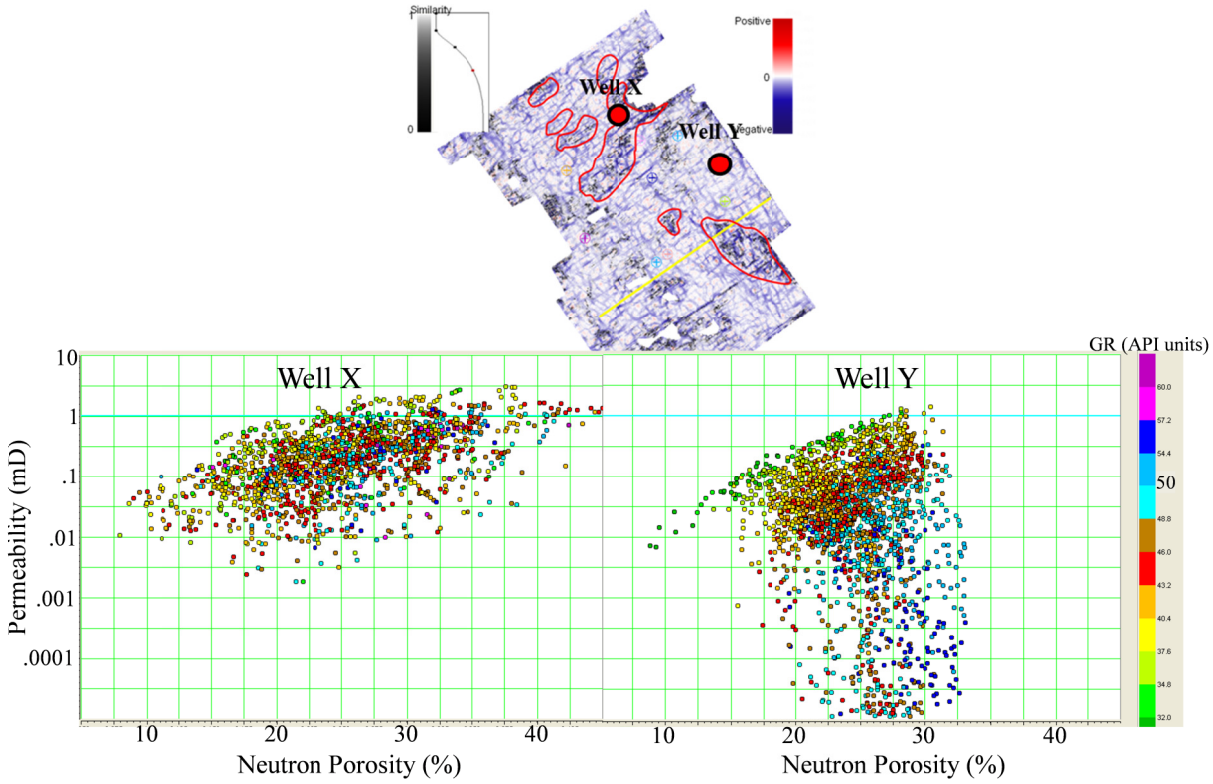

Figure 13. Neutron porosity vs. permeability crossplot from well C 435 (inside a mapped polygon) and well H 118 (outside the mapped polygons).

CONCLUSIONS

Although the presence of volcanic bodies within the reservoir zone adds to the complications of the tight and complex Chicontepec reservoir system, they show potential to increase the fracture intensity in the reservoir near the contact zone. These potential fracture zones can be mapped near the top of the Chicontepec reservoir units by integrating curvature and coherence attributes at the first regionally interpretable surface below the volcanics. These volcanic-influenced natural fractures create a dual porosity system incorporating the intragranular porosity from the carbonate rock fragments. The mapped zones of potential higher permeability near the volcanic-sedimentary contact zone can be considered as additional targets within the stacked Chicontepec reservoirs.

REFERENCES

Alzaga-Ruiz, H., M. Lopez, F. Roure, and M. Seranne, 2009, Interactions between the Laramide Foreland and the passive margin of the Gulf of Mexico: Tectonics and sedimentation in the Golden Lane area, Veracruz State, Mexico: Marine and Petroleum Geology, **26**, 951-973.

Bermúdez, J. C., J. Araujo–Mendieta, M. Cruz–Hernández, H. Salazar–Soto, S. Brizuela–Mundo, S. Ferral–Ortega, and O. Salas–Ramírez, 2006, Diagenetic history of the turbiditic litharenites of the Chicontepec Formation, northern Veracruz: Controls on the secondary porosity for hydrocarbon emplacement: Gulf Coast Association of Geological Societies Transactions, **56**, 65–72.

Chopra, S., and K. J. Marfurt, 2010, Integration of coherence and volumetric curvature images: The Leading Edge, **29**, 404-414.

Chopra, S., and K. Marfurt, 2007, Curvature attribute applications to 3D surface seismic data: The Leading Edge, **26**, 1092-1107.

Delpino, D.H. and A.M. Bermudez, 2009, Petroleum systems including unconventional reservoirs in intrusive igneous rocks (sills and laccoliths): The Leading Edge, **28**, 804-811.

Tristán-González, M., G. J. Aguirre-Díaz, G. Labarthe-Hernández, J. R. Torres-Hernández, and H. Bellon, 2009, Post-Laramide and pre-Basin and Range deformation and implications for Paleogene (55–25 Ma) volcanism in central Mexico: A geological basis for a volcano-tectonic stress model: Tectonophysics, **471**, 136-152.

Magoon, L.B., Hudson, T.L., and Cook, H.E., Pimienta-Tamabra (!)-A giant supercharged petroleum system in the southern Gulf of Mexico, onshore and offshore Mexico, in Bartolini, C., Buffler, R. T., and Cantu-Chapa, A., eds., The Western Gulf of Mexico Basin - Tectonics, Sedimentary Basins, and Petroleum Systems: AAPG Memoir **75**, 83-126.

Morán -Zenteno, D., 1994, Geology of the Mexican Republic: AAPG Studies in Geology, **39**, 160 p.

Chapter 5

Generation of sea-level curves from depositional patterns as seen through seismic attributes –seismic geomorphology analysis of an MTC-rich shallow sediment column, northern Gulf of Mexico

Supratik Sarkar, Kurt J. Marfurt, Roger M Slatt, University of Oklahoma

Detailed interpretation of seismic attributes along horizon slices or stratal slices reveals changes in depositional pattern and seismic geomorphology within a sediment column that are controlled by eustatic and local sea level changes. In this study we analyze seismic geomorphologic features of a shallow sedimentary column within a salt minibasin in the Northern Gulf of Mexico, and attempt to predict the relative sea level curve. We then calibrate these predictions against biostratigraphic markers and compare with existing eustatic cycles and events. Systematic analysis of amplitude and attribute data within a seismic geomorphologic framework reveals high resolution sequence stratigraphic patterns that might otherwise be overlooked.

INTRODUCTION

Our study area is located within the tabular salt minibasin tectono-stratigraphic province (Diegel et al, 1995) of the northern Gulf of Mexico (GOM) margin (Figure 1a). Salt constrains the minibasin on the eastern, western, and southern sides; the main

sediment fairway is from the northeastern side (Figure 1b). Due to the constrained sediment fairway, limited accommodation space, and deposition by "fill-and-spill" processes (e.g. Winker, 1996), the geomorphology of deep-water deposits within salt minibasins differs from that in unconfined marine conditions.

Deepwater clastic deposits consist of four main architectural or depositional elements: channels, thin bed levees, basin floor fans or sheets and mass transport complexes (MTC). The shallow sediment column we are studying here is dominated by MTCs along with other architectural elements. MTCs generally form due to slope failure or slumping from the shelf-slope area when sea level falls rapidly, exposing the shelf-slope area and changing sediment pore pressure. Sediment accumulation in the system of salt minibasins takes place by "fill-and-spill" process (e.g. Winker, 1996) from upslope to downslope areas, thereby preserving the basin floor fan and channel-levee sediments related with the basinal processes. While traditionally MTCs go from upslope to downslope from shelf to slope regions, in areas of salt tectonism, MTCs can also have a local origin due to slope failure or enhanced salt diapirism. Mass transport complexes can be subdivided into i) slide, ii) slump and iii) debrites, or any combination of the three. Where slide and slump is related to sliding and slumping of previously deposited sediments, debrites are high density flows in which coarser particles are supported by matrix strength. Although, there are examples of reservoir units from each type of MTC, these are rare in nature. In general, mass transport complexes exhibit a chaotic seismic reflection pattern. This chaotic pattern differentiates MTCs from more layered fans, channel sands and pelagic shales.

METHODOLOGY

In this study, we analyzed a 100 km^2 prestack depth-migrated 3D seismic volume that covers almost the entire minibasin (Figure 2). Well logs and sparse biostratigraphic data constrain our seismic interpretation. We identify three MTC units (denoted as MTC 1, 2 and 3) as well as seismic sequences containing sheet sands and channels (Figure 2).

In addition to the migrated seismic amplitude, we generated a suite of seismic attribute volumes including RMS amplitude, coherent energy (the square of the RMS amplitude of the coherent component of the data), energy ratio similarity, generalized Sobel filter edge detectors, amplitude gradients, and spectral decomposition components. Although attributes such as RMS amplitude, coherence, and curvature are mathematically independent, they are often coupled through the underlying geology. For this reason, some the features can be identified on all the attributes while others were illuminated by only one or two attributes.

SEQUENTIAL SEISMIC GEOMORPHOLOGIC ANALYSIS.

MTC 1 and underlying sequence 1:

We start with "sequence 1" underlying the MTC 1 (Figure 1c), where attribute expressions indicate the presence of a channel system (Figure 2a). In Figure 2b, we display the phantom horizon slice through blended coherent energy and inline amplitude gradient volumes, approximately 125 m below the top of sequence 1. The low-amplitude deposits in Figure 2b indicate fine-grained sediments throughout the minibasin.

We identify a few striations or grooves at the base of the MTC 1 unit (Figure 3a), which are characteristic features of MTC created due to dragging of coarser blocks

within the MTC, and also indicate the flow direction (Posamentier, 2003). These grooves appear prominently in edge detection attributes such as the Sobel filter attribute (Figure 3b). The relatively rare occurrence of these features indicates a relatively low energy of the initial flow, containing a minimal amount of blocky material.

Attribute slices along the base of MTC 1 indicate a relatively continuous flow coming from the northeast. For instance, the horizon slice generated by blending coherent energy and inline amplitude gradient (Figure 4a) indicates the presence of a moderate to highly reflective coarser grain matrix; however, this seismic geomorphologic pattern becomes very chaotic upward through MTC 1 (Figure 4b). Extending this observation to the vertical seismic profiles, we subdivide MTC 1 into flows A and B (Figure 1c). Flow B is much more erosive in nature and gives rise to a chaotic seismic geomorphologic texture compared to flow A (Figure 4b). It encroaches into flow A from both the southeast and northeast (Figure 4a), eroding into underlying sequences in some places near the main conduit (Figure 1c). Within the overall incoherent pattern of flow B, some coherent high-amplitude blocks are entrapped as imaged in the stratal slice (Figure 4b) corendering coherent energy, amplitude gradient with low coherent part of energy ratio similarity attribute.

Towards the top of MTC 1 flow B, we see relatively continuous stratification and some large entrapped high-amplitude blocks (Figure 4c). The strength and confined character of these bright spots suggest that they are hydrocarbon-charged sand bodies. If these bodies are sufficiently large, they can be exploited as a secondary exploration objective. More commonly they are considered to be a potential drilling hazard to be avoided.

Although flows A and B are part of a large MTC unit, we interpret them as having completely different origins. Sandy debrites in flow A were generated due to basinal slope failure. These debrites entered into the salt minibasin as part of a "fill-and-spill" process, resulting in much reduced original force and holding only a few coarser blocks. Consequently flow A was much less erosive, shows a relatively less chaotic pattern, exhibits a broader flow conduit and created very few striations or groove at the base.

In contrast, flow B is extremely erosive and exhibits a highly chaotic seismic geomorphologic pattern. We interpret flow B of MTC 1 to have a local origin and formed due to collapse of sediment from in and around the minibasin in response to either salt diapirism or differential sediment loading.

Basin floor fan unit overlying MTC 1:

Several stratal slices have been generated through the seismic sequence overlying MTC1. We identify a basin floor fan within the seismic sequence in some stratal slices. A stratal slice (dotted line (ii) in Figure 5a) as shown in Figure 5c reveals the basin floor fan by plotting peak magnitude against peak frequency volumes. Distributaries and complex sediment distribution patterns within the fan are clearly seen on Figure 5e, which is a display of the coherent energy attribute blended with the inline coherent amplitude gradient attribute along this stratal slice. We abbreviate the sequence dominated by this basin floor fan as the BFF sequence. Two other stratal slices extracted at the top and bottom of the seismic sequence (5a) by blending peak magnitude with peak frequency exhibit a monotonous, relatively low amplitude pattern (5b and 5d). The feeder channels

of the basin floor fan can be observed along a stratal slice at a shallower level (Figure 5a and 5f) to the main fan unit.

MTC 2:

The basin floor fan sequence is overlain by MTC 2. The overall seismic geomorphologic pattern is chaotic in nature. MTC 2 does not have any erosional impact on the underlying and overlying units; consequently it had significantly lower energy compared to flow B of MTC 1. MTC 2 contains some small slump blocks along with some debrites, and undifferentiated MTC deposits (Figure 6a, 6b). Overall analysis indicates that MTC 2 was related to basin-wide deposition rather than to salt tectonism. One of the most interesting features within MTC 2 is the presence of a higher-amplitude internal channel-submarine fan unit within the chaotic sediments as revealed by coherent energy and inline gradient blended stratal slice (Figure 6d). This channel appears as a high-amplitude strip within the MTC 2 unit in vertical seismic sections (6b). The chaotic sediments of MTC 2 are overlain by another blanket of low-amplitude sediments (Figure 6e).

MTC 3:

MTC 3 is the uppermost sequence within the sedimentary column where the seismic data quality allowed geomorphologic analysis. MTC 3 does not yield any systematic depositional pattern from detailed seismic interpretation and seismic geomorphologic study. The overall chaotic facies includes debris flows (Figure 6f) as well as combinations of slumps and debrites. Another low-amplitude interval is detected from seismic geomorphology at the top of this seismic sequence (Figure 6g).

Sequence stratigraphic interpretation from sequential seismic geomorphologic patterns.

Excellent vertical stacking patterns and well-defined seismic sequences created predominantly by the "fill-and-spill" processes are characteristic of salt minibasins (Winker, 1996). Sequential seismic geomorphologic analysis based on seismic attributes through these sequences provides us with a unique opportunity to estimate the relative sea level changes and sequence stratigraphy of the minibasin as well as the whole basin. First, we attempted to define the sequence stratigraphic patterns from seismic geomorphologic studies alone. Then we made modifications in the relative sea level curve by including the biostratigraphic information, and finally compared the prediction with existing Quaternary eustatic cycles for the Gulf of Mexico (GOM).

Sequential seismic geomorphologic analysis as described previously indicates that sequence 1 culminates with fine-grained sediments or shaly deposits which are in turn overlain by flow A of MTC 1. Since we interpreted flow A to be part of a basinal mass transport event, we hypothesize that the shaly deposit at the top of sequence 1 (Figure 2b) was formed as part of a Transgressive Systems Tract (TST) and/or a Highstand Systems Tract (HST). Sequence 1 was followed by flow A of MTC 1 (figure 4b) in the early Lowstand Systems Tract (LST) of the following sequence. We interpret the base of MTC 1 flow A to be a sequence boundary. An increased sedimentation rate and differential loading caused enhanced salt diapir movement throughout the basin, which resulted in the initiation of flow B above flow A within the same LST (Figure 4c). We interpret the monotonous relatively low-amplitude reflection pattern at the base of seismic sequence BFF to be finer clastics deposited during the next TST (TST 2) atop the MTC 1 unit

(Figure 5b). Basin floor fans are formed during LST time, such that the prominent basin floor fan in the sequence BFF was formed in the LST of the next sea level cycle (Figure 5c, 5e). The feeder channel or canyon for this basin floor fan can be identified in the next shallower level (Figure 5f). Coarser sediments through the feeders were carried to the basin floor fan, such that the channel conduits were open or filled with finer clastics. With start of sea level rise during the next TST (TST 3) following the LST time, the depositional axes of the basin began to change such that the channels were backfilled with coarser grained material, making them visible through amplitude-sensitive seismic attributes. This TST 3 again deposited a blanket of finer clastics on the BFF sequence (Figure 5d). MTC 2 was a basinal event, formed during the next fall in sea level, bringing some chaotic sediment into the minibasin. The buried channel-submarine fan unit was also formed during this LST and was buried within MTC2. An additional blanket of low-amplitude sediments above MTC 2 is interpreted to be part of the next TST event (TST 4) (Figure 6e). We conclude our sequence stratigraphic analysis at MTC 3 (Figure 6f), which we interpret have been deposited during the next sea level cycle, occurring during a LST with finer clastics above it, indicating the beginning of a TST (TST 5) (Figure 6g). From this sequence stratigraphic interpretation based only on seismic geomorphology, we draw the preliminary relative sea level curve shown in Figure 7.

The above sequence stratigraphic interpretation can be made during the early exploration stage, when only seismic data are available. In the following section we incorporate biostratigraphic information within our sequence stratigraphic framework for a more comprehensive picture before comparing our prediction with the available GOM eustatic cycles.

Incorporating biostratigraphy within the seismic sequence stratigraphic interpretation.

Biostratigraphy provides the ground truth for any sequence stratigraphic interpretation. Incorporating biostratigraphic information from the few wells in the area to the seismic sequence stratigraphic interpretation allowed us to make necessary calibration and changes to the existing curve (Figure 8a). We also verified whether we placed the MTCs in their proper sequence stratigraphic context. Table 1 shows the name of the key microfossils (corresponding to the sequences starting from top of sequence 1 to top of MTC 3), their type and age of last appearance datum (LAD) as obtained from the biostratigraphic chart for the Neogene section of the GOM. According to the biostratigraphic chart, these biomarkers either represent maximum flooding surfaces or a sequence boundary. Figure 8a shows the relative sea level curve constrained by biostratigraphic age, showing that we are examining fourth order sequences (10^5- 10^6 years).

Table 1: Last appearance datum of microfossils, their type and corresponding sequences in this study. (Biostratigraphic age data from Paleo Data, Inc., 2009).

Geologic Time (Ma)	Calcareous Nanoplankton	Planktonic Foraminifera	Benthic foraminifera	Corresponding sequence Top
0.13		Globorotalia flexuosa		MTC3
0.44	Pseudoemiliania lacunose A			MTC2
0.51		Globorotalia truncatulinoides		BFF
0.64			Trimosina A	MTC1
0.85	P. lacunosa variety			SEQUENCE1

Comparison with existing eustatic cycles from the Neogene GOM

Finally we matched the newly constructed relative sea level curve with the corresponding part of the Quaternary eustatic cycles from Wornardt and Vail (1991) (Figure 8b). The sea level curve can be well correlated for the first two sequences - sequence 1 and MTC 1. BFF and MTC 2 correspond to a single sea level cycle in the published curve, indicating that seismic data can sometime lead to finer scale sea level change information especially within such shorter geologic time intervals. Denser biostratigraphic information is needed to understand its sequence stratigraphic significance. The next eustatic cycle does not match the newly constructed sea level curve. Since the deposition of sediment within a minibasin predominantly follows the "fill and spill" pattern, sediments corresponding to this cycle might have bypassed, due to the lack of accommodation space left within the minibasin. The final part of the sea level curve corresponding to MTC 3 and planktonic foraminifera Globorotalia flexuosa can be well-correlated with the eustatic cycle.

The relative sea level curve we constructed from sequential seismic geomorphologic analysis corresponds reasonably well with the Neogene eustatic cycles. However, we observed that limited accommodation space within the minibasin may lead to some mismatch due to absence in the sedimentary record. At the same time, some part of the sediment column may contain deposits resulting from local processes such as salt tectonics as happened in the case of flow B of MTC 1. Consequently, a one-to-one correspondence of the constructed sea level curve for the sediments within the minibasin to the basin scale sea level curve may not always be possible. However, the points of mismatches may yield valuable information about missing or bypassed strata.

SUMMARY AND CONCLUSIONS

Seismic geomorphologic features in the MTC-rich sediment column within a GOM minibasin were illuminated through seismic attributes. A bottom to top sequential geomorphology study of these features helped to build a sequence stratigraphic framework.

We showed how to construct a relative sea level curve from sequential seismic geomorphology and seismic sequence stratigraphic interpretation. This curve correlates fairly well with the published eustatic cycles. In the absence of biostratigraphic data, the sequential seismic geomorphologic analysis from multi-attribute studies can provide a sequence stratigraphic framework for more detailed sand prediction. Combined with biostratigraphic information, such analysis may even reveal finer details not predicted by the regional sea level curves.

ACKNOWLEDGEMENTS

We want to acknowledge Hess Inc., for the use of their deepwater GOM data volume for research and education and Schlumberger for providing the Petrel Software, in which the interpretation was done. We acknowledge Belinda Ferrero Hodgson, who did her MS thesis on this data and thus providing the starting point of our work. Much of the attribute software and financial support for the first author was funded by industry support for the Attribute-Assisted Seismic Processing and Interpretation consortium at OU.

REFERENCES:

Diegel, F. A., J. F. Karlo D. C. Schuster R. C. Shoup and P. R. Tauvers P. R., 1995, Cenozoic structural evolution and tectono-stratigraphic framework of the northern Gulf coast continental margin, AAPG Memoir 65, 109-151.

Ferrero-Hodgson, B., 2007, An integrated 3d Seismic Sequence-Stratigraphic Analysis of the Pleistocene Strata Above Baldpate Field, Garden Banks, Deep Water Gulf of Mexico: M.S Thesis, University of Oklahoma, Norman, Oklahoma, 1-186.

Okuma, A.F., R. R. Pressler, D. B. Walker, and K., Kemp, 2000, Baldpate Field Exploration History, Garden Banks 260, Gulf of Mexico, Gulf Coast Section -SEPM Foundation 20th Annual Bob F. Perkins Research Conference. 739-755

Paleo-data Inc., 2009, Biostratigraphic chart, gulf Basin, USA- Neogene.

Posamentier, H.W., 2003, Depositional elements associated with a basin floor channel-levee system: case study from the Gulf of Mexico, Marine and Petroleum Geology, 20, 677-690.

Winker, C.D., 1996, High-resolution seismic stratigraphy of a late Pleistocene submarine fan ponded by salt-withdrawal mini-basins on the Gulf of Mexico continental slope, Proceedings of the 28th annual Offshore Technology Conference, 619-628.

Wornardt, W.W., and P. R. Vail, 1991, Revision of the Plio-Pleistocene cycles and their application to sequence stratigraphy and shelf and slope sediments in the Gulf of Mexico, GCAGS Transactions, XLI, 719-744.

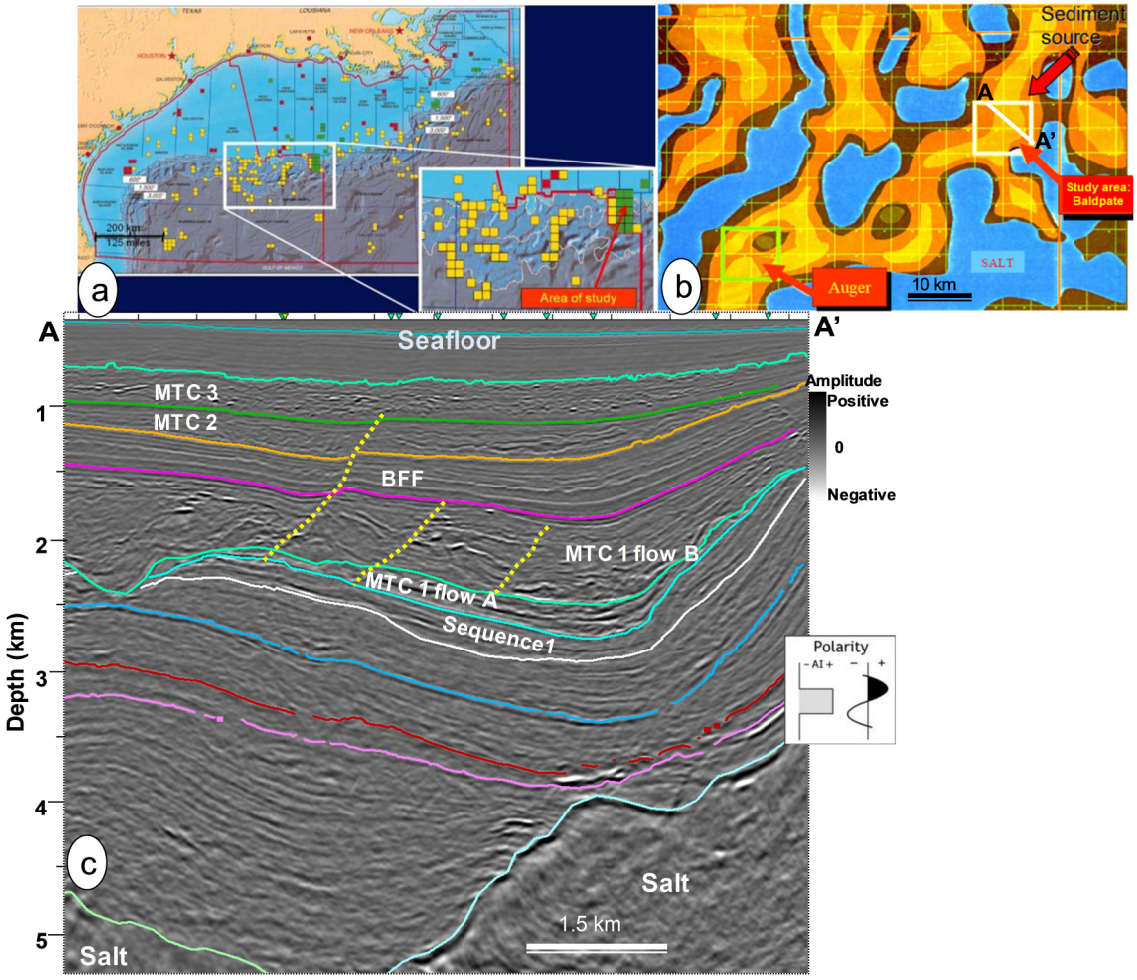

Figure 1. Location of the study area within the northern Gulf of Mexico salt minibasin tectonostratigraphic province. (Okuma et al., 2000). (b) Regional sediment fairway map. Yellow and orange represent sediments, blue represent salt bodies. White square indica tes the 3D area. (modified from Okuma et al., 2000). (c) Seismic Line AA' from the 3D seismic survey showing the interpreted seismic sequences from Sequence 1 (white line is the base of sequence 1) up through MTC 3. Portions of the salt bodies surrounding the minibasin are also imaged at the bottom. MTC = Mass Transport Complex. BFF= Basin Floor Fan. Dotted lines indicate rotated fault blocks.

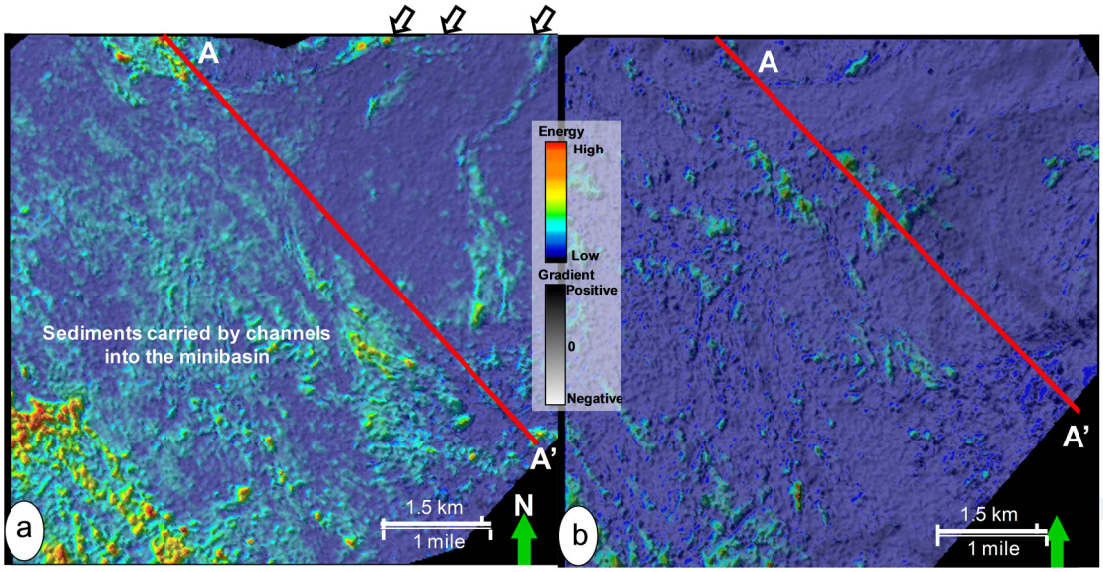

Figure 2. Phantom horizon slices blending coherent energy and inline gradient attributes approximately (a) 250 meters below and (b) 125 m below the top of Sequence 1(Figure 1c), computed using a three trace by three trace by five sample analysis window (75 m by 75 m by 45 m). In (a) arrows indicate a channel system coming from the northeast and (b) exhibits an overall low amplitude character.

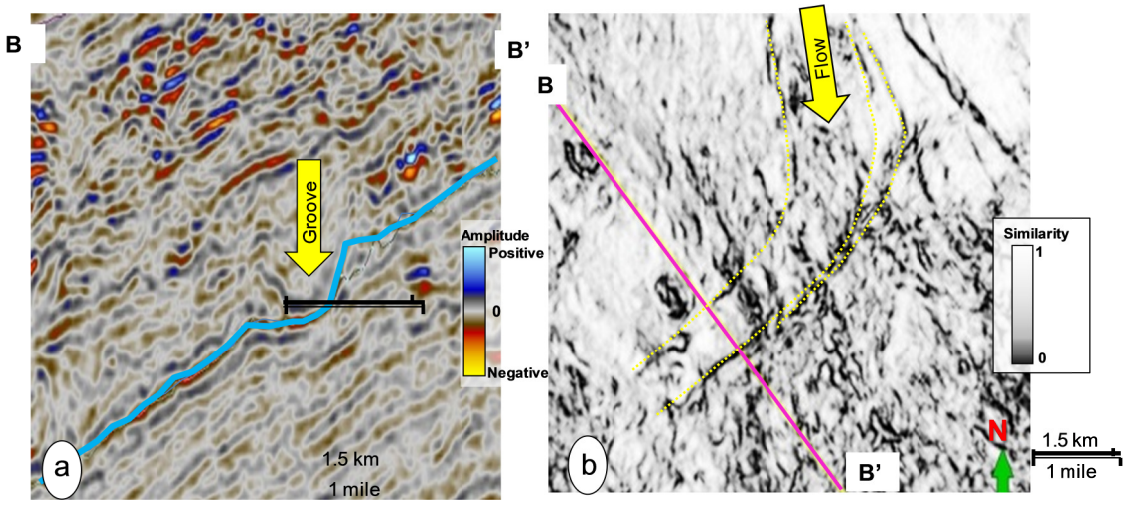

Figure 3.Striation or groove seen in (a) vertical seismic indicated by yellow arrow and (b) horizon slice along the cyan pick on (a) through the generalized Sobel filter similarity volume. Dotted yellow lines in (b) indicate the edges of the groove while arrow indicates the flow direction.

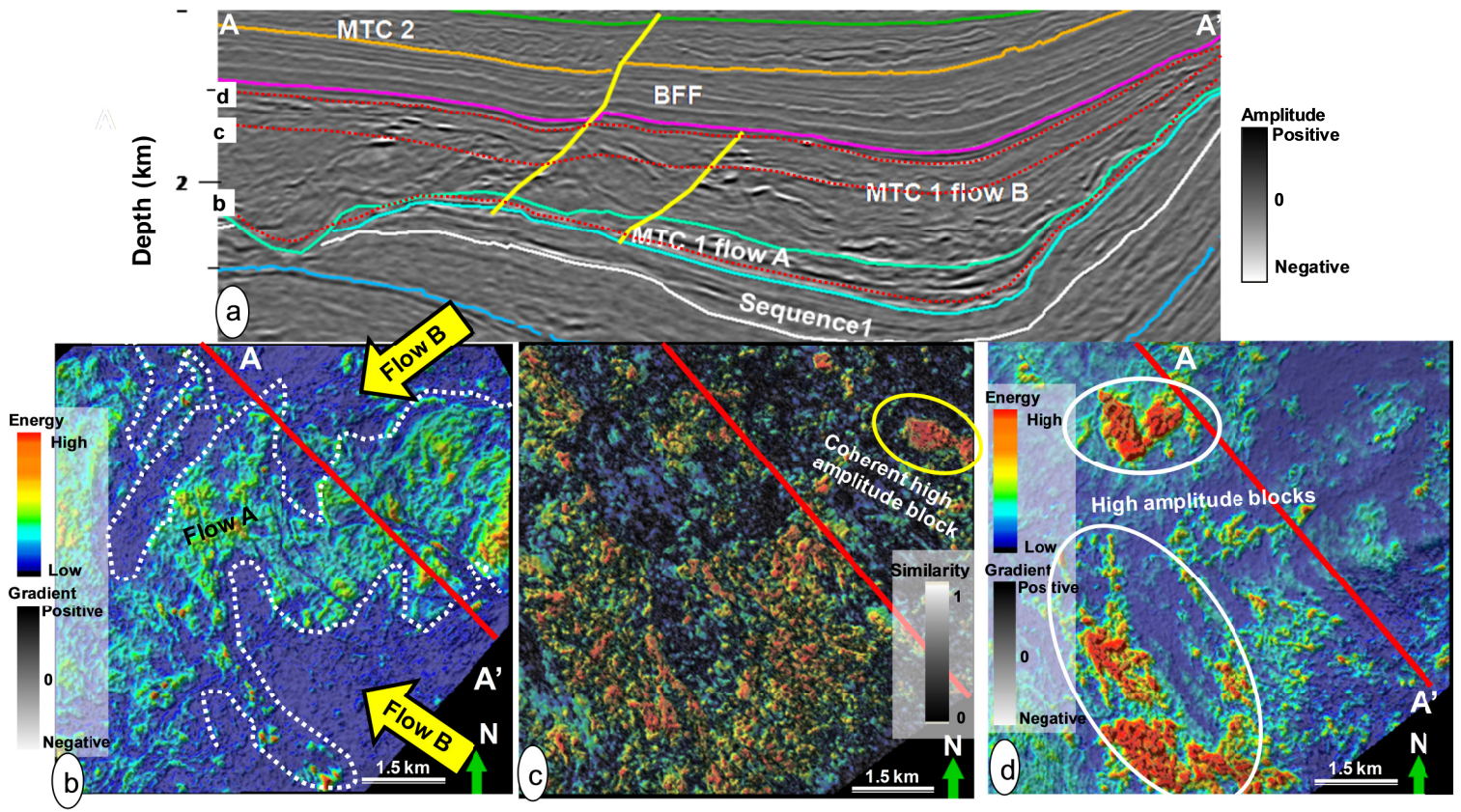

Figure 4. Stratal slices through MTC1 sequence by corendering coherent energy and inline gradient volumes. Red dotted lines b,c,d in vertical seismic section in (a) represent stratal slices corresponding to the figures (b), (c), and (d) respectively. In (b) white dotted line indicates encroachment of flow B into relatively continuous flow A from two directions. Stratal slice in (c) is also blended with low coherent part of energy ratio similarity attribute to identify coherent blocks and overall incoherent nature of flow B. High amplitude entrapped blocks towards the top of MTC 1 flow B are illuminated in (d).

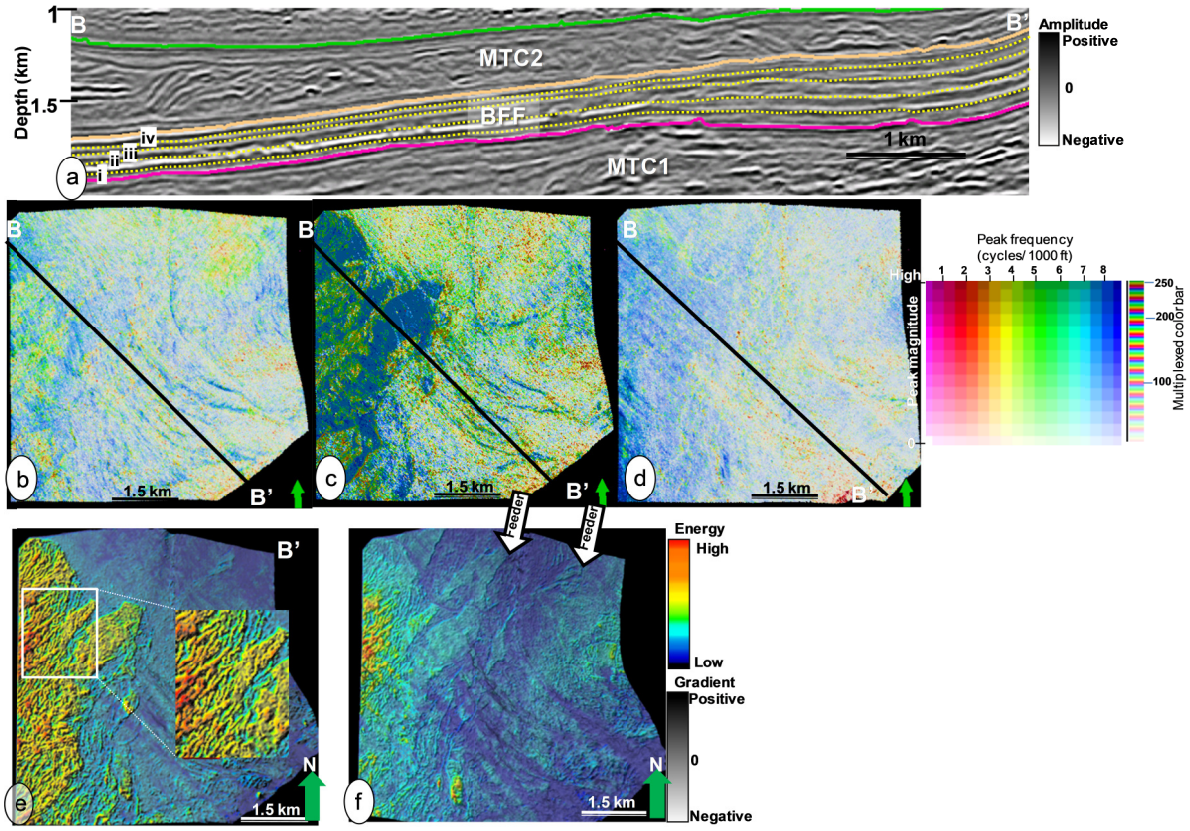

Figure 5. Stratal slices through basin floor fan (BFF) sequence. White dotted lines (i), (ii) and (iv) on vertical seismic profile in (a) corresponds to stratal slices represented respectively in (b), (c), and (d) by blending peak magnitude with peak frequency volume against 2D hue-lightness colour bar. Stratal slices (e) and (f) are generated by corendering coherent energy and inline gradient volume and they correspond to yellow dotted lines (ii) and (iii) respectively in (a). Dotted line (ii) in (a) goes through the basin floor fan, whereas (i) and (iv) goes through TST2 and TST3 respectively. Complex internal distributaries of the basin floor fan are illuminated in (e). (f) reveals fan feeder channels.

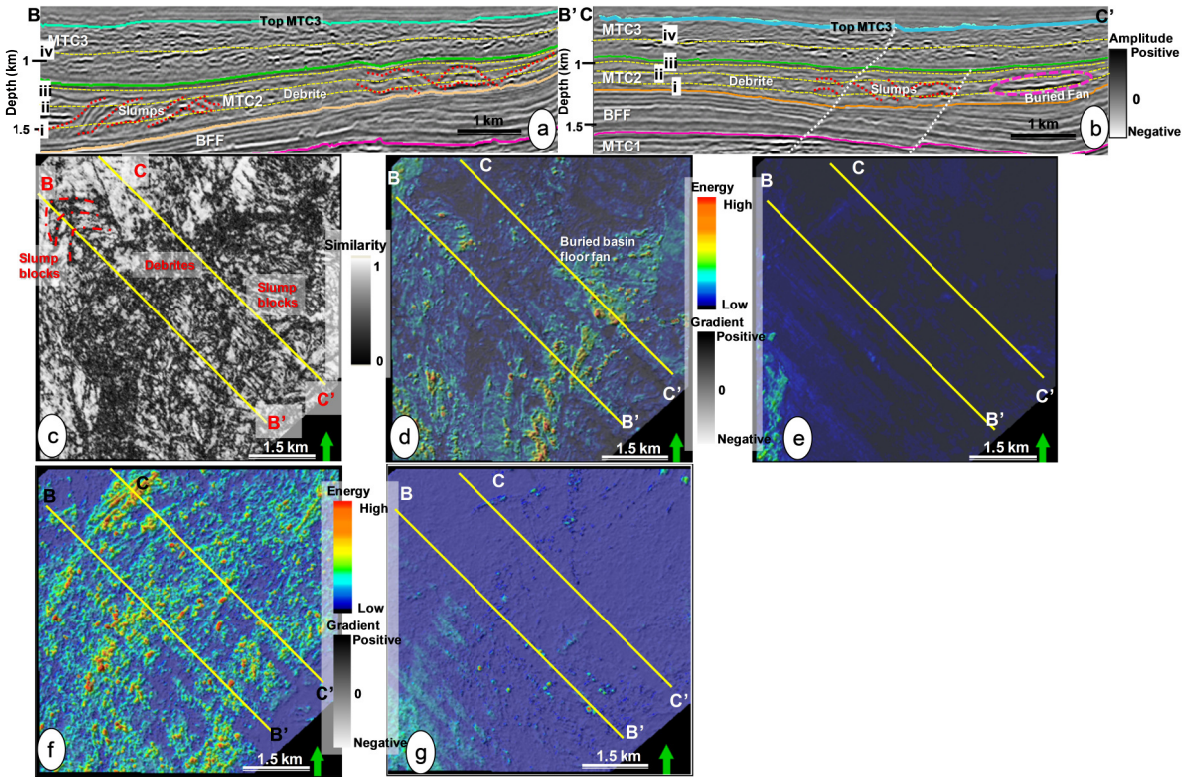

Figure 6. Stratal slices through MTC 2 and MTC 3 sequences. In vertical seismic lines(a) and (b), slumps and debrites are interpreted within MTC 2. Yellow dotted lines (i), (ii), (iii), (iv) in (a) and (b) corresponds to stratal slices shown in (c), (d), (e) and (f) are generated by blending coherent energy with inline amplitude gradient attributes. (d) images a buried basin floor fan within MTC 2 indicated by the pink ellipse in (b). (e) represents monotonous low amplitude deposits of TST 4 at the top of MTC 2. Sandy debris flow within MTC3 is seen in (f). In (g), horizon slice at Top MTC3 horizon indicates initiation of low amplitude blanket at TST 5.

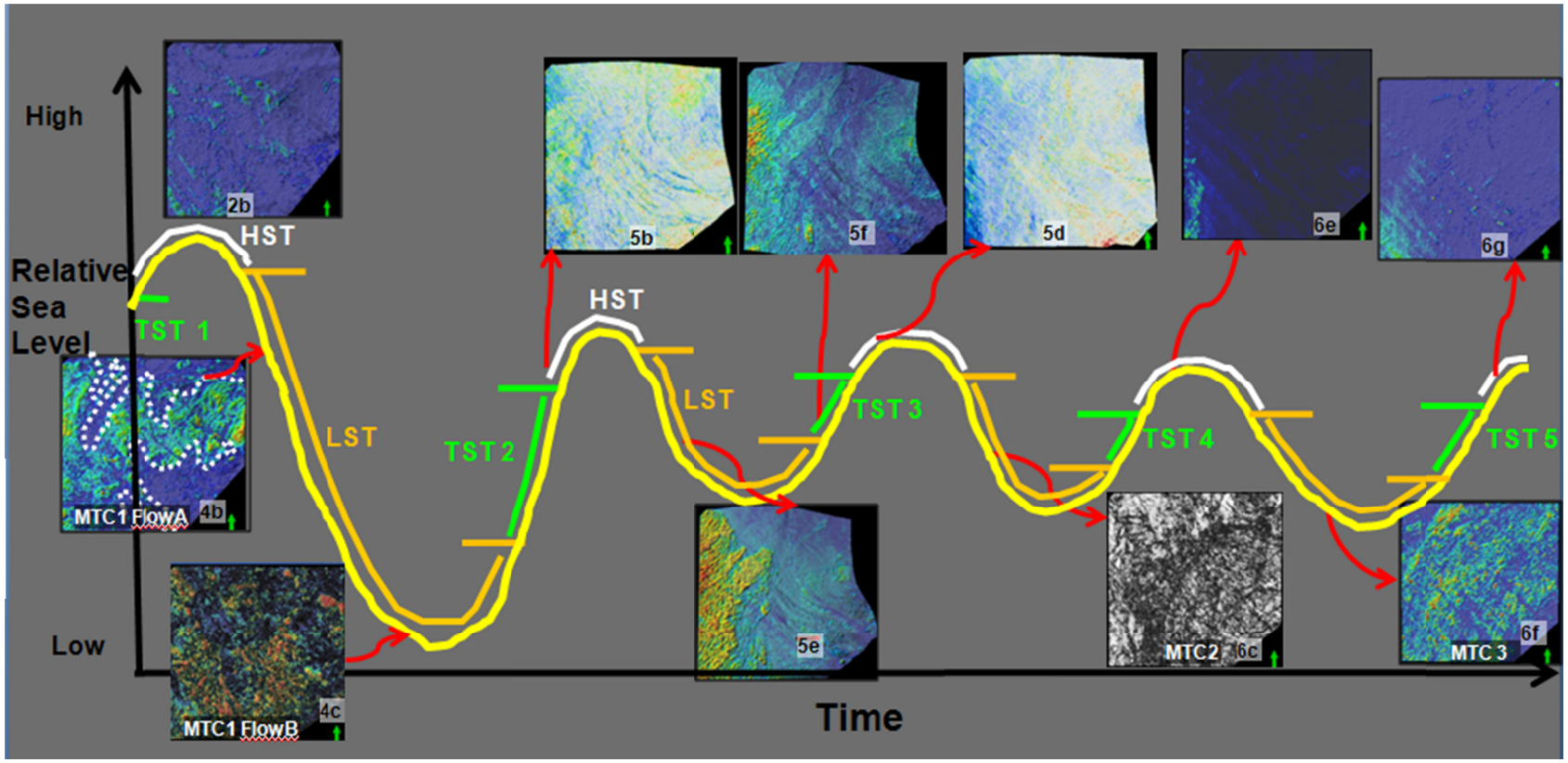

Figure 7. Generalized sea level curve from sequential seismic geomorphology study. Orange, green and white portions in each cycle represents respectively LST, TST and HST respectively. The numbers associated with the images corresponds to the original figure numbers associated with the images corresponds to the original figure numbers.

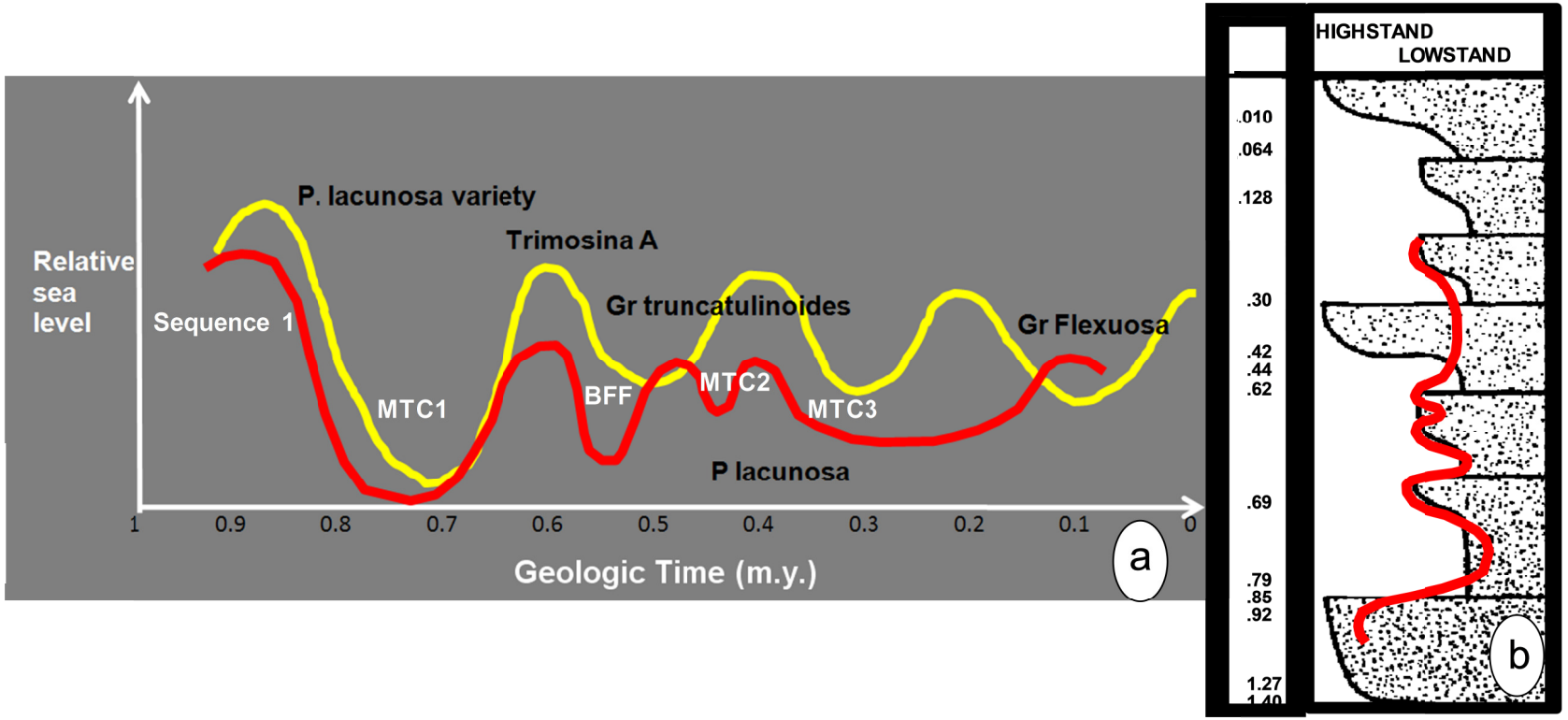

Figure 8. Curve in Figure 7 (in yellow) is modified (in red) after constraining it with geologic age obtained from biostratigraphic data. (b) Overlaying the sea level curve generated from our analysis on the published Quaternary eustatic cycles of Gulf of Mexic o from Wornardt and Vail (1991) (after Lamb et al., 1987).

Chapter 6

Conclusions

The new depositional history model established for the northern part of the Chicontepec basin shows that the turbidites that formed the Chicontepec reservoirs were deposited within five stratigraphic units equivalent to 3rd order global sequences (Haq et al., 1987) from Upper Paleocene to Early Eocene. Turbidite assemblages in the basal Chicontepec sequence were dominated by a system of basin axis-parallel channel systems coming from the far northern part of the basin. The facies assemblages changed dramatically from late Upper Paleocene with significantly enhanced sediment supply from the direction of the Sierra Madre Oriental with the initiation of a Laramide Orogeny tectonic pulse and a smooth basin gradient development. These basin axis-perpendicular channel fan system dominated the turbidite assemblages in the Early Eocene sequences. The mixed depositional system evolved from the interaction of the basin axis-parallel and -perpendicular systems within the Chicontepec foredeep can be considered as a 'type' depositional concept for foreland basin turbidite systems. The change in progressive turbidite depositional pattern is linked with improved reservoirs within the sequences from the lower part of the Early Eocene.

Petrophysical analysis of turbidite reservoirs within the low-permeability productive intervals corresponds to a small window in $\lambda\rho$-$\mu\rho$ space, corresponding to rock types with good fracability. Calibration of prestack simultaneous inversion $\lambda\rho$-$\mu\rho$, V_P/V_S volumes with the petrophysical analysis and seismic geomorphology provides a

volumetric estimation of rock types within the stratigraphic units and provide us a means to predict prospective areas beyond well control.

Shallow volcanic bodies, which are an integral part of Chicontepec sedimentary units show potential to increase the fracture intensity in the reservoir near the contact zone in many areas. These potential fractured areas may give rise to increased permeability zones and can be mapped near the top of the Chicontepec reservoir units by corendering curvature and coherence attributes. The 'dual' porosity system created by this process incorporates intragranular pores within the carbonate fragments and makes it a candidate for consideration as an additional target.

Relative sea level curve and sequence stratigraphy corresponding to a sediment column can be derived from a bottom-to-top sequential geomorphology study of the seismic attribute-illuminated depositional features. Biostratigraphy calibrates the seismic geomorphologic interpretation so that in the absence of biostratigraphic data, the sequential seismic geomorphologic analysis from multiattribute studies can provide a sequence stratigraphic framework for more detailed sand prediction even within a structurally confined deepwater salt minibasin.

Recommendation

The Chicontepec basin is one of the most important hydrocarbon plays for Mexico. It is very important to reconstruct the turbidite depositional history in the entire basin and extend the depositional model I proposed here to the other parts of the basin. Gustavo Diaz (2008) proposed a sequence stratigraphic framework in the southern part of the basin. I recommend a comprehensive study in the middle part of the Chicontepec

basin that establishes a connection between the two parts and reconstruct the complex geological history of the Chicontepec basin as a whole.

Appendix

Outcrop section consisting of basalt flow within the Chicontepec Sandstone